DISSERTATION

Collision-Induced Scattering in Simple Liquids Investigated with Stimulated Gain Spectroscopy at Ambient and High Pressures

Submitted by

Cheryl Bigelow Gratias

Physics Department

In partial fulfillment of the requirements
for the degree of Doctor of Philosophy

Colorado State University
Fort Collins, Colorado, USA

SUMMER 2003

COLORADO STATE UNIVERSITY

May 27, 2003

WE HEREBY RECOMMEND THAT THE DISSERTATION PREPARED UNDER OUR SUPERVISION BY CHERYL BIGELOW GRATIAS ENTITLED **COLLISION-INDUCED SCATTERING IN SIMPLE LIQUIDS INVESTIGATED WITH STIMULATED GAIN SPECTROSCOPY AT AMBIENT AND HIGH PRESSURES** BE ACCEPTED AS FULFILLING, IN PART, REQUIREMENTS FOR THE DEGREE OF DOCTOR OF PHILOSOPHY.

Committee on Graduate Work

____

____

____

____

____
Adviser

____
Department Head

ABSTRACT OF DISSERTATION

Collision-Induced Scattering in Simple Liquids Investigated with Stimulated Gain Spectroscopy at Ambient and High Pressures

Stimulated gain spectroscopy (SGS) provides an excellent tool for the investigation of low frequency dynamics of molecular liquids, with sufficient resolution and signal-to-noise ratio to reflect intermolecular interactions. Liquid CCl_4 was selected for investigation because its isotropic polarizability ensures that depolarized scattering is due only to intermolecular interactions, thus providing a good test of various models for collision-induced (CI) anisotropy based on different interaction distances, *r*. The depolarized spectrum for CCl_4 was decomposed phenomenologically into two modeled components: a narrow Lorentzian function with a damping rate, Γ, representing diffusive reorientation and a broad weighted exponential function of the form $\omega^s \exp(-\omega/\omega_c)$ corresponding to collision-induced scattering with a characteristic frequency, ω_c. Different values for s correspond to different sources for the induced anisotropy and provide distinct models for fitting to the measured spectrum. A model with s = 1.571, indicating a collision-induced electronic repulsive force with a r^{-9} dependence provided the best fit to the CCl_4 spectrum. The best fitted values are $\Gamma = 2.2 \pm 0.5$ cm^{-1} and $\omega_c = 17.1 \pm 0.1$ cm^{-1}, in general agreement with earlier results from spontaneous light scattering and coherent time-domain techniques, which were usually unable to determine all three parameters from a single measured spectrum.

These results in CCl_4 enable comparison with liquids comprised of nearly spherical, linear and planar molecules. While a three-component model which decomposes the CI component into an intermediate frequency term and a librational term is generally best for less isotropic molecules, the application of the two-component model for diffusive reorientation and CI scattering fit many molecules surprisingly well, indicating that, for many molecular liquids, binary collisions dominate depolarized scattering even at liquid densities.

In a second experiment, high pressure is incorporated into the SGS experiment and benzene spectra at atmospheric pressure and at 350 bars are analyzed using a curve-fitting model comprised of a low frequency diffusive reorientational term, a high frequency librational term, and an intermediate frequency term. The 3% increase in liquid density resulted in a 17% decrease in the rate of reorientational diffusion and a librational component with a 12% higher center frequency and a 31% reduction in inhomogeneous broadening. The intermediate frequency term exhibited the strongest pressure sensitivity, resulting in a broader, higher intensity component with a 32% higher characteristic frequency.

The effects of pressure on the Brillouin spectrum of liquid benzene is also investigated with stimulated Brillouin gain measurements made at 1, 540, and 880 bars of pressure. Results indicate a Brillouin shift with pressure of 1.92 GHz/kbar.

Cheryl Bigelow Gratias
Physics Department
Colorado State University
Fort Collins, CO 80525

Summer 2003

ACKNOWLEDGMENTS

This dissertation would not have been possible without the help and contributions of many others. The research and experiments presented here build on work done by Jonathan Friedman. I appreciate the time he spent introducing me to his research and to the lab and lasers used for this work.

I owe a debt of gratitude to my adviser, Professor Chiao-Yao She, for in many ways making this project feasible. I especially appreciate our many discussions which have clarified physical insights and have both shaped and given focus to the direction of this research. Thank you, Joe, for your encouragement and patience with what has turned out to be a longer process than any of us anticipated. I also want to thank my committee members, each of whom has contributed in one or more ways with technical support, insightful and challenging discussions and a contagious enthusiasm for tackling questions of science. The high pressure portions of this work would not have been possible without Professor H. Dieter Hochheimer generously sharing his time, expertise and equipment.

I cannot count the times my family and friends have stepped in with help and encouragement. I especially want to thank my parents who have always been willing to offer their time in ways to free up mine. My husband, Ray Gratias, should be knighted for his amazing patience and constant support, and I thank him from the bottom of my heart. Finally, thank you, Benjamin, for always cheering your Mom on!

DEDICATION

This work is dedicated to the memory of Marjorie Anne Bigelow for her unwavering faith in my ability to accomplish whatever I set my mind and heart to, for the hope she had to see this degree completed, and for her loving support and encouragement every step of the way. Faith. Hope. Love. Thanks, Mom.

TABLE OF CONTENTS

LIST OF FIGURES

1 Introduction

1.1 Introduction

Despite the important role that liquids play in nearly every aspect of life on earth, the microscopic structure of the liquid state of matter remains difficult to fully understand. Being both dense and highly disordered, liquids cannot be approximated using the models generally applied to either gases or crystals. Furthermore, the variety of intermolecular interactions and inhomogeneities in the transient local environment found in the liquid state involve a wide range of time and distance scales. This results in a broad light scattering spectrum with generally few distinct features making it difficult to unambiguously interpret the spectral information in terms of the underlying dynamics and structure of the liquid. Many questions remain despite significant efforts on the part of both experimentalists and theorists for over three decades[1-9] to improve our understanding of liquid structure and dynamics. Recent technical advances[9] in experimental, theoretical and computational tools are now bringing new life to the investigation and hold promise for further distinguishing the different contributions to the liquid spectrum.

Laser spectroscopy provides an effective probe of the microscopic dynamics of matter since an electric field incident on matter induces a polarization of the medium. In response to the induced polarization, the molecules will scatter light with frequency shifts, polarization, and intensity that are determined by the size, shape, and interactions of the molecules within the scattering volume. In liquids, molecular motions include collective thermal motions, intermolecular interactions (involving collisions, diffusive reorientations and oscillations), and intramolecular vibrations. These motions will scatter light into a spectrum with frequency shifts ranging over about 1000 cm^{-1}. This work focuses on that portion of the spectrum which covers frequencies between approximately 10 - 150 cm^{-1}, generally attributed to the translational and rotational motions of the molecules. Commonly termed the Rayleigh wing, it is the most complex and certainly the least understood portion of molecular liquid spectra. Understanding the intermolecular interactions that scatter light into this broad nearly featureless region of the spectrum is primary to the characterization of the liquid state.

Interaction-induced effects have been investigated experimentally by means of spontaneous light scattering (LS),[2] tunable-laser induced gain (TLIG) spectroscopy,[10] and stimulated gain spectroscopy (SGS)[11-13] in frequency domain, or by impulsive stimulated scattering (ISS),[14] and several optical-heterodyne-detected techniques: induced phase modulation (OHD-IPM),[15] optical Kerr effect (OHD-OKE),[16] and Raman-induced Kerr effect (OHD-RIKES)[17] in time domain. Each experimentally measured spectrum may be expressed in terms of a response function, $G(\omega)$ or $G(t)$, in frequency- or time-domain respectively, depicting motion dynamics of a liquid in question. These dynamics are most often discussed in terms of

diffusive reorientation (diffusive long time region), oscillations or libration within transient local potential wells (inertial components in a short time region), and collision-induced dynamics (intermediate time range).

This picture of the material response has been modeled as a collection of underdamped, critically damped, and overdamped harmonic oscillators[18] to account for a spectrum that is both oscillatory and dissipative in nature, and is widely used in analysis of time-domain experiments. The validity of this approach has recently been questioned, especially with respect to the origin of the intermediate dynamics.[19,20] One suggestion is that anharmonic couplings among the numerous microscopic oscillators play the critical role in the intermediate region, with a major difference being that there should exist a strong temperature dependence for the anharmonic model while the harmonic oscillator picture should be independent of temperature.[20] The classical harmonic oscillator (HO) representation was very recently improved upon with an inhomogeneously broadened quantum mechanical harmonic oscillator description of dynamics in molecular liquids.[21] While many of the conclusions of the new analysis are similar to those of the earlier HO model, the quantum mechanical oscillator model does a better job of recovering the behavior of the intermediate frequency intermolecular dynamics.[21]

This study examines interaction dynamics in simple molecular liquids using stimulated gain spectroscopy (SGS). This technique has a proven ability to differentiate various liquids with enough resolution to correlate qualitative differences in the liquid spectra with their molecular characteristics.[13,22] SGS was applied to carbon tetrachloride at ambient pressure and to benzene under high pressure. The results and interpretations are reported in this dissertation, as outlined below.

The purpose of Chapter 2 is to provide an understanding of SGS as it is applied to scattering in molecular liquids. It thus begins with a review of the physical processes that produce light scattering in liquids and how these relate to the structure of the resulting molecular spectra. The stimulated gain scattering process is then introduced through a discussion of induced polarization and the third-order nonlinear susceptibility. Stimulated gain scattering involves mixing two laser fields to coherently drive molecular normal mode oscillations at the laser difference frequency. When the difference frequency is in resonance with a normal mode oscillation, the stimulated gain signal is significantly enhanced. This technique offers several advantages for investigation of molecular liquids, including (a) an ability to do frequency-domain spectroscopy with a high frequency resolution over a large frequency range, (b) the ability to smoothly range from negative to positive frequency differences (including a zero frequency measurement) without interference from the unwanted strong central Rayleigh scattering which dominates conventional light scattering spectroscopy, and (c) since SGS probes only the imaginary part of the response function, $\chi^{(3)}$, it is more sensitive to small changes in the spectrum than spectroscopies that detect a scattering intensity that is proportional to the square of the response function, such as transient laser induced grating spectroscopy and impulsive stimulated scattering techniques. The time domain optically heterodyned optical Kerr effect (OHD-OKE) technique has been shown to be an exact Fourier analog of SGS and provides a valuable comparison for investigations of liquid dynamics.[23,24] However, since SGS has a laser bandwidth (0.02 cm^{-1}) that is very narrow compared to the width of the spectrum (~150 - 200 cm^{-1}) there is no need to deconvolve any instrumental lineshape from the spectrum, whereas

an accurate deconvolution of the laser pulse from the observed spectrum is necessary to obtain the correct response function using time domain OHD-OKE . These features make SGS an excellent tool for the study of molecular liquids. In view of its purpose to provide an understanding of SGS as it is applied to scattering in molecular liquids, Chapter 2 continues with a description of the SGS experimental set-up, apparatus and procedure in Section 2.4.

Chapter 3 will discuss the application of SGS to liquid carbon tetrachloride (CCl_4). Liquid CCl_4 was selected for investigation because its isotropic polarizability ensures that light scattered with polarization perpendicular to that of the incident light (depolarized scattering) arises from intermolecular interactions. With no strong orientational scattering to complicate the analysis of the spectrum, the depolarized scattering from CCl_4 will be due to translational collisions which can be described by a simple model for collision-induced (CI) scattering. Previous work in our lab[13,22] investigated the effects of molecular geometry on the depolarized spectra of several simple liquids, and at that time the measurement of a spectrum for carbon tetrachloride was attempted without success. A primary purpose of this work is to obtain and carefully characterize the spectrum for CCl_4 to enable valuable comparisons both to other generally spherical chlorinated methanes, as well as to molecules with very different geometries (linear CS_2 and planar C_6H_6), already in the existing SGS body of data.[22] Since CCl_4 offers a picture of CI dynamics unobscured by rotational motions, such comparisons can help resolve entangled translational and rotational interactions in less symmetric molecular liquids.

In order to compare different spectra there needs to be a quantitative framework for describing the data. In its ability to highlight relative differences in various spectra being compared, lineshape modeling provides a useful tool for understanding the intermolecular response of simple molecular liquids.[13,19,22,25-37] To interpret an experimental spectrum, the possible types of motion a molecule can undergo in a liquid environment are first considered, then curve-fits based on phenomenological models are applied to describe the frequency responses of those motions. While lineshape analysis can offer insight into the physical mechanisms producing scattering, it is important to keep in mind the challenge presented to unambiguously separate the various contributions to any liquid spectrum. Section 3.2 will detail the development of a lineshape model for CCl_4 and address both the success and the limitations of multimode curve-fitting as applied to the analysis of intermolecular scattering. The resultant fit to the spectrum for liquid CCl_4 is presented in Section 3.3. A two component model consisting of a narrow Lorentzian lineshape function with a damping rate, Γ, to represent diffusive relaxation and a weighted exponential function with a characteristic frequency, ω_c, corresponding to scattering from a collision-induced electronic repulsive force provides the best fit among the several models fitted to the CCl_4 liquid spectrum.

The last half of Chapter 3 first considers collision-induced scattering in other molecular liquids by comparing the SGS results in CCl_4 to results for the same model applied to the SGS spectra of chloroform, methylene chloride, carbon disulfide and benzene liquids. The liquid spectra, except for CCl_4, are also fit to a three component model that includes an inhomogeneously broadened Gaussian lineshape to fit librational dynamics.

Such comparisons will not only test the quality of the models used, but can also reveal correlations between molecular physical parameters and the observed spectra and thereby offer further insight into the mechanisms producing scattering.

Incorporating high pressure into the SGS experiment is the subject of Chapter 4. When density is increased in a liquid sample it is reasonable to expect changes in the intermolecular dynamics that will be apparent in the scattered light. Density effects have been studied by varying temperature at atmospheric pressure, but the spectra produced reflect both the change in kinetic energy of the molecules as well as the change in the average volume available for the motion of the molecule. Spontaneous light scattering experiments under pressure and over a wide range of temperatures have generally found that the characteristic frequencies of molecular liquid spectra exhibit a density dependence that is very different than the temperature dependence.[38-41] Experiments at high pressure reflect changes in the liquid density only, and thereby can separate the competing effects of temperature and density on the molecular motions[38] to provide additional information about interactions in a liquid.

Although incorporating high pressure into the SGS experiment is technically quite challenging, spectra can be obtained with a signal-to-noise ratio comparable to that from experiments at ambient pressure. Liquid benzene, with a stimulated gain signal that is nearly an order of magnitude larger than that of CCl_4, was selected to facilitate the initial experiment. The changes necessary to the basic SGS experimental set-up in order to apply high pressure to the experiment are detailed in Section 4.2. Section 4.3 discusses the technical challenges encountered, particularly with additional

stray scattered pump light and with polarization that is both rotated and scrambled by the sapphire windows used.

The depolarized stimulated gain spectrum for liquid benzene at 1 bar and 350 bars pressure is presented in Section 4.4 and the three component lineshape model developed in Chapter 3 will be applied to the spectral data. Although relatively few high pressure studies of the Rayleigh wing of molecular liquids exist, these will be reviewed and compared to the SGS results in benzene.

A nice feature of the SGS experiment is that it can easily be altered to obtain either a broad depolarized Rayleigh-wing spectrum or a spectrum dominated by a narrow bandwidth Brillouin (polarized) component by orienting the probe polarization to be perpendicular or parallel to the pump polarization. In Section 4.5 results of a stimulated Brillouin gain experiment at 1, 540, and 880 bars pressure will be presented.

The results and conclusions of this investigation of intermolecular dynamics in liquids using stimulated gain spectroscopy will be summarized in Chapter 5.

1.2 References

1. H. B. Levine and G. Birnbaum, "Collision-induced light scattering," Phys. Rev. Lett. **20**, 439 (1968).

2. J. P. McTague, P. A. Fluery and D. B. DuPre, "Intermolecular light scattering in liquids," Phys. Rev. **188**, 303 (1969).

3. J. A. Bucaro and T. A. Litovitz, "Rayleigh scattering: Collisional motions in liquids," J. Chem. Phys. **54**, 3846 (1971).

4. H. E. Howard-Lock and R. S. Taylor, "Induced anisotropy and light scattering in liquids. II," Can. J. Phys. **52**, 2436 (1974).

5. W. M. Gelbart, "Review of calculations and analyses of available measurements on depolarized scattering of light by simple fluids," Adv. Chem. Phys. **26**, 1 (1974).

6. B. J. Berne and R. Pecora, *Dynamic Light Scattering* (John Wiley and Sons, New York, 1975).

7. G. Birnbaum, ed., *Phenomena Induced by Intermolecular Interactions*, NATO ASI Series B **127** (Plenum, New York, 1985).

8. D. Steele and J. Yarwood, ed., *Spectroscopy and Relaxation of Molecular Liquids*, Studies in Physical and Theoretical Chemistry, Vol. **74** (Elsevier Science Publishers, Amsterdam, 1991).

9. J. T. Fourkas, ed., *Liquid Dynamics*, ACS Symposium Series **820** (American Chemical Society, Oxford University Press, 2002).

10. R. Trebino, C. E. Barker, and A. E. Siegman, "Tunable-laser-induced gratings for the measurement of ultrafast phenomena," IEEE J. Quantum Electron. **22**, 1413 (1986).

11. M. A. Scarparo, J. H. Lee, and J. J. Song, "Near-zero-frequency stimulated Raman gain spectroscopy in CS_2," Opt. Lett. **6**, 193 (1981).

12. J. S. Friedman, M. C. Lee and C. Y. She, "Depolarized stimulated gain spectra of liquid CS_2 and benzene at room temperature," Chem. Phys. Lett. **186**, 161 (1991).

13. J. S. Friedman and C. Y. She, "The effects of molecular geometry on the depolarized stimulated gain spectra of simple liquids," J. Chem. Phys. **99**, 4960 (1993).

14. K. A. Nelson, D. R. Lutz, M. D. Fayer, and L. Madison, "Laser-induced phonon spectroscopy. Optical generation of ultrasonic waves and investigation of electronic excited-state interactions in solids," Phys. Rev. B **24**, 3261 (1981).

15. T. Hattori, A. Tersaki, T. Kobayashi, T. Wada, A. Yamada, and H. Sasabe, "Optical-heterodyne-detected induced phase modulation for the study of femtosecond molecular dynamics," J. Chem. Phys. **95**, 937 (1991).

16. E. P. Ippen and C. V. Shank, "Picosecond response of a high-repetition-rate CS_2 optical Kerr gate," Appl. Phys. Lett. **26**, 93 (1985).

17. G. L. Eesley, M. D. Levenson, and W. M. Tolles, "Optically heterodyned coherent Raman spectroscopy," IEEE J. Quant. Electron. **14**, 45 (1978).

18. D. McMorrow and W. T. Lotshaw, "Dephasing and relaxation in coherently excited ensembles of intermolecular oscillators," Chem. Phys. Lett. **178**, 69 (1991).

19. S. Kinoshita, Y. Kai, and Y. Watanabe, "Origin of initial rise process of ultrafast exponential response in liquids," Chem. Phys. Lett. **301**, 183 (1999).

20. S. Kinoshita, Y. Kai, Y. Watanabe and J. Watanabe, "Femtosecond optical Kerr effect measurement on initial process of liquid dynamics," J. Lumin. **87-89**, 706 (2000).

21. D. McMorrow, N. Thantu, V. Kleiman J. S. Melinger, and W. T. Lotshaw, "Analysis of intermolecular coordinate contributions to third-order ultrafast spectroscopy of liquids in the harmonic oscillator limit," J. Phys. Chem. A, **105**, 7960 (2001).

22. J. S. Friedman, Ph.D. dissertation, "Stimulated Rayleigh-Brillouin spectroscopy for studying low frequency dynamics in simple liquids," Colorado State University, (1992).

23. P. Cong, J. D. Simon and C. Y. She, "Intermolecular spectral densities of liquids: A quantitative comparison of time-domain and frequency-domain techniques," J. Chem . Phys. **104**, 962 (1996).

24. D. McMorrow and W. T. Lotshaw, "The frequency response of condensed-phase media to femtosecond optical pulses: spectral-filter effects," Chem. Phys. Lett. **174**, 85 (1990).

25. H. L. Gabelnick and H. L. Strauss, "Low-frequency motions in liquid carbon tetrachloride. II. The Raman spectrum," J. Chem. Phys. **49**, 2334 (1968).

26. W.S. Gornall, H. E. Howard-Lock, and B. P. Stoicheff, "Induced anisotropy and light scattering in liquids," Phys. Rev. A, **1**, 1288 (1970).

27. V. Volterra, J. A. Bucaro and T. A. Litovitz, "Molecular motion and light scattering in liquids," Ber. Bunsenges. Phys. Chem. **75**, 309 (1971).

28. H. E. Howard-Lock and R. S. Taylor, "Induced anisotropy and light scattering in liquids. II," Can. J. Phys. **52**, 2436 (1974).

29. R. A. Stuckart, C. J. Montrose and T. A. Litovitz, "Comparison of interaction induced light scattering and infrared absorption in liquids," Faraday Symp. Chem. Soc. **11**, 94 (1977).

30. M. Cho, S. J. Rosenthal, N. F. Scherer, L. D. Ziegler, and G. R. Fleming, "Ultrafast solvent dynamics: connection between time resolved fluorescence and optical Kerr measurements," J. Chem. Phys. **96**, 5033, (1992).

31. M. Cho, M. Du, N. F. Scherer, G. R. Fleming, and S. Mukamel, "Off-resonant transient birefringence in liquids," J. Chem. Phys. **99**, 2410 (1993).

32. H. Deuel, P. Cong, and J. Simon, "Probing intermolecular dynamics in liquids by femtosecond optical Kerr effect spectroscopy: Effects of molecular symmetry," J. Phys. Chem. **98**, 12600 (1994).

33. P. Vöhringer, C. C. Arnett, R. A. Westervelt, M. J. Feldstein, and N. F. Scherer, "Optical dephasing on femtosecond time scales: Direct measurement and calculation from solvent spectral densities," J. Chem. Phys. **102**, 4027 (1995).

34. Y. J. Chang and E. W. Castner, Jr., "Intermolecular dynamics of substituted benzene and cyclohexane liquids, studied by femtosecond nonlinear-optical polarization spectroscopy," J. Phys. Chem., **100**, 3330 (1996).

35. M. Neelakandan, D. Pant, E. L. Quitevis, "Structure and intermolecular dynamics of liquids: Femtosecond optical Kerr effect measurements in nonpolar fluorinated benzenes," J. Phys. Chem. A, **101**, 2936 (1997).

36. N. A. Smith and S. R. Meech, "Ultrafast dynamics of polar monosubstituted benzene liquids studied by the femtosecond optical Kerr effect," J. Phys. Chem. A, **104**, 4223 (2000).

37. B. -R. Hyun, S. V. Dzyuba, R. A. Bartsch, and E. L. Quitevis, "Intermolecular dynamics of room-temperature ionic liquids: Femtosecond optical Kerr effect measurements on 1-akyl-3-methylimidazolium bis(trifluoromethyl)sulfonyl," J. Phys. Chem., **106**, 7579 (2002).

38. J. Jonas, "Pressure--An essential experimental variable in spectroscopic studies of liquids," in *Phenomena Induced by Intermolecular Interactions*, NATO ASI Series B 127 (Plenum, New York), 525 (1985).

39. X. Song, J. Jonas, and T. W. Zerda, "Total intensity measurements of depolarized Rayleigh scattering from linear molecules," J. Phys. Chem. **93**, 6887 (1989).

40. B. Hegemann and J. Jonas, "Temperature study of Rayleigh and Raman line-shapes in liquid carbonyl sulfide," J. Phys. Chem. **88**, 5851 (1984).

41. B. Hegemann, K. H. Baker, and J. Jonas, "Temperature and pressure effects on the collision-induced depolarized Rayleigh line-shapes of liquid carbon disulfide," J. Chem. Phys. **80**, 570 (1984);
B. Hegemann and J. Jonas, "Separation of temperature and density effects on collision-induced Rayleigh and Raman line shapes of liquid carbon disulfide," J. Chem. Phys. **82**, 2845 (1985).

2 Stimulated Gain Spectroscopy in Molecular Liquids

2.1 Introduction

The purpose of this chapter is to provide a basic understanding of stimulated gain spectroscopy (SGS) as applied to molecular liquids. To this end, Section 2.2 begins with an overview of light scattering described in terms of the various fluctuations in density and orientation produced by the motion of the molecules in a liquid state. These molecular motions are then identified with different components comprising the structure and form of the resulting molecular spectra.

The theory underlying stimulated gain scattering is presented in Section 2.3 by first considering the simpler case of linear susceptibility and the induced polarization responsible for spontaneous scattering. A brief discussion of how coherent, stimulated scattering processes differ from spontaneous ones is followed with a qualitative description of SGS. A semi-classical approach is then taken to derive expressions for the third order susceptibility and polarization of interest for SGS. These are used to understand how propagation of the laser field through a nonlinearly polarized

medium produces stimulated gain and to derive a gain coefficient for the process.

To complete a description of stimulated gain spectroscopy as applied to molecular liquids, Section 2.4 describes the experimental set-up and procedures used in the lab.

2.2 Density Fluctuations and Molecular Liquid Spectra

Light traveling through any medium is scattered by variations in the dielectric constant. In a liquid, random thermal motions and intermolecular interactions produce time-dependent fluctuations in the density and orientation of molecules thus varying the dielectric constant. The frequency of the light scattered in passing through a liquid produces a spectrum which reflects the time dependence of these fluctuations. In order to understand the processes which produce molecular liquid spectra, it is useful to consider the variety of density fluctuations present in liquids, on both macroscopic and microscopic scales.

Density fluctuations that occur on a macroscopic scale can be connected to the hydrodynamic properties of the liquid as a whole and can be monitored by thermodynamic parameters such as pressure and temperature. Work by Leon Brillouin[1] describing light scattering in isotropic media in terms of frequency distribution accurately predicted a frequency shifted doublet centered around the incident light frequency due to thermally excited density fluctuations. When the first light scattering experiments in liquids were conducted,[2] the Brillouin doublet was observed as well as a strong

unshifted central line. Both of these spectral features can be understood in terms of thermodynamic fluctuations in density.[3,4] By expressing the thermodynamic fluctuations in density, $\Delta\rho$, as due to entropy and pressure fluctuations, ΔS and ΔP, respectively, we can describe two types of light scattering independently:

$$\Delta\rho = (\partial\rho / \partial P)\Big|_S \Delta P + (\partial\rho / \partial S)\Big|_P \Delta S \qquad [2.1]$$

The first term describes density fluctuations produced by propagating fluctuations of pressure at constant entropy. These pressure fluctuations can be thought of as sound waves propagating through the liquid and scattering light at Doppler-shifted frequencies. The doublet produced is identified as Brillouin scattering, and exhibits a frequency shift, ω_B, with respect to the incident laser frequency which is proportional to both the sound velocity, v, in the medium and the propagation wave vector, k, of the density fluctuation such that

$$\omega_B = \pm vk \, . \qquad [2.2]$$

The magnitude of k is defined by the Bragg condition:

$$k = (4\pi/\lambda)\sin(\theta/2) \qquad [2.3]$$

with θ being the scattering angle and λ is the wavelength of the incident light.

The density fluctuations described by the second term of Eqn. [2.1] are produced by non-propagating fluctuations of entropy at constant pressure and give rise to the observed central, or Rayleigh, line. Although not shifted in

frequency, the light scattered from entropy fluctuations will be broadened by the diffusion of energy through the liquid. Scattering from both pressure and entropy fluctuations is isotropic, resulting in a signal with the same polarization as the incident light. Generally referred to together as Rayleigh-Brillouin scattering, these reflect large scale collective motions which are relatively slowly changing and thus contribute intensity to the very low frequency (MHz to 10GHz) region of spectrum. For historical reasons, the correct name for Rayleigh scattering is under dispute. According to She,[5] the term Cabannes-Brillouin scattering is preferred.

In addition to thermodynamic density fluctuations in the collective ensemble, there are local fluctuations in the dielectric constant due to intermolecular interactions in the form of translational and rotational collisions between molecules. These collisions will anisotropically scatter light. Translational collisions occur when atoms or molecules come into close enough contact for electron clouds to interact and be redistributed. In the simplest case, consider an atomic liquid which, having no rotational or vibrational degrees of freedom, might be expected to scatter light with the same polarization as the incident light. Collisions, however, can break the former symmetry and change the polarizability for the duration of the interaction. This leads to depolarized scattering for otherwise isotropic scatterers.

In liquids of anisotropic molecules, the orientation of a molecule will vary as it rotates either randomly or in response to an applied field. This rotation causes neighboring molecules to rearrange in response to the new orientation of the first molecule and the reorientation then diffuses through the liquid as it relaxes to equilibrium. Rates for diffusive Debye reorientation

depend on the geometry of the molecules involved, as will be discussed in some detail in Chapter 3. In addition to diffusive reorientations, anisotropic molecules may experience displacement or rotational oscillation (libration) within a potential well formed by its nearest neighbors. As in solids, these neighbors provide a restoring force on the molecule. Within a liquid, however, this restoring force is transient in that neighboring molecules will attempt to readjust their own positions and orientations to accommodate the rotation or displacement. The transient potential well formed by near neighbors is referred to as a solvent cage[6] within which a molecule will oscillate until the cage readjusts to a new equilibrium thereby damping out the oscillations.

The spectrum that results from scattering due to intermolecular interactions (i.e., collisions and hindered rotations) is inhomogeneously broadened, consistent with the wide distribution of molecular environments present locally in a liquid at a given instant in time. Since for many molecular liquids the time scales for the librational dynamics overlap with those for translational collisions, these two are often grouped together under the single designation of "collision-induced" (CI) scattering. The time required for the relaxation of the induced polarizability anisotropy which produces CI scattering is usually much less than the time necessary for atoms or molecules to diffusionally reorient.[7-9] In many cases, this makes it possible to differentiate the spectral component due to diffusive reorientation from those due to other collisions. Taken together, these intermolecular interactions comprise the Rayleigh-wing of the molecular liquid spectrum, covering approximately 1-100 cm^{-1}, with the diffusive reorientations generally in the region below 10 cm^{-1} and the other CI dynamics contributing to frequencies

higher than 10 cm^{-1}. Understanding the structure of this broad region in liquid spectra remains an area of difficulty for both light scattering experimentalists and molecular dynamics theorists, and is the focus of the depolarized SGS study presented in this work.

Finally, the microscopic dynamics occurring in liquids also include intramolecular vibrations. A given molecule will have one or more normal modes of vibration from which light is scattered into the high frequency portion of the spectrum, usually at 100-1000s of wavenumbers. Light scattered from these modes is termed vibrational Raman scattering. Vibrational Raman scattering has provided a rich field of study, yielding a great deal of information on the structure of molecules. Earlier investigations in this lab have also included measurement of supersonic flow velocities using vibrational Raman techniques, and temperature and density measurements in the supersonic flow with rotational-vibrational Raman information.[10] While much can be learned in this high frequency region of the spectrum, it is the scattering resulting from molecular interactions in the Rayleigh-wing that is of primary concern in this study.

In an idealized situation of a single molecule or an extremely dilute gas, scattering from these molecular motions would appear in a spectrum as quantized modes for rotational or vibrational excitations. As density is increased, these modes are broadened or smeared out due to molecular interactions as discussed above, resulting in a spectrum for a molecular liquid represented schematically in Fig. 2.1. As can be seen in this figure, stimulated gain spectroscopy (SGS) is able to discriminate against Rayleigh scattering and effectively enhance the weaker structure found in the wings. SGS measures the change in scattered intensity as a function of the frequency

difference between a pump laser and a probe laser as the frequency of one of the laser is varied. When the laser frequencies are equal, competing gain and loss processes cancel one another so that there is neither a net gain nor loss on the probe beam. As a result, SGS is able to smoothly range from negative to positive frequency differences, including a zero frequency measurement without interference from Rayleigh scattered light, efficiently measuring the complete intermolecular spectrum. This provides SGS with an excellent advantage for the study of molecular liquids.

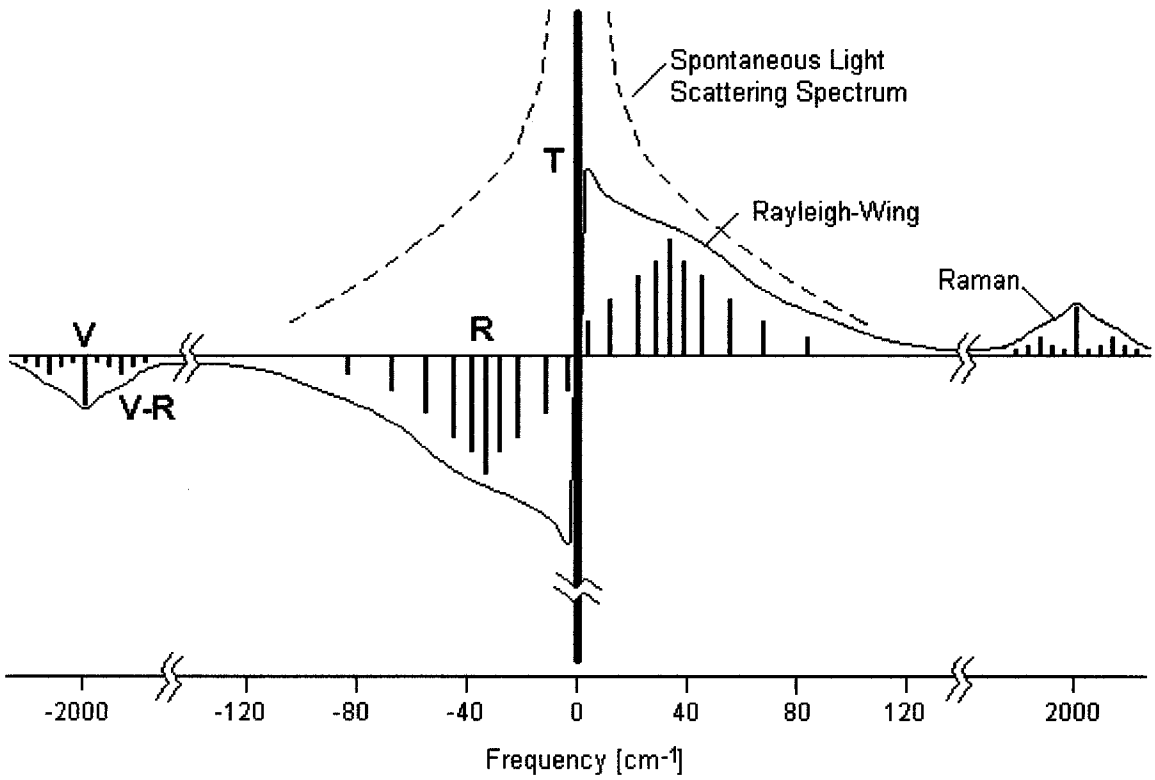

Figure 2.1 Representation of a molecular liquid spectra showing schematically the modes for translational (T), quantized rotational (R), and quantized vibrational (V) molecular motions and the broadened spectrum. The dashed line represents the spontaneous light scattering spectrum and the solid line represents the spectrum obtained with stimulated gain spectroscopy.

2.3 The Theory of Stimulated Gain in Liquids

A variety of laser techniques for both time- and frequency-domain exist for the study of molecular spectra,[11-22] several of which will be discussed and compared to stimulated gain spectroscopy (SGS) in Chapter 3. SGS is a coherent technique for frequency-domain spectroscopy which offers several advantages over the more widely known spontaneous light scattering (LS) spectroscopy for the study of molecular liquids. While, in principle, yielding the same information as spontaneous scattering, stimulated techniques do so with signal levels nine orders of magnitude larger.[23] In SGS, the combined laser fields at two different frequencies drive molecular oscillations at the frequency difference. The motions of the molecules then modulate the dielectric constant, resulting in fluctuations that can change the frequency, intensity, or polarization of the incident laser beam to yield a signal containing information about the molecular motions. Like other coherent Raman techniques, SGS is the result of a nonlinear optical process which can be considered in two steps. When the intense light of a laser beam (pump) travels through matter, it induces a nonlinear electric polarization in a process that is governed by the susceptibility of the material. This induced polarization then causes a modulation of the (probe) optical fields. The theory underlying stimulated gain scattering presented here will follow this two step process. A discussion of the origins of the nonlinear optical response in liquids starts with the simpler case of linear susceptibility and induced polarization responsible for spontaneous scattering before moving on to the third order nonlinear susceptibility, $\chi^{(3)}$, responsible for stimulated gain. A classical harmonic oscillator model is used to describe motions of the

molecules in order to determine how these motions modulate the polarization induced by the incident electric fields. Expressions for $\chi^{(3)}$ and the polarization of interest for SGS are derived. Next, the propagation of an optical electric field through this nonlinearly polarized medium and the resultant stimulated gain signal will be considered. An expression for the gain coefficient will be derived and related to experimentally measurable quantities. Since susceptibility is physically related to the microscopic structure of a medium, a rigorous evaluation is properly the domain of quantum mechanics. There are several excellent texts specific to nonlinear optics which treat coherent Raman scattering quantum mechanically.[23-25] The semi-classical approach taken here however has proven useful in its ability to offer physical insight into the light-matter interaction and provide a simple means of understanding stimulated gain scattering.

Induced Polarization

In the formulation of the electromagnetic theory of light, the dielectric polarization of a material is approximately linearly proportional to the amplitude of the applied electric field,

$$\mathbf{P} = N\varepsilon_0\chi \cdot \mathbf{E} = N\alpha \cdot \mathbf{E} \qquad [2.4]$$

where the susceptibility tensor, χ, is the frequency-domain polarization response function which fully characterizes the optical properties of the medium. In this equation, N is the number of molecules per unit volume, ε_0 is the permittivity of free space and **E** is the applied electric field. The quantity $\varepsilon_0\chi$ is also referred to as the polarizability, α, which for small fields,

is independent of E. High intensity laser beams belong to the realm of nonlinear electromagnetic phenomena so that the susceptibility is no longer independent of the electric field and can be expanded as

$$\chi^{NL} = \chi^{(1)} + \chi^{(2)}E + \chi^{(3)}E^2 + \cdots \qquad [2.5]$$

and the polarization in Eqn. [2.4] becomes

$$P^{NL} = N\varepsilon_o\{\chi^{(1)}(\omega)E(\omega) + \chi^{(2)}(\omega=\omega_i+\omega_j)E(\omega_i)E(\omega_j) + \chi^{(3)}(\omega=\omega_i+\omega_j+\omega_k)E(\omega_i)E(\omega_j)E(\omega_k) + \cdots\}. \qquad [2.6]$$

The linear and nonlinear susceptibilities describe various scattering phenomena. The linear, $\chi^{(1)}$, term is responsible for quasi-elastic spontaneous light scattering. Its real part is related to the index of refraction and its imaginary part is related to the absorption coefficient of the medium. In isotropic media, such as the liquids studied here, the second-order, $\chi^{(2)}$, term vanishes due to inversion symmetry. The lowest order nonlinear effects arise from $\chi^{(3)}$ and include third-harmonic generation and inelastic stimulated gain scattering.

In any dielectric material the effect of an electric field is to induce a polarization according to Eqn. [2.4]. Usually, fields at optical frequencies oscillate too fast for the heavy atomic nuclei to follow and affect the electrons only. However, with the mixing of two input fields that occurs with SGS and other coherent Raman techniques, the difference frequency of the two fields is slow enough for the heavier nuclei to follow. Consider a driven harmonic oscillator model for a molecule such that the electronic forces binding the

atoms together are treated as springs. This then allows the nuclei to vibrate at a characteristic frequency, Ω, thereby modulating the induced polarization. If we treat q as a generalized coordinate which can represent vibrations, rotations or displacement of a molecule, then the polarizability of a single molecule can be written as

$$\alpha(t) = \alpha_o + (\partial\alpha / \partial q)\, q(t)\,, \qquad [2.7]$$

the sum of a static term, α_o, representing the average intrinsic molecular polarizability and a dynamic quantity, $(\partial\alpha / \partial q)\, q(t)$, that represents the fluctuations in polarizability due to intermolecular interactions. Intramolecular motions are also represented by the time-dependent term, but occur at frequencies that are too high to contribute to the Rayleigh-wing scattering which is of interest here.

If we consider the case where q(t) is independent of the applied electric field, the dielectric polarization of a molecular liquid in an optical field of amplitude E_o and frequency ω can be written[23]

$$\begin{aligned} \mathbf{P}(t) &= N\alpha(t)\, E_o e^{-i\omega t} \\ &= N\alpha_o E_o e^{-i\omega t} + N(\partial\alpha/\partial q) q E_o \{e^{-i(\omega+\Omega)t} + e^{-i(\omega-\Omega)t}\}, \end{aligned} \qquad [2.8]$$

where the last terms reflect interactions of the incident field with a molecular normal mode of frequency Ω. This induced polarization, comprised of terms which oscillate at ω and $\omega \pm \Omega$, can spontaneously emit light leading to light scattering. In terms of an energy level diagram, Fig 2.2 (a), the majority of spontaneous emission is quasi-elastic Rayleigh scattering emitting photons

with a center frequency unshifted from the incident laser light or Doppler broadened due to the translational motion of the molecule. This interaction is described by the permanent molecular polarizability, α_0, contribution of Eqn. [2.8] and results in the strong central line seen in a LS frequency spectrum, Fig. 2.2(b). There is also a much smaller probability that an incident photon interacts with the molecule in such a way that energy is exchanged with the molecule and a photon is emitted at a shifted frequency, $\omega \pm \Omega$. Such interactions with molecular modes produce Raman scattering and are the time dependent induced polarizability contributions of the second term in Eqn. [2.8]. When the emitted photon has less energy than the incident one, the internal energy of the scattering medium is increased and it is referred to as Stokes scattering. Anti-Stokes scattering removes energy from excited molecular modes and emits photons with higher energy than the incident photon. Both the Stokes and Anti-Stokes processes are also shown in Fig. 2.2. In the case of liquids, the molecular modes are primarily rotational modes hindered by interactions between molecules producing Rayleigh-wing scattering.

In contrast to spontaneous scattering, stimulated gain scattering involves mixing two laser fields to coherently drive molecular normal mode oscillations at the laser difference frequency. When the difference frequency is in resonance with a normal mode oscillation, the stimulated gain signal is significantly stronger. Figure 2.3 highlights schematically several of these differences. Two lasers are used to provide an intense pump beam at frequency ω_l and a weaker probe beam at ω_s, one of which is tunable in frequency. In terms of an energy level diagram, Fig. 2.3(a), when the

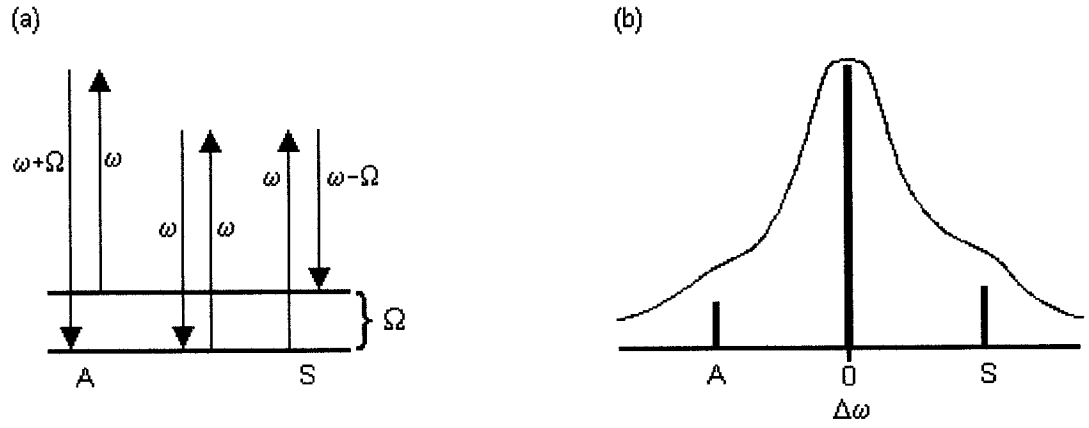

Figure 2.2 Energy level diagram (a) and representation of spectrum for intensity of spontaneous light scattering (b). The unshifted Rayleigh-Brillouin scattering dominates the spectrum. The Stokes (S) and Anti-Stokes (A) components shown in (b) have been exaggerated for illustration purposes.

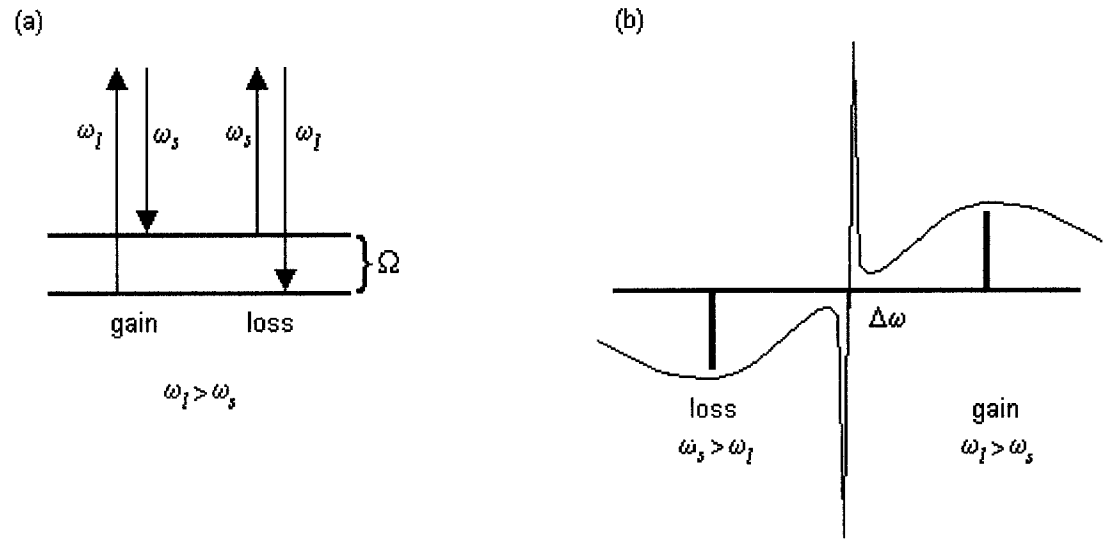

Figure 2.3 Energy level diagram and representation of spectrum for stimulated gain spectroscopy. The energy level diagram (a) is shown for $\omega_l > \omega_s$ where ω_l is the pump laser frequency, ω_s is the probe frequency and Ω is a molecular normal mode frequency, and $\Delta\omega = (\omega_l - \omega_s) \equiv \Omega$. Here the gain process dominates, due to the larger population in the ground state as compared to the excited state at thermal equilibrium. The resultant SGS spectra is shown in (b). In liquids, there exists a continuous distribution of normal modes leading to a gain/loss spectrum as shown. The sharp, polarized Brillouin components shown near $\Delta\omega = 0$ are eliminated in depolarized gain spectra, i.e., when the polarization of the pump and probe beams are orthogonal. Note that when $\omega_l = \omega_s$ the competing gain and loss processes cancel one another to yield a zero intensity in the SGS signal.

difference between the two laser frequencies, $\Delta\omega$, is equal to a characteristic frequency of the molecule two processes occur concurrently. One process involves the destruction of a high frequency photon, the energy of which is divided between driving a molecular normal mode and the emission of a lower frequency photon, so that the lower frequency laser beam gains energy. The opposite process is also occurring, where a high frequency photon is created from the energy of the normal mode and the destruction of a low frequency photon. In each case, photons are either added to or taken from the probe beam whose gain or loss in intensity is then monitored as a function of the frequency difference between the lasers. As a result of competing gain and loss processes, when the pump and probe laser frequencies are equal, the gain and loss completely cancel one another. This eliminates the strong center line that results from thermal scattering in the spontaneous LS spectra, Fig. 2.3b.

These differences lead to qualitative differences in the spectra obtained with the two techniques. With the strong center peak suppressed, the weaker wing structure is effectively enhanced in SGS experiments, as can be seen in Figures 2.4 and 2.5. The spectra for an LS experiment[26,27] in liquid CS_2 is reproduced in Fig. 2.4 for both polarized and depolarized scattering, with a linewidth that is spectrometer limited at about 0.4 cm^{-1}. The polarized LS spectrum results from light scattered with a polarization that is the same as that of the incident light. As depicted in Fig. 2.4, it consists of unresolved Rayleigh and Brillouin scattering and a wing due to the intermolecular interactions. The depolarized spectrum, shown at ten times intensity, consists of light scattered with polarization perpendicular to the incident light, and eliminates the polarized Rayleigh-Brillouin scattering. In order to analyze the

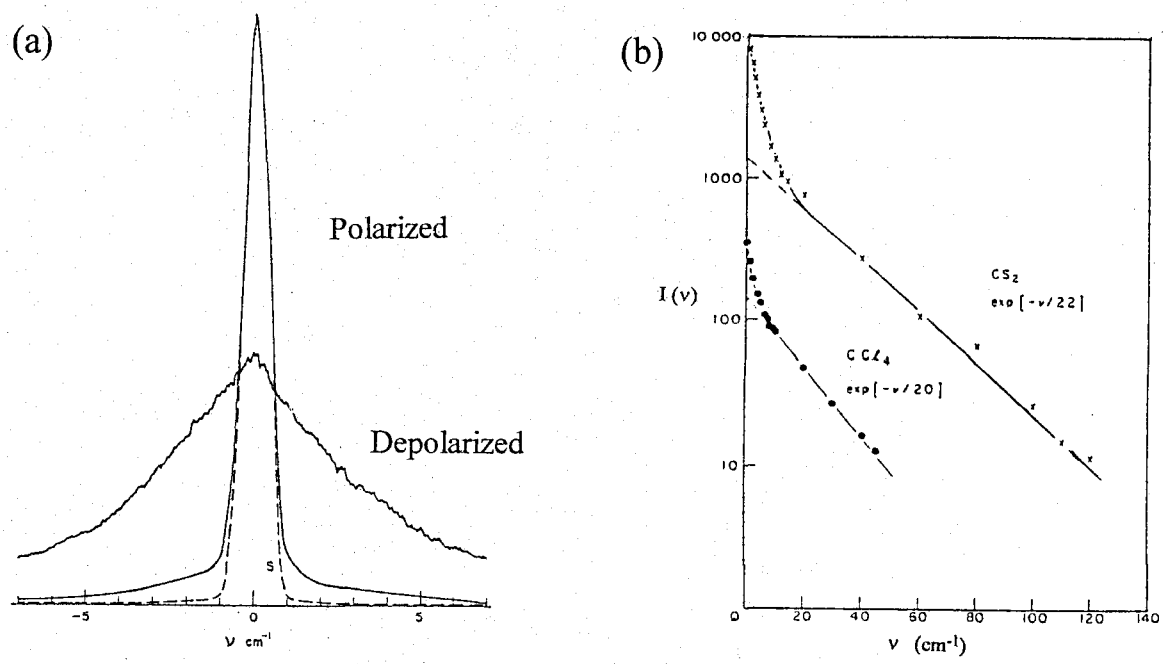

Figure 2.4 (a) Spontaneous light scattering spectra for liquid CS_2.[26] The polarized LS spectrum consists of unresolved Rayleigh and Brillouin lines and a wing due to intermolecular interactions. The dashed line indicates the spectrometer resolution of 0.4 cm^{-1}. The depolarized spectrum intensity has been enhanced by a factor of 10. (b) The same depolarized CS_2 data is replotted on a semilog scale with a larger frequency range. Also shown is the depolarized spontaneous LS data for CCl_4.[27]

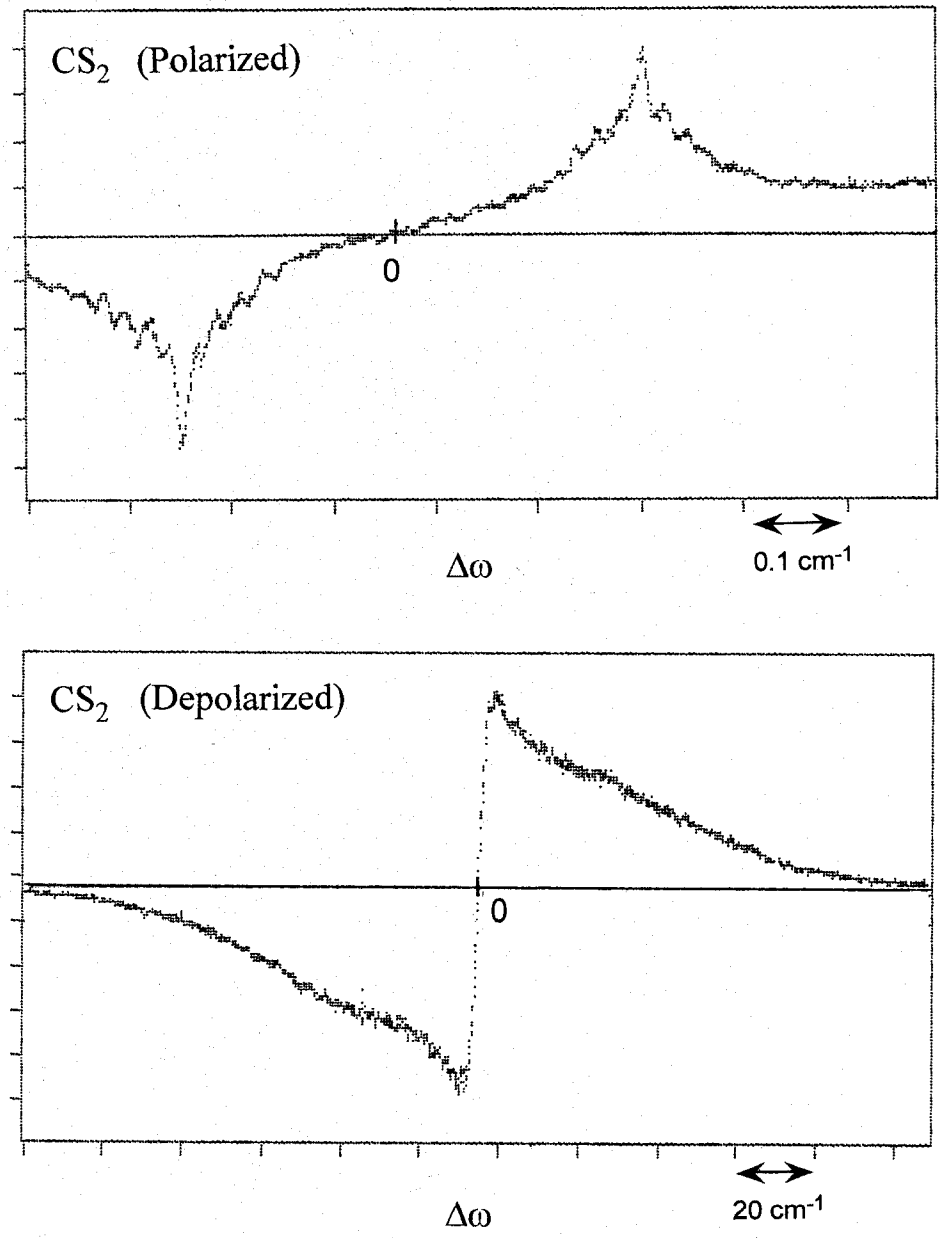

Figure 2.5 Stimulated gain scattering spectra for liquid CS_2. (a) The polarized SGS spectrum, covering 30 GHz, clearly resolves the Brillouin doublet. Resolution is limited by the pump laser linewidth at 500 MHz. (b) The depolarized SGS spectrum effectively enhances the relatively weak Rayleigh wing structure when compared to the spontaneous scattering spectrum.

structure of the depolarized data, it is replotted on a semilog scale.[27] In this representation, diffusive reorientational dynamics are apparent below 20 cm^{-1} and a few data points at higher frequencies are fitted with an exponential curve. The raw data itself is quite noisy with no structure observable. By contrast, the SGS spectra in Fig. 2.5(a) and (b) are presented as the full data rather than as a fit. Again both polarized and depolarized data are presented, which for a SGS experiment corresponds to a probe laser polarization parallel (polarized) or orthogonal (depolarized) to the pump laser polarization. The resolution is laser linewidth limited at 500MHz (0.017 cm^{-1}). Brillouin scattering is the focus of the polarized data, so laser frequency was scanned only 30 GHz, covering a range of $\Delta\omega = (\omega_s - \omega_l) = \pm 0.5$ cm^{-1}. The depolarized spectrum ranges over $\Delta\omega = \pm 120$ cm^{-1}, similar to the LS semilog plot. The signal to noise for this single scan is excellent at more than 10:1 and the weaker Rayleigh wing structure is clearly discernible.

Every coherent process involves at least two laser fields. In stimulated gain spectroscopy, the beating of two laser fields drives a molecular coordinate, q(t), with an amplitude proportional to the product of the two laser fields. If driven resonantly, whenever $\Delta\omega = (\omega_s - \omega_l) = \Omega$, a large amplitude results. The magnitude of the molecular coordinate can be described with the equation of motion for a damped harmonic oscillator

$$\zeta\left(\partial^2 q/\partial t^2 + \gamma\,\partial q/\partial t + \Omega^2 q\right) = F_q, \qquad [2.9]$$

where ζ is a generalized mass, (ie., equal to mass for translations or vibrations, but able to represent the moment of inertia for rotations), γ is the damping constant (such that the damping force, $\gamma\,\partial q/\partial t$, accounts for

spontaneous relaxation), and F_q is the external driving force. An expression for F_q can be obtained by considering a molecule with no intrinsic, permanent dipole moment but which has an induced dipole moment. The interaction energy for an induced dipole in an applied field is

$$W(t) = -1/2\ \mathbf{p} \cdot \mathbf{E} = -1/2\ (\partial\alpha/\partial q)q(t)|\mathbf{E}|^2 . \qquad [2.10]$$

The optical electric field can be written as the total electric field, **E**, due to the laser pump field, $\mathbf{E}_l$, and the laser probe field, $\mathbf{E}_s$,

$$\mathbf{E} = \mathbf{E}_l + \mathbf{E}_s = 1/2\{E_{ol}\exp(-i\omega_l t) + E_{os}\exp(-i\omega_s t) + c.c.\} \qquad [2.11]$$

where *c.c.* denotes complex conjugate terms. Thus the force on the induced dipole moment is then given by

$$F_q = -\frac{\partial W}{\partial q} = \frac{1}{4}\left(\frac{\partial\alpha}{\partial q}\right)\left\{E_{ol}E_{os}^{*}\exp\left[-i\left(\omega_s - \omega_l\right)\right] + c.c.\right\} \qquad [2.12]$$

where, in order to couple to the oscillation frequency, Ω, of the molecule, only the difference frequency terms (ω_s-ω_l) are kept. Eqn. [2.9] can now be solved to yield a solution of the form

$$q(t) = 1/2\ [q_o \exp(-i\omega t) + c.c.] \qquad [2.13]$$

with

$$q_o = \frac{1}{4\zeta\Omega}\left(\frac{\partial\alpha}{\partial q}\right)\left\{\frac{E_{ol}E_{os}^{*}}{\left[\Omega-(\omega_s-\omega_l)\right]-\frac{i\gamma}{2}}\right\}. \qquad [2.14]$$

The amplitude of the driving fields, E_{os} and E_{ol}, and the match between the driving difference frequency (ω_s- ω_l) and the molecular frequency, Ω, determine the amplitude of the molecular coordinate. It is this driven molecular coordinate that is responsible for the time-dependent change in the polarizability of the molecular liquid, which in turn induces a driven nonlinear polarization

$$P^{NL}(t) = N\,(\partial\alpha / \partial q)\, q(t)\; E(t)\,. \qquad [2.15]$$

Substituting Eqns. [2.11] and [2.13] into [2.15] yields

$$P^{NL}(t) = \frac{N}{4}\left(\frac{\partial\alpha}{\partial q}\right)\left\{q_o^{*}E_{os}\exp\left[-i(2\omega_s-\omega_l)t\right] + q_oE_{os}\exp\left[-i\omega_l t\right] + q_oE_{ol}\exp\left[-i(2\omega_l-\omega_s)t\right] + q_o^{*}E_{ol}\exp\left[-i\omega_s t\right] + c.c\right\}. \qquad [2.16]$$

The induced polarization thus results in radiated fields at four different frequencies which taken from the first term to the fourth, can be identified with coherent Stokes Raman scattering (CSRS), inverse Raman scattering, (IRS), coherent anti-Stokes scattering (CARS), and stimulated Raman gain scattering (SRGS), respectively. While Herring[10] has solved the expression for $P^{NL}(t)$ fully for each of different frequency terms, the polarization of interest here is the stimulated gain term. Substituting the expressions for q_o

and q_o^* into the last term of Eqn. [2.16], we find the amplitude for the polarization of interest of SGS in molecular liquids to be

$$P_{os}(\omega) = \frac{N}{8\zeta\Omega}\left(\frac{\partial\alpha}{\partial q}\right)^2 \frac{|E_{ol}|^2 E_{os}}{[\Omega-(\omega_s-\omega_l)]+\frac{i\gamma}{2}} \cdot \qquad [2.17]$$

Note that all the quantities in P_{os} are experimentally measurable with the exception of $(\partial\alpha/\partial q)$. This factor may in principle be calculated quantum mechanically for a specific liquid and it can be related to measurable quantities by making a connection to the differential scattering cross section for spontaneous Raman scattering.[10,28] The differential scattering cross section, $d\sigma/d\Omega$, is defined as the power radiated into a unit solid angle divided by the incident intensity

$$\frac{d\sigma}{d\Omega} = \frac{1}{I_o}\frac{d\wp}{d\Omega} \qquad [2.18]$$

where $\wp$ denotes power and I_o is the incident intensity. By treating the induced dipole as a classical oscillating dipole antenna, the power radiated per unit solid angle in a direction at 90° to the dipole axis, is[29]

$$\frac{d\wp}{d\Omega} = \frac{ck^4\left(\frac{\partial\alpha}{\partial q}\right)^2 q^2 E_o^2}{32\pi^2\varepsilon_o} \qquad [2.19]$$

Combining Eqns. [2.18] and [2.19] and converting the field, E_o, to intensity with

$$I_o = \frac{1}{2}\varepsilon_o cn|E_o|^2 \qquad [2.20]$$

results in an expression for $(\partial\alpha/\partial q)$ in terms of known quantities

$$\left(\frac{\partial\alpha}{\partial q}\right)^2 = \frac{16\pi^2\varepsilon_o^2 n}{q_{spont}^2}\left(\frac{c}{\omega}\right)^4 \frac{d\sigma_\perp}{d\Omega} \qquad [2.21]$$

where $d\sigma_\perp/d\Omega$ is the differential cross section for spontaneous scattering at frequency ω and at 90° to the dipole axis, n is the index of refraction of the scattering medium and q of Eqn. [2.19] is now identified as q_{spont}, the molecular coordinate associated with spontaneous radiation. To describe the spontaneous radiation, a quantum mechanical model of a harmonic oscillator can be used for which fluctuations in the molecular coordinate, q_{spont}, are due to quantum zero-point fluctuations with

$$\left\langle q_{spont}^2 \right\rangle = \frac{\hbar}{2\zeta\Omega} \qquad [2.22]$$

where ζ and Ω are defined as in Eqn. [2.9]. Using this expectation value in Eqn. [2.21] and then substituting that back into [2.17], we can finally write

$$P_{os} = \frac{4\pi^2\varepsilon_o^2 n}{\hbar}\left(\frac{c}{\omega_s}\right)^4 \frac{d\sigma_\perp}{d\Omega} \frac{N|E_{ol}|^2 E_{os}}{\left[\Omega - (\omega_s - \omega_l) + \frac{i\gamma}{2}\right]}, \qquad [2.23]$$

describing the amplitude for the nonlinear polarization for SGS. Rewriting this expression in the form of Eqn. [2.6],

$$P(\omega_s) = N\,\varepsilon_o\,\chi^{(3)}(\omega_s)|E_{ol}|^2E_{os} \qquad [2.24]$$

identifies the third order term in the nonlinear susceptibility as responsible for stimulated gain scattering. An expression for $\chi^{(3)}$ follows directly from Eqn.[2.23]

$$\chi^{(3)}(\omega_s) = \frac{4\pi^2\varepsilon_0 n}{\hbar}\left(\frac{c}{\omega_s}\right)^4 \frac{d\sigma_\perp}{d\Omega}\frac{1}{\left[\Omega-(\omega_s-\omega_l)+\frac{i\gamma}{2}\right]}. \qquad [2.25]$$

Whenever the frequency difference between the two lasers equals a normal mode frequency of the molecule, $(\omega_s - \omega_l) = \Omega$, the real part of the third order susceptibility is zero and the polarization amplitude becomes a negative imaginary number corresponding to amplification. To understand how this produces stimulated gain on the probe beam, it is necessary to examine the propagation of the probe laser field through the medium, consider the coupling between it and the induced polarization and derive a gain coefficient for the SGS process. This is the topic of the next section.

Wave Propagation in a Nonlinear Medium

In order to derive the gain coefficient for the SGS technique, we start with the propagation of the probe laser field through a nonlinearly polarized medium. The wave equation for an optical electric field traveling through a medium with a nonlinear polarization, $\mathbf{P}^{NL}$, is given by[24]

$$\nabla^2 \mathbf{E}_s(\omega) + \frac{\omega^2}{c^2}(1+N\chi)\mathbf{E}_s(\omega) = -\omega^2 \mu_o \mathbf{P}^{NL}(\omega) \qquad [2.26]$$

where, for simplification, $\mathbf{E}_s(\omega)$ is assumed to be a plane wave of the form

$$\mathbf{E}_s(\omega) = \hat{\mathbf{e}}_S E_s \exp[i(kz - \omega t)] \qquad [2.27]$$

where E_s is the amplitude of the probe laser field and $\hat{\mathbf{e}}_S$ is a unit vector in the polarization direction of the $\mathbf{E}_S$ vector, with $\hat{\mathbf{e}}_S \cdot \mathbf{z} = 0$. Our interest in the gain coefficient means that we are only concerned with the variation in **E** along the direction of propagation, **z**, making this assumption a reasonable one. It is also reasonable to assume that the variations of $\mathbf{E}_S(\omega)$ are small over distances on the order of a wavelength, and thus employ the slowly varying amplitude approximation[24]

$$\left|\frac{\partial^2}{\partial z^2}\mathbf{E}_S(\omega)\right| << \left|k\frac{\partial}{\partial z}\mathbf{E}_S(\omega)\right| << k^2 z \ . \qquad [2.28]$$

Applying this approximation to the wave equation Eqn. [2.26] yields an expression for the change in the probe field along **z** as a function of the induced polarization,

$$\frac{\partial}{\partial z}E_s = \frac{i}{2}\frac{\omega_s}{\varepsilon_o nc}P^{NL} \qquad [2.29]$$

where P^{NL} is the amplitude of the nonlinear polarization. Substituting Eqn. [2.24] for the induced polarization in a SGS experiment and expressing

the susceptibility as the sum of its real and imaginary parts, $\chi^{(3)} = \chi' + i\chi''$, we have

$$\frac{\partial}{\partial z} E_s = \frac{i}{2} \frac{\omega_s}{\varepsilon_o nc} \left\{ N\varepsilon_o (\chi' + i\chi'') |E_{ol}|^2 E_{os} \right\}. \qquad [2.30]$$

Converting this expression for the field E_s to intensity with Eqn. [2.20] and using the equality

$$\frac{\partial |E_s|^2}{\partial z} = E_s^* \left(\frac{\partial E_s}{\partial z} \right) + E_s \left(\frac{\partial E_s^*}{\partial z} \right) \qquad [2.31]$$

we have an expression in the form of Beer's law for gain

$$\frac{\partial I_s}{\partial z} = g I_s = -\frac{\omega_s N}{\varepsilon_o n^2 c^2} \chi'' I_l I_s. \qquad [2.32]$$

This can be integrated over some distance, l, through the medium to give

$$I_s(l) = I_{os} \exp(gl) = I_{os} \exp\left\{ \left(-\frac{\omega_s N}{\varepsilon_o n^2 c^2} \chi'' I_l \right) l \right\} \qquad [2.33]$$

where a gain coefficient, g (in units of m^{-1}), can be identified as the quantity inside the inner parentheses. Note from Eqn. [2.25] that χ'' is negative when the laser difference frequency matches a molecular normal mode frequency, $(\omega_s - \omega_l) = \Omega$, so that gain is produced in the probe laser beam intensity as it travels through the polarized medium.

2.4 The SGS Experimental Set-up and Procedure

Stimulated gain spectroscopy (SGS) is a coherent technique, most readily understood in the frequency-domain, that can easily be altered to obtain either a broad depolarized Rayleigh-wing spectrum or a spectrum dominated by a narrow bandwidth Brillouin (polarized) component by orienting the probe polarization to be perpendicular or parallel to the pump polarization. A thorough description of the basic SGS experimental procedure used previously in our lab has been presented by Friedman,[28] some of which will be reiterated here for the sake of completeness. The Friedman work, which compared the low frequency dynamics of several molecular liquids, also attempted to measure the depolarized spectrum for CCl_4 without success. The depolarized signal intensity detected for the symmetric CCl_4 molecule was found to be only about 3% of CS_2, or 12% of that for liquid benzene, and as such can be difficult to distinguish above background noise. Much of the discussion here will therefore emphasize the careful and systematic reduction in noise arising from multiple sources that was necessary in order to obtain this spectrum.

Following an overview of the experimental set-up, the pulsed laser system, optical components and monitoring involved in providing the pump beam line will be described. The discussion continues with the cw laser system which provides the probe beam and will also include remarks about mitigating the effects of power fluctuations and plasma noise in the argon ion laser used.

The next section deals with experimental procedure and data acquisition. It includes information about sample preparation, the detectors, the integrating and averaging electronics used and the computer interface.

This section also includes comments about reducing radio frequency (rf) noise originating primarily from the Q-switched YAG laser and steps taken to monitor and subtract any stray scattered light that would affect the SGS signal. A final section on the tools used for data analysis follows, comprised of information about the software used, error analysis, accurate zeroing and frequency scaling.

The SGS Experimental Set-up

The SGS experimental arrangement is shown in Figure 2.6. It contains two beams which are counterpropagated through the sample liquid with a crossing angle of about 178°. The pump beam is supplied by a pulsed dye laser (PDL) pumped by the second harmonic of a Q-switched Nd:YAG laser. The PDL linewidth is about 500 MHz and is tunable over 300 cm^{-1}. The pump beam is passed through a Glan-Thompson polarizer and then directed through a focusing lens into the sample cell. A 50 cm focal length lens is used to ensure that the focal depth of the beam waist lies entirely within the scattering medium in order to provide maximum signal. Shorter focal length lenses run the risk of vaporizing the volatile molecular liquids used and generating bubbles that appear as sharp spikes in the spectra obtained. One of two quartz sample cells (1.2 cm or 5 cm in length) is positioned at an angle to the beam path to prevent the pump beam reflected off the cell surface from traveling back along the signal line. The 1.2 cm long cell worked well for the strongly scattering CS_2 or benzene, as the shorter passage through produced less heating of the liquid and therefore fewer bubbles. Also the shorter cell could be turned as much as 25°off the beam path to reduce backscattered pump light. A longer 5 cm cell was necessary for the

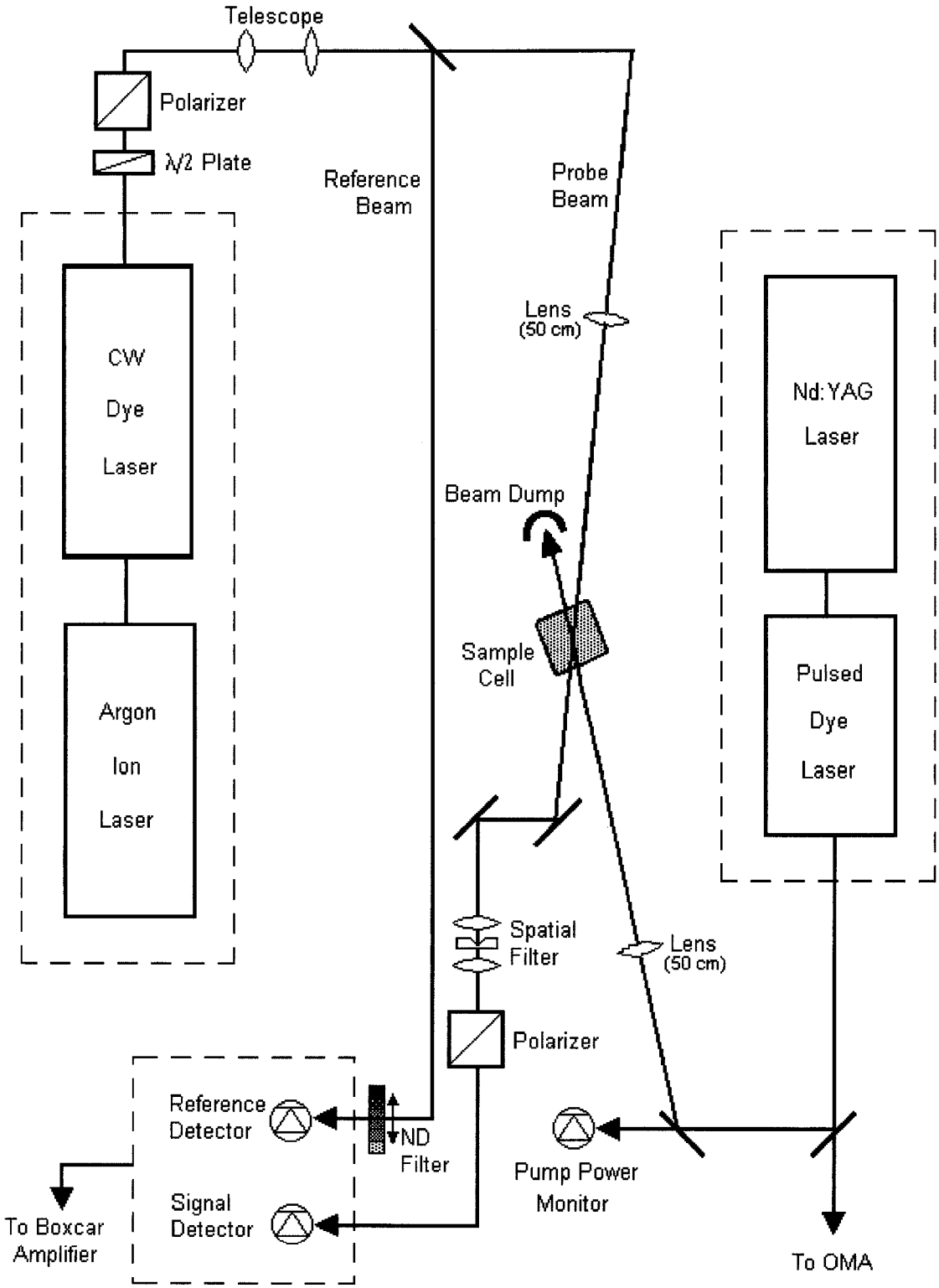

Figure 2.6 The experimental set-up for stimulated gain spectroscopy.

experiments in CCl_4, where a longer interaction region could be contained in order to produce greater gain. A beam dump captures the transmitted pump beam. In order to monitor beam quality, a small portion of the pump beam is directed to an optical multichannel analyzer (OMA). The OMA provides a means of monitoring the PDL laser output during alignment and scanning in order to reduce or eliminate fluctuations in the pump power due to fluorescence or to mode competition. In order to obtain a Rayleigh-wing spectrum, the pump laser needs to be frequency tuned about 200 - 300 cm^{-1}. Since this range covers much of the dye gain curve, the pump power will vary as a given spectrum is measured. In order to normalize the signal to the pump power supplied, a pump intensity spectrum is taken simultaneously with the signal spectrum, as will be described in the next section.

The probe beam is furnished by a cw dye laser pumped by an argon ion laser. This beam passes through a half-wave plate and polarizer to set the polarization with respect to that of the pump. A chopper in the probe beam path eliminates overheating and bubbles in the sample. It is also used to trigger the Q-switch of the YAG laser to synchronize timing of the pump and probe lasers. Following the chopper, a beam splitter reflects a portion of the light to be used as a reference beam in a detector circuit to subtract out fluctuations in the probe laser. Irises on both the pump and probe paths provide spatial filtering necessary to block stray scattered light traveling adjacent to the beam paths. A telescope is used to expand the beam so that its size matches that of the pump beam when each enters its respective focusing lens. Both focusing lenses have a 50 cm focal length and are positioned symmetrically around the sample cell. After the probe beam is focused through the sample cell it is recollimated and directed, along with the

reference beam, to its respective detector. The detectors for the probe and reference beams are arranged in a circuit that subtracts the intensities of the two beams, thereby eliminating fluctuations present in the probe laser in the absence of the pump pulse. Signal detection will be discussed in more detail in the section on data acquisition which follows later in this chapter.

Pulsed Pump Laser

The pump beam is generated by a pulsed dye laser (PDL) from Pegasus Enterprises. This PDL is a modified Littman style[30] pumped by the second harmonic of a Quanta-Ray DCR-1 Q-switched Nd:YAG laser. When rhodamine 610 is used for the dye, the laser could be frequency tuned over 300 cm^{-1} with a bandwidth of 500 MHz and a center frequency of about 585 nm. The Pegasus laser uses a four prism beam expander and a pair of gratings arranged as shown in Fig. 2.7. A thorough description of this laser is given in Friedman.[28] A cylindrical lens focuses the pump light (532 nm) into a line along the laser path in the dye cell. Behind the cell is the rear high-reflector and in front of the dye cell is the beam expander. The laser light is expanded to cover the surface of the first grating, G1, and the zero diffraction order is used as the laser output while the first order diffracted light is caught by the second grating, G2. In order to tune the output frequency, grating G2 can be rotated using a motorized micrometer (Oriel Motor Mike) which pushes on a sine bar attached to the support post of the grating. A higher diffraction order (third to fifth) from G2 was returned to the laser cavity in order to narrow the linewidth.

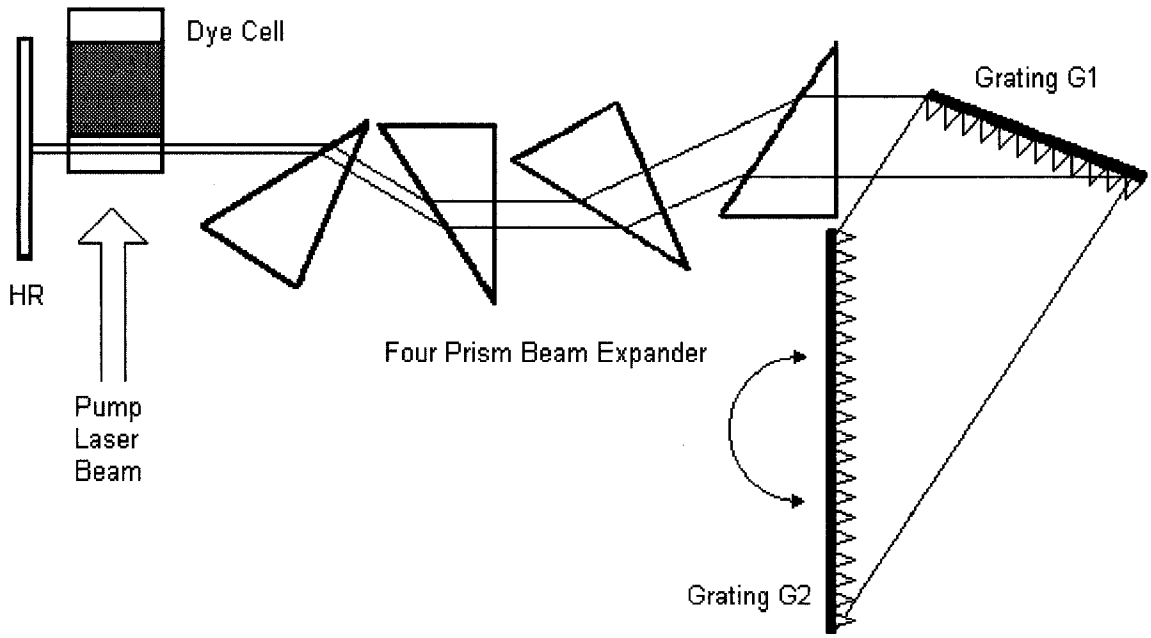

Figure 2.7 The pulsed dye laser with 4-prism beam expander and grating pair.

Since the depolarized Rayleigh wing spectrum covers a very broad frequency range there are exacting alignment requirements for the PDL. In order to tune the frequency while using a fourth order diffraction from G2, the sine bar is pushed about 20 μm (0.2 mrad rotation) for every cm^{-1} change in frequency.[30] Thus a 250 cm^{-1} spectrum requires the sine bar to travel a full 5 cm for a 50 mrad rotation of G2. To ensure that the output beam would remain spatially stable during this much rotation of the grating, it was absolutely necessary to have the grating lines of G1 and G2 parallel. This was done by adjusting pitch and yaw on grating G2 so that, when examined

on a screen set several meters away, the various diffraction orders from both gratings are aligned on the same horizontal plane. A second complication due to the large frequency range scanned is that a large portion of the dye gain curve is used resulting in a pump laser power that closely follows the amplitude of the gain curve. To normalize the effects of changes in the pump intensity during scanning, as well as pulse to pulse fluctuations in the PDL, a pump intensity spectrum is taken simultaneously with the signal spectrum. This helps reduce noise in the spectrum and eliminates skewing due to large changes in the pump intensity during the scanning. One alternative to using the low intensity edges of dye curve is to scan only the gain side of curve, or about 120 cm^{-1}. It is still necessary to run a the pump intensity spectrum for normalization purposes. Another alignment concern is that of eliminating fluorescence over the entire tuning range. Fluorescence, or amplified spontaneous emission, does not contribute to the signal in the SGS spectra but does add to the intensity detected at the diode monitoring the pump beam. Thus the normalization process will actually introduce effects of fluorescence into the spectrum. It is important therefore to be certain that fluorescence remain well separated from the laser light throughout the frequency range of the scan. This is accomplished by monitoring the PDL output with an optical multichannel analyzer (OMA) on loan from Dr. George Collins of the Electrical Engineering Department here at Colorado State University. The laser light and fluorescence are both displayed, with the broad bandwidth fluorescence generally blue shifted from the narrow laser line. By using the OMA while peaking alignment and selecting a favorable portion of the dye curve, the fluorescence can be avoided over the whole tuning range. The

OMA display is checked between scans and the PDL alignment periodically peaked to maintain beam quality.

Cw Laser System/Probe Beam

In addition to its ability to obtain broad Rayleigh-wing spectra, the SGS experiment can also access the narrow polarized Brillouin signal. Brillouin scattering requires a narrow laser linewidth over a shorter frequency range of $\pm$10 - 15 GHz. These requirements are met by scanning a Coherent 599-21 single mode, standing wave, stabilized cw dye laser (CWDL). When pumped at 3 watts using an argon-ion laser, all lines, the CWDL provides stability in both frequency and output power, with output powers between 50 to 100 mW, frequency tunability of 30 GHz and an average linewidth of 1 MHz. It was noted that for a given dye the gain curve in the CWDL is red-shifted about 15 nm relative to the PDL,[28] so Rhodamine 590 dye is used in order to better match the dye gain curve of the PDL. While the experimental linewidth here is limited by the 500 MHz linewidth of the PDL, our research group has also demonstrated stimulated Brillouin gain spectroscopy in SF_6 gas with spectral resolution improved to better than 4 MHz.[31,32] This was accomplished using a tunable cw single-mode ring dye laser as the pump laser in place of the pulsed dye laser for studies that do not require the large frequency shifts necessary for Rayleigh-wing spectra.

The CWDL was found to require an argon pump power of at least 2W for stable operation. Due to a lack of research funding, the work presented here was done using a series of Argon ion lasers that gave only borderline performances. Most often the problem was that the tube pressure was too high, resulting in low output power and poor stability. The gain for an ion

laser is strongly dependent on gas pressure.[33] Population inversion in an argon ion laser is created after two collisions of an argon atom with free electrons. The first collision ionizes the argon atom from its ground state and the second collision pumps the ion either directly to the upper level of visible lasing transitions (4p energy level) or to the doubly ionized ground state, from which it cascades almost immediately to 4p. When operating at optimal conditions, the tube pressure is relatively low in order to increase the time between collisions with free electrons and thereby increase the average electron energy. This creates conditions favorable to the high energy collisions required to excite argon ions to the Ar^{++} state. Pressure that is too high results in too many low energy collisions that do not populate the upper energy level. Stable performance also requires a uniform pressure distribution along the length of the discharge. If the pressure distribution is uneven, regions of gain and loss may compete with one another causing a noisy, unstable output. The effect of plasma noise and other power fluctuations from the argon ion laser is to add noise at various frequencies to the probe light.

When working with CCl_4, the SGS gain is only 0.06% on a probe beam with about a 120 mV dc level. (All voltage values cited here are values before amplification as detected by EG&G FND-100 photoconductive diodes). Thus it was critical that the amplitudes of noise contributions be less than about 0.05 mV. When light directly from the argon laser was examined, oscillations at 120Hz, 20MHz and 150MHz were observed. A passive high pass filter placed after the signal detector to block frequencies below 10 MHz eliminated the lower frequency noise. The differential detection, Section 2.4.4, using the probe and reference beams was necessary

to reduce higher frequency probe fluctuations. The probe and reference beams had initially been set up to eliminate relatively slow fluctuations in power from the CW dye laser and the two paths were not precisely matched. The high frequency argon plasma noise necessitated a path length match that was accurate to ± 3 cm out of a 7 meter total length to counter these fast oscillations. This was sufficient to reduce the amplitude of the 20 MHz oscillation by 98% and the fast 150 MHz oscillation by 87%, enabling detection of a SGS signal of about 0.07 mV.

Data Acquisition

The SGS experiments that are the subject of this report examined molecular interactions in liquid CCl_4 at ambient conditions and the effects of high pressure on molecular motions in liquid benzene. Both liquids were Spectranalyzed grade supplied by Fischer Scientific. A 5 cm long glass cell with a teflon stopper was used to contain the carbon tetrachloride sample for experiments at room temperature and pressure. The experiment in benzene at high pressure required a specialized cell and equipment which are described along with the sample preparation in chapter 4. However, in addition to the pressurized sample, a glass cell was filled with benzene and used to precisely match the pump and probe laser wavelengths. Due to their toxicity and volatile natures, all samples used at ambient conditions were loaded under a chemical fume hood. The samples were filtered into the cells and the teflon stoppers sealed with a teflon based high-vacuum sealant to prevent outgassing. The samples were allowed to sit for a period of several hours to allow turbulence and bubbles introduced in the filling process to settle out of the liquid. This significantly reduced the amount of stray scattered pump light

seen in the spectra and on the monitoring oscilloscope when data was taken immediately after filling.

With the samples in place, data acquisition could begin. Since the SGS signal is detected on top of the probe laser intensity, amplitude fluctuations of the probe laser significantly impact the experiment. As discussed above, random amplitude noise may overwhelm the signal if not minimized. Thus, the experiment is started by blocking the pump beam and carefully balancing the probe and reference beam intensities using a variable neutral density filter placed in the reference beam. The beams are detected using EG&G FND-100 photoconductive diodes arranged in a circuit to subtract the signals, Figure 2.8. The detectors are biased by 90 volt batteries as shown, and have sensitivities on the order of 0.3 amps/Watt and rise times of less than 1 nsec. The output for the signal is taken between the anode of the signal diode and the cathode of the reference diode. When identical light intensities impinge on the two diodes, there will be no current through the output load resistor, R_L and no output voltage. This will eliminate intensity fluctuations that are in the probe laser before the beamsplitter thus allowing the signal to be seen above laser noise.

When the pump beam is sent through the sample, interaction with the probe produces gain on the probe beam but not on the reference beam resulting in an output signal. Since the SGS signal can occur only with the interaction of the probe and pump pulse, the chopper set in the probe line is used to externally trigger the YAG laser at a 10 Hz rate to ensure that the pump pulse arrives at the sample during the chopped probe beam. Then, using the variable output from the YAG laser, the boxcars and an oscilloscope are triggered by an electrical pulse synchronous with its

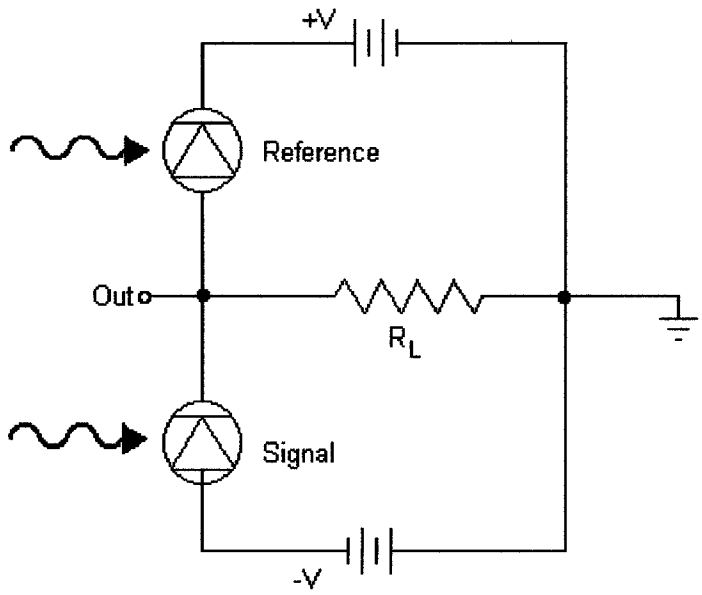

Figure 2.8 The probe/reference beam detection circuit designed to subtract identical light intensities incident on the two diodes and to output a voltage only when an excess intensity is detected at one diode and not the other.

Q-switch. The detected signal is passed through a 200 pf capacitor to a 10x, pre-amplifier (Phillips model 6950). Together the 50Ω input load resistor of the pre-amp and the capacitor form a passive high pass filter to block frequencies below a few megahertz. The signal is then amplified another 10x (Phillips model 770 amplifier) and sent to the input of a gated integrator (EG&G PAR model 165) and a boxcar averager (EG&G PAR model 162). The pump intensity monitor goes to an identical electronic system and then both signals are sent to a Stanford Research Systems model SR245 computer interface which does analog to digital conversion of the signal. For the broad

spectrum Rayleigh-wing experiments, the SR245 is triggered externally by a square pulse output from the controller of the Oriel motorized micrometer used to tune the PDL. In the Brillouin gain experiment, the Coherent Model 251 Spectrum Analyzer Controller controls the frequency tuning for the CWDL and the trigger to the computer interface. The signals are then sent to both the monitoring oscilloscope and an IBM pc compatible computer where Stanford Research software (SR265 v.3.1) saves the data. This data acquisition apparatus has been described in careful detail previously.[28]

The detection circuit, with its batteries and amplifiers, proved to be very sensitive to radio frequency (rf) pick-up. The Q-switched YAG laser used was an older model, Quanta-Ray DCR-1, which, because of its age was a large source of rf noise, producing significant amplitudes at about 80MHz. A number of steps were taken to minimize this. Although the probe and reference detectors were mounted in a cast aluminum box with a ground strap to the table, the shielding provided was insufficient. Additional improvement resulted from wrapping both the batteries and the umbilical cord to YAG power supply with aluminum foil and placing a Faraday cage around the YAG laser itself. These steps, combined with careful repositioning of the batteries to find a quiet spot, lowered the rf noise amplitude by almost 75%. The remaining noise amplitude, at about 0.5 mV, was still unacceptably large. A wire cage was constructed to contain the subtraction circuit housing, batteries and preamp. With this bolted down to the optical table and the cables for the amplifiers also wrapped, the rf noise was finally reduced to well below 0.05 mV, so that the stimulated gain signal in CCl_4 was easily observed on the oscilloscope used for monitoring and alignment.

Once the optics are aligned and the signal is peaked up, the procedure for collecting a Rayleigh-wing spectrum involves steps to define a zero intensity baseline for both the gain spectrum and the power intensity spectrum that is collected concurrently. This is accomplished by collecting approximately the first 50 to 100 data points (out of about 2500 data points for a typical spectrum) with both lasers blocked to prevent any light from entering the detectors. This data is later used to set the zero baseline for the pump intensity monitor. The light from the pump laser only is allowed to pass for about the next 100 data points to provide a zero gain intensity level for the spectrum. At the end of the spectrum, the probe beam is again blocked for the last 150 to 200 data points. The lasers were blocked remotely, using solenoids and black anodized aluminum plates, to avoid physically moving around the room during the data collection. This was necessary because of the sensitivity of the detectors to both the rf output from the YAG and other equipment, and to any changes in scattered background light levels.

Despite every effort to locate and eliminate stray scattered pump light, some backscattering often remained and made its way into the signal detector. Slight differences in the zero signal intensity levels at the beginning and end of some scans indicated that the level of scattered light was changing over the course of a spectrum. When a full spectral scan was run with the probe beam blocked, the scattered light was found to be either increasing or decreasing steadily over the course of the scan. This was most likely due to slight spatial offsets in the pump beam as it was tuned over the large range. For the low gain experiments in CCl_4, it was necessary to subtract out the effects of the changing scattered light. In order to be able to do this, a scatter spectrum was

run (with the probe beam blocked) after every few signal spectra. Later these scans could be used to correct any skewing that resulted from stray scattering regardless of the source.

Data Handling

To get the experimental data into a form suitable for curve fitting analysis, it was corrected for variations in pump laser power and stray scattered light, the zero point was determined for both the signal intensity and $\Delta\omega$, the frequency difference between the pump and probe lasers, as described below, then several spectra were added together for each of the final data sets analyzed.

A new program was written specifically to convert the raw data files into the normalized, frequency-scaled spectra presented here. With each stimulated gain spectrum run, a pump intensity spectrum was collected simultaneously and both are stored by the SR265 program as a data point number, signal voltage and pump monitor voltage. This enabled a point by point normalization of signal intensity to the pump power provided. Whenever they were used, the scatter scans were also normalized to their respective pump intensity scans. Typically, about 2500 data points are recorded for each spectrum, corresponding to roughly 300 cm^{-1} (or 0.119 cm^{-1} per data point, as will be described with frequency scaling).

A zero intensity baseline was set by taking an average of the signal intensity for the last 150 data points. These points coincided with the portion of the spectrum for which the probe laser was blocked. The signal data points were then shifted by the average value so that the blocked region

would have a zero value. A check on this baseline value was supplied by comparing the maximum and minimum intensity values, since for the small gain values involved the Stokes and Anti-stokes scattering should be equal. Consistently, very similar values were obtained whether the intensity zero level was set using the blocked portion of the spectrum or the symmetry of the gain and loss curves. In the benzene data for example, these methods determined a set point for the intensity baseline which differed by only 1 or 2 units of relative intensity on a scale of between 220 to 330 relative intensity units.

Before individual (normalized) spectra could be added together or a scatter scan subtracted from the signal, the data point for which the laser frequency difference was equal to zero had to be precisely determined. This was accomplished as follows. The CCl_4 spectra had been obtained with a small amount of polarized light intentionally "leaked" to supply a Brillouin signal as a marker to aid in locating the weak signal and optimizing alignment. This sharp feature provided an accurate means of locating the frequency zero, allowing the program to determine the location of the maximum and minimum signal for the spectrum and to set the frequency zero midway between. For the completely depolarized benzene spectra, the maximum and minimum were not as sharp as a Brillouin spike, and could be off by as much as $\pm$ 5 - 7 points due to noise. This is a significant problem for adding spectra together as it could result in broadening the narrow low frequency spectral component found in the molecular liquids. For this reason, a different approach was taken for the benzene data collected. After the intensity baseline was set and the data shifted, the data point which held the intensity value closest to zero was determined to be the zero frequency.

Concern about inaccuracy due to reliance on the set baseline proved to be unnecessary because of the large amplitude changes in the signal as it passes through zero. It was determined that the intensity zero value would have to be incorrect by over 15% to result in an error of just one data point in the location of the frequency zero. An error of one point translates to 0.119 cm^{-1} out of about 250 to 300 cm^{-1} for a full spectrum. With the zero frequency point set, individual spectra could be aligned with one another and added together to improve the signal to noise levels. The depolarized SGS spectrum for CCl_4, presented in Chapter 3, is the sum of 12 individual spectra. In Chapter 4, the spectrum for liquid benzene at ambient pressure is comprised of 14 individual data sets and the spectrum at 350 bars pressure consists of 7 data sets added together .

The frequency scaling was done using 300 cm^{-1} scans to produce spectra that include the first vibrational Raman line[34] for CCl_4 at 217.9 cm^{-1}. Additional certainty in converting the number of data points scanned to a wave number range was provided by obtaining spectra for a range of frequency differences from 200 cm^{-1} to 500 cm^{-1}, thus including the vibrational Raman lines[34] at 217.9, 314.0, and the resolved triplet at 459 cm^{-1}. By taking difference ratios between various peaks, a frequency scale was arrived at with less than 1% uncertainty.

Curve fitting techniques will be covered in depth in Chapter 3. The lineshape modeling was done using the nonlinear curve fitting capabilities of the Kaleidagraph® program by Synergy Software. The quality of fits to the data was determined using both a linear correlation factor (Pearson's r) and by minimizing Chi-square. Finally, the Kaleidagraph® program simplified formatting the final spectra for publication.

2.5 References

1. L. Brillouin, Comptes Rendus, **158**,1331 (1914); L. Brillouin, Ann. Phys. **17**, 88 (1922).

2. E. Gross, Nature, **126**, 201 (1930); E. Gross, Nature, **129**, 722 (1932).

3. L. D. Landau and G. Placzek, Phys. Zeit. Sow. **5**, 172 (1932).

4. R. D. Mountain , "Spectral distribution of scattered light in a simple fluid," Rev. Mod. Phys. **38**, 205 (1966).

5. C. -Y. She, "Spectral structure of laser light scattering revisited: Bandwidths of nonresonant scattering lidar," Appl. Opt. **40**, 4875 (2001).

6. R. M. Lynden-Bell and W. A. Steele, "A model for strongly hindered molecular reorientation in liquids," J. Chem. Phys. **88**, 6514 (1984).

7. A. J. C. Ladd, T. A. Litovitz, and C. J. Montrose, "Molecular dynamics studies of depolarized light scattering from argon at various fluid densities," J. Chem. Phys. **71**, 4242 (1979).

8. P. M. Madden, in *Spectroscopy and Relaxation of Molecular Liquids*, edited by D. Steele and J. Yarwood, Studies in Physical and Theoretical Chemistry, Vol. 74 (Elsevier Science Publishers, Amsterdam, 1991).

9. D. Frenkel and J. P. McTague, "Molecular dynamics studies of orientational and collision-induced light scattering in molecular fluids," J. Chem. Phys. **72**, 2801 (1980).

10. G. C. Herring, "Coherent Raman spectroscopy for supersonic flow measurements," Ph.D. dissertation, Colorado State University, (1987).

11. J. P. McTague, P. A. Fluery and D. B. DuPre, "Intermolecular light scattering in liquids," Phys. Rev. **188**, 303 (1969).

12. R. Trebino, C. E. Barker, and A. E. Siegman, "Tunable-laser-induced gratings for the measurement of ultrafast phenomena," IEEE J. Quantum Electron. **22**, 1413 (1986).

13. M. A. Scarparo, J. H. Lee, and J. J. Song, "Near-zero-frequency stimulated Raman gain spectroscopy in CS_2," Opt. Lett. **6**, 193 (1981).

14. J. S. Friedman, M. C. Lee and C. Y. She, "Depolarized stimulated gain spectra of liquid CS_2 and benzene at room temperature," Chem. Phys. Lett. **186**, 161 (1991).

15. K. A. Nelson, D. R. Lutz, M. D. Fayer, and L. Madison, "Laser-induced phonon spectroscopy. Optical generation of ultrasonic waves and investigation of electronic excited-state interactions in solids," Phys. Rev. B **24**, 3261 (1981).

16. T. Hattori, A. Tersaki, T. Kobayashi, T. Wada, A. Yamada, and H. Sasabe, "Optical-heterodyne-detected induced phase modulation for the study of femtosecond molecular dynamics," J. Chem. Phys. **95**, 937 (1991).

17. E. P. Ippen and C. V. Shank, "Picosecond response of a high-repetition-rate CS_2 optical Kerr gate," Appl. Phys. Lett. **26**, 93 (1985).

18. G. L. Eesley, M. D. Levenson, and W. M. Tolles, "Optically heterodyned coherent Raman spectroscopy," IEEE J. Quant. Electron. **14**, 45 (1978).

19. M. Khalil, N. Demirdoven, O. Golonzka, C. J. Fecko, and A. Tokmakoff, "A phase-sensitive detection method using diffractive optics for polarization-selective femtosecond Raman spectroscopy," J.Phys. Chem. A, **104**, 5711 (2000).

20. A. Tokmakoff and G. R. Fleming, "Two-dimensional Raman spectroscopy of the intermolecular modes of liquid CS_2," J. Chem. Phys. **106**, 2569 (1997).

21. S. Takagi and H. Tanaka, "Phase-coherent light scattering spectroscopy. II. Depolarized dynamic light scattering," J. Chem. Phys. **114**, 6296 (2001).

22. C. J. Fecko, J. D. Eaves, and A. Tokmakoff, "Isotropic and anisotropic Raman scattering from molecular liquids measured by spatially masked optical Kerr effect spectroscopy," J. Chem. Phys. **117**, 1139 (2002).

23. M. D. Levenson and S. S. Kano, *Introduction to Nonlinear Laser Spectroscopy,* Academic Press, (1988).

24. P. N. Butcher and D. Cotter, Cambridge Studies in Modern Optics, Vol. 9, *The Elements of Nonlinear Optics*, Cambridge University Press, (1990).

25. Y. R. Shen, *Principles of Nonlinear Optics*, John Wiley & Sons, (1984).

26. S. L. Shapiro and H. P. Broida, "Light scattering from fluctuations in orientations of CS_2 in liquids," Phys. Rev. **154**, 129, (1967).

27. J. P. McTague, P. A. Fluery and D. B. DuPre, "Intermolecular light scattering in liquids," Phys. Rev. **188**, 303 (1969).

28. J. S. Friedman, "Stimulated Rayleigh-Brillouin spectroscopy for studying low frequency dynamics in simple liquids," Ph.D. dissertation, Colorado State University, (1992).

29. J. D. Jackson, *Classical Electrodynamics*, Wiley, New York, (1975).

30. Model PE-201 Pulsed Dye Laser User's Manual, Pegasus Enterprises.

31. S. Y. Tang, C. Y. She, and S. A. Lee, "Continuous-wave Rayleigh-Brillouin-gain spectroscopy in SF_6," Opt. Lett. **12**, 870 (1987).

32. S. Y. Tang, "Light scattering in fluids," Ph.D. dissertation, Colorado State University, (1992).

33. Model 2020-5 Argon Ion Laser User's Manual, Spectra-Physics.

34. G. Herzberg, *Molecular Spectra and Molecular Structure*, vol. 2, "Infrared and Raman Spectra of Polyatomic Molecules", (Van Nostrand Reinhold Company, New York, 1945).

3 Depolarized Stimulated Gain Spectrum of Liquid CCl_4

3.1 Introduction

Light scattered from simple liquids results in spectra that is broadened and depolarized by the motions of the molecules. In the case of anisotropic molecules, depolarized scattering is generally described as resulting from diffusive reorientation, collisions, and oscillations (libration) within transient local potential wells, each producing a characteristic spectral shape which can be represented phenomenologically by a model with low, intermediate and high frequencies.[1-6] Collisions change the polarizability for the duration of the interaction and lead to depolarized scattering even for isotropic scatterers.[7-9] The details of these interactions and how the anisotropy in the polarizability varies as a function of the distance r between interacting molecules have been the subject of much study.[10,11]

In the effort to understand collision-induced (CI) scattering, carbon tetrachloride (CCl_4) is an attractive sample molecule due to an isotropic polarizability. With no strong orientational scattering to complicate the analysis of the collision-induced spectra, the depolarized scattering from CCl_4 will be dominated by purely translational CI effects which can be described

by a simple model. Although more regulated and difficult to obtain today due to its impact on atmospheric ozone, CCl_4 was often selected for investigation of CI effects using either spontaneous light scattering (LS) techniques[9,12-17] or time-domain techniques,[18-20] thus providing a basis for comparison and evaluation of SGS results.

Lineshape modeling has proven to be a useful tool for understanding experimental spectra. Our main objective in line shape modeling is to consider possible types of motion a molecule can undergo in a liquid environment and to apply phenomenological models to describe the frequency responses of the motions. The resolution of SGS enables a distinction between several models based on different interaction distances, *r*. Furthermore, by making comparisons and connections among various liquids (carbon tetrachloride, chloroform, methylene chloride, carbon disulfide and benzene) we hope to both test the quality of the models used and to better understand the effects of molecular physical parameters on the observed spectra, thereby furthering insight into the mechanisms producing scattering.

3.2 Lineshape modeling for collision-induced scattering

Early spontaneous light scattering (LS) studies showed that collision-induced scattering is present universally in both gases and liquids[7-10,12,13,17,18,21,22] producing a broad exponential tail in the wings of the depolarized spectra. Both phases exhibit a similar line shape, although the spectra for liquid densities are much weaker in intensity and broader in frequency than seen in gases.[8] For anisotropic molecules a second

component due to reorientational relaxation appears as a Lorentzian line centered at zero frequency shift.

In gases comprised of atoms or isotropic molecules, depolarized scattering is the result of transient anisotropic polarizability produced primarily in colliding pairs by a dipole-induced dipole (DID) effect.[23-24] DID involves fluctuations in both magnitude and direction of the local field as seen by one scatterer due to the dipole moments induced on its near neighbors by the incident laser field. This relatively long range effect produces a force proportional to r^{-3} extending over several atomic radii. While DID scattering dominates in gases, the nearly symmetric environment that results from the close-packed nature of liquids produces a cancellation of long range field effects and thereby a reduction in scattered intensity. Clearly, shorter range mechanisms become more important as densities are increased and interactions become more complex.

One such short range mechanism, first proposed by Levine and Birnbaum,[7] involves the overlap of electronic clouds during binary collisions. In contrast to DID, the electronic overlap (EO) mechanism does not experience cancellation at high densities since even in a multiple collision there is low probability for a molecule to simultaneously overlap with more than one neighbor. In this sense, EO is essentially a binary effect even at liquid densities. These short range effects can dominate at high densities and account for the higher frequency components seen in the liquid spectra.

By assuming that the collision-induced anisotropy of polarizability, $\Delta\alpha(r)$, of a pair of scatterers is related to their separation, r, as

$$\Delta\alpha(r) \sim r^{-m}, \qquad [3.1]$$

Bucaro and Litovitz[9] were able to derive explicit formulas in the form of a weighted exponential for spontaneous light scattering spectra,

$$I(\omega) \sim \omega^{2(m-7)/7}\exp(-\omega/\omega_c), \qquad (\omega>\omega_c) \qquad [3.2]$$

where ω_c, the collision frequency, is related to the inverse average time duration of a collision. Different values of m describe different physical mechanisms for induced anisotropy of polarizability, and as will become clear below, r^{-m} is proportional to the interaction forces involved. Calculations[9] based on a deformable shell model for argon atoms indicate that electronic overlap results in an induced anisotropy proportional to r^{-9}. For molecular systems, EO may also cause a distortion in the molecular frame and thus change the polarizability of the colliding molecules for the duration of the collision. In the absence of theoretical calculations, Bucaro and Litovitz make the intuitive assumption that any frame distortion which occurs will be proportional to the repulsive part of the interaction force. Using a Lennard-Jones 6-12 potential to describe the molecular interactions results in an interaction force, and associated polarizability anisotropy, with a r^{-13} dependency.[9] The Bucaro and Litovitz values of m = 9 or 13, corresponding to electronic overlap effect in isotropic 'atomic' liquids or distortion of anisotropic molecular frames in molecular liquids, respectively, were later tested and confirmed by Howard-Lock and Taylor[15] for a series of fifteen simple liquids. It was noted that liquids composed of quasi-spherical molecules (CCl_4 included) were better fitted by the isotropic atomic model than by the molecular model Bucaro and Litovitz had initially applied to them.

As noted in chapter 2, much of the superior resolution of the SGS technique is due to directly probing the imaginary portion of the spectral density, $\chi^{(3)}$, whereas LS spectra detect the same material response function divided by the angular frequency.[9] Thus for SGS, Eqn. [3.2] needs to be modified to

$$g(\omega) = \mathrm{Im}\,[G(\omega)] \sim \omega^{s}\exp(-\omega/\omega_c), \qquad (\omega>\omega_c) \qquad [3.3]$$

where s=1+[2(m-7)/7], so that s=1.571 and 2.714 for atomic and molecular liquids, respectively. This expression provides an important model for CI scattering and has been applied to data obtained by several different techniques.[3-5,12-16,18,25-31] The ability with SGS to distinguish between various values of s (or equivalently, m) corresponding to different induction processes, despite the presence of a strong exponential function, can offer meaningful information about interaction-induced dynamics not available through the exponential alone.

Additional understanding of molecular interactions in liquids has been provided by molecular dynamics (MD) simulations, using a generalization of the dipole-induced-dipole effect which includes higher order effects for the evaluation of collision-induced polarizability.[32] These effects arise from two sources: higher order molecular multipoles (field induced quadrupoles and octopoles) and multiple order gradients in the local field due to contributions from moments induced in near neighbors. This introduces a dipole-quadrupole polarizability describing both the quadrupole induced by an incident field and the dipole induced by a field gradient, each of which has a pair polarizability varying as r^{-4}. A dipole-octopole polarizability, varying as

r^{-5}, has contributions from both the field induced octopole and the dipole induced by the second derivative of the field.

To provide a simplified understanding of these interactions, recall from Chapter 2 that the light scattering process consists of an incident light field, $\mathbf{E}_i$, that induces a dipole moment, $\mathbf{p}$, which then re-emits radiation modulating the optical field. Depending on the symmetry of the molecule in question, multipole moments can also be induced by the incident field with the induced quadrupole, octopole or higher moments each being proportional to the incident field. For a single, isolated molecule, its dipole moment, $\mathbf{p} = \alpha_0 \mathbf{E}_i$, is due its intrinsic molecular polarizability, α_0, and the increase of the molecular potential energy is the result of work done by the incident electric field. However, with millions of molecules within a small interaction volume, there are additional contributions to the polarizability resulting from forces that are due to the induced moments on the neighboring molecules and which leadto a local field, $\mathbf{E}_{loc}$ on the molecule in question. Considering one such molecule with an induced dipole moment, its potential energy, U, is increased by

$$\Delta U = \mathbf{E}_{loc} \cdot d\mathbf{p} = \mathbf{F} \cdot d\mathbf{r}_d \qquad [3.4]$$

as a result of work done by a force, $\mathbf{F}$, that is due to the induced moments on the neighboring molecules. Here $d\mathbf{r}_d$ represents the change in the charge distribution of the molecule under consideration. $\mathbf{E}_{loc}$ is a combination of the incident laser field, $\mathbf{E}_{inc}$ plus a term due to contributions from the neighboring molecular moments and proportional to the polarizability (Eqn. [2.7]) such that we can write $\mathbf{E}_{loc} = (1 + \Delta\alpha(r)/\alpha_0)\mathbf{E}_{inc}$. We can thus see that induced moments on neighboring molecules introduce a r dependence, with

associated spatial derivatives, in the local electric field. Depending on the symmetry of the molecule in question, the incident field could induce a dipole, quadrupole, octopole moment, etc., leading to dipole-dipole, dipole-quadrupole, and dipole-octopole interactions with the force proportional to both the incident electric field and to $\Delta\alpha(r)$ with r^{-3}, r^{-4}, and r^{-5} dependences, respectively, as discussed earlier.

For tetrahedral molecules such as CCl_4 an isotropic molecular dipole polarizability does not allow pure rotational scattering. The dipole-quadrupole and dipole-octopole polarizabilities however are nonzero and anisotropic and result in a pair polarizability that is modulated by the rotation of the molecules. These extra contributions, which occur over somewhat shorter interaction distances ($r^{-4}$and r^{-5}) and therefore faster timescales than DID scattering, appear at rotational transition frequencies augmenting the higher frequency portion of the spectrum, and are generally referred to as collision-induced rotational Raman scattering (CIRRS).[32-34]

Molecular dynamics studies have compared spectra calculated with DID and the first order CIRRS terms to experimental data and found good correlation in gaseous methane.[35] Results for heavier molecular gases [CF_4, SF_6, $C(CH_3)_4$] have been less satisfactory with excess intensity remaining in the higher frequency portion of the spectra. This excess cannot be accounted for with the addition of CIRRS second order (dipole-octopole) terms.[35,36] In condensed phases, the contribution from the leading DID term is expected to be greatly reduced due to cancellation effects, allowing the shorter range higher order terms to become more significant (although they too are subject to cancellation). However, in dense liquids the rotational motions producing the higher frequency contributions are almost always overdamped, thus

moving to somewhat lower frequencies. This may make the CIRRS contribution even more difficult to detect in liquids.[36] In their investigation of depolarized Rayleigh scattering in tetrahedral molecules, Neumann and Posch[37] distributed the polarizability over the molecule to represent the same physical effect which leads to CIRRS. They found for CCl_4 that the high frequency character of CIRRS was damped as anticipated in the liquid phase and that the calculated spectra was very similar to a calculation for a simple center-to-center DID spectrum thus leaving a portion of the higher frequency intensity unaccounted for. Neumann and Posch also investigated the frequency dependence of the depolarization factor in liquid CCl_4 and again concluded that a mechanism other than DID is the principal contributor to the depolarized spectrum for large frequency shifts.[37] A more recent (2002) MD simulation[38] has taken DID, induced multipole, and electronic overlap effects all into account in an approximate way to study collision-induced effects in CS_2. The inclusion of multipole and EO effects considerably improved the quality of the theoretical description based solely on DID effects.

Although the MD formulation is rigorous and is preferred in theoretical studies,[11,36,39,40] there remains a need for higher order, shorter range effects to fully account for the intensity seen in the higher frequency portion of the spectrum. Regrettably at present the complexity of molecular liquids precludes a predictive theory for a well defined, closed functional form to fit the experimental spectrum. It is this lack of a simple functional form for a CIRRS model with sufficient higher order terms that has led us to base our models for lineshape fitting on the expression of Eqn. [3.3]. It provides a means of quantitatively comparing and categorizing CI scattering in various liquids while offering insight into the interaction mechanisms responsible for

the scattering. Additionally, there exists a significant body of experimental data[3-5,12-16,18,25-31] fit to the Bucaro and Litovitz equation available for comparison with this present work. The various models and induction mechanisms for anisotropy of polarizability discussed above are summarized in Table 3-1. Also included is the model most often used in coherent time-domain work[18,25-30] which is based on a uniform distribution of critically damped (or Ohmic) oscillators and has a value of s = 1.

While line shape analysis can offer insight into the physical mechanisms producing scattering, it is important to keep in mind the challenge presented to unambiguously separate the various contributions to any liquid spectrum. By separating the spectrum into distinct components to represent the various contributing mechanisms, we make the assumptions that these scattering intensities are additive and that there is a clear separation between time scales of diffusive reorientational (OR) and the non-diffusive collision-induced dynamics. For anisotropic liquids, such as benzene, the separation between reorientational and translational/rotational CI components is often assumed. Molecular dynamics (MD) studies have shown however that CI-OR interference is significant in many instances, and at times even larger than either the purely CI or reorientational contribution to spectral intensities.[39,40] In calculations for CO_2 and several light diatomic molecules, it was noted that adding the contribution of this interference to the sum of the OR and CI components has the effect of broadening the spectrum and should not be neglected.[39] However, there are molecular liquids in which diffusive reorientational motions are significantly hindered with respect to the CI effects, and for these a clear time scale separation may be possible.[36,41-43] One such liquid is that of the heavy elongated CS_2 molecule, where

Table 3-1. Models for induced anisotropy of polarizability in molecular liquids. The collision-induced anisotropy of polarizability is $\Delta\alpha \sim r^{-m}$ and s is as defined in Eqn. 3.3.

Model	Mechanism	m	s
Hard sphere (Levine & Birnbaum)[7]	Electronic overlap (EO)	8.75	1.5
Deformable shell[9] Isotropic/Atomic	Electronic overlap (EO)	9	1.571
Anisotropic/Molecular[9]	Molecular frame distortion	13	2.714
Ohmic Model[53] (Time-domain work)[18,25-30]	Distribution of critically damped oscillators	7	1
DID[23,24]	Dipole-induced dipole effect	3	---
CIRRS,DQ[33,34]	Dipole-quadrupole effects	4	---
CIRRS, DO[33,34]	Dipole-octopole effects	5	---

calculated OR and CI spectra[36,41,42] have appreciably different shapes, well separated in frequency, and whose experimental data may be well fitted to a component resolved spectrum. A time scale separation for reorientational and interaction-induced scattering in methylene chloride (CH_2Cl_2) and chloroform ($CHCl_3$) may also be more valid than for the diatomic liquids and CO_2 of the MD studies due to slightly larger shape anisotropies and significantly higher densities to slow reorientational relaxation with respect to the CI dynamics. The symmetry of the CCl_4 molecule with no permanent anisotropy precludes any librational contribution and also makes cross correlation between the small amplitude diffusive component and CI effects negligible. Furthermore, the high liquid density of CCl_4 will tend to hinder the diffusive relaxation with respect to the CI effects resulting in a clear separation in frequency for these components.

3.3 CCl_4 Spectrum

Following the procedures described in chapter 2, data were obtained on liquid CCl_4 and a variety of line shapes were compared with the observed spectra to determine a best fit. Spontaneous LS spectra for atomic liquids[8,9,13,14] have shown that collision-induced scattering is well fitted with the weighted exponential form of Eqn. [3.2]. Later work involving several different techniques[2,44-46] used combinations of Lorentzian and Gaussian lineshapes to fit the complex intermolecular interactions of many molecular liquids. Expecting the dominance of purely translational CI scattering for CCl_4, our observed spectrum was fitted first with several single lineshapes:

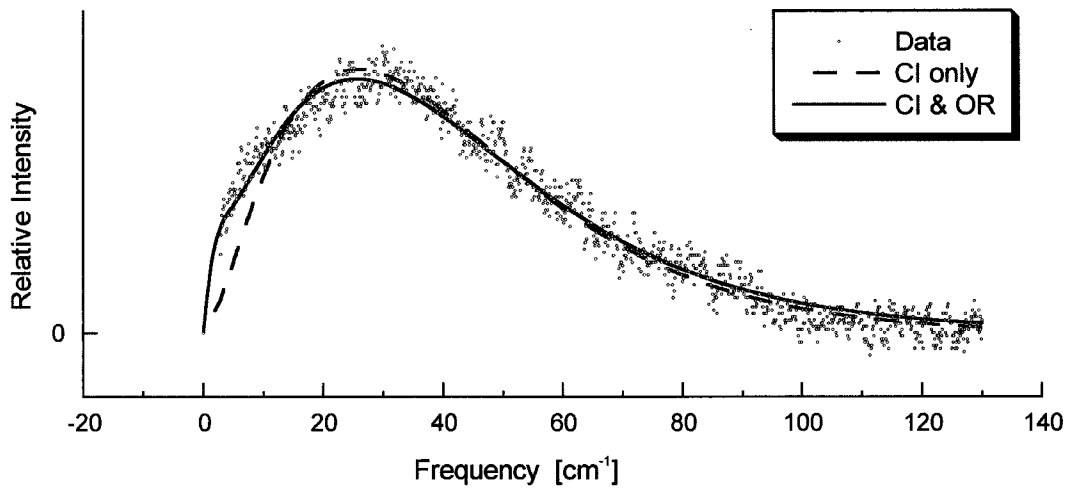

Figure 3.1 One vs. two component model for collision-induced scattering fitted to the SGS spectrum of CCl_4. Dashed line: spectrum fitted with only a weighted exponential (CI term) shows excess intensity below 10 cm^{-1}. Solid line: the spectrum fitted with weighted exponential (CI term) and a Lorentzian (OR) component provides a better match to data. Both fits are to the isotropic model, s = 1.571.

Lorentzian, Gaussian, and weighted exponential. Satisfactory fits were found only for the weighted exponentials. Additionally, as can be seen in Fig. 3.1, the spectrum showed an excess intensity in the low frequency (<10 cm^{-1}) region when a one-component fit was used, so a second component was added. Fits made with a Lorentzian centered at zero, with characteristic decay frequency, Γ, and a weighted exponential,

$$g(\omega) = \mathrm{Im}[G(\omega)] = A\omega[1/(\omega^2+\Gamma^2)] + B\omega^s \exp(-\omega/\omega_c) \qquad [3.5]$$

were found to describe the observed data well. As mentioned, most molecular liquids require one or more additional components to account for the complex interactions of translational/rotational character in CI scattering,

often modeled by a Gaussian lineshape to characterize librational caging at higher frequencies. Efforts to fit CCl_4 with a three-component model failed to provide meaningful results (see Section 3.7). This reflects the symmetry of the CCl_4 molecule and the fact that there are no strong electrostatic interactions to exert the intermolecular torque necessary for librational dynamics, further distinguishing CCl_4 as an isotropic liquid.

It is because of this symmetry that a low frequency Lorentzian component, such as appears in the liquid spectra of anisotropic molecules, is somewhat unexpected in CCl_4. Although this component has been noted earlier,[14,17,47] some uncertainty seems to remain as to its origin. A similar Lorentzian component is also found in monatomic liquids where it is attributed to a simple Debye diffusion mechanism.[21,48-51] For an atom in the liquid state, a brief period of free motion will be interrupted by intermolecular collisions and the resulting distortion produces anisotropy in the polarizability which will then relax through diffusive motions with a characteristic decay frequency, Γ. MD simulations which calculate the polarizability anisotropy autocorrelation functions corresponding to two-, three- and four-particle contributions to depolarized Rayleigh scattering (DRS) at various fluid densities further support this picture.[49] It has been shown that these individual correlation functions decay very slowly in the case of dense fluids, with relaxation times on the order of 5 picoseconds compared to about 0.4 ps for the total summed correlation function responsible for the depolarized scattering. The rapid decay of the total correlation function is largely due to the cancellation effects that liquid densities produce in the pair, triplet and quadruplet contributions to the scattering. A more physical description is simply that the long time tail of the pairs correlation function reflects the

longer time necessary for atoms to diffusionally separate as compared to the time required for relaxation of fluctuations in induced polarizability anisotropy caused by the small movements of near neighbors which produce the CI scattering. That a similar diffusion process provides the optical anisotropy responsible for the low frequency spectral component in isotropic molecular liquids is supported by measurements of the Lorentzian linewidths at various temperatures in CCl_4 and $GeCl_4$, suggesting the existence of a diffusion process related to viscosity.[17] The picture for CCl_4 is likely more complex than for a monatomic liquid. Evidence from neutron and x-ray diffraction data for liquid CCl_4[52] indicates significant orientational correlations due to some interlocking of the molecular structure which will also influence diffusive motion. Understandably, for even a relatively simple molecular liquid, there are significant difficulties in accurately deriving equations for spectral density from intermolecular forces involving up to four-body correlations between the forces on one pair of scatterers and the positions of another pair, making the more phenomenological curve-fitting approach an attractive alternative for the investigation and characterization of molecular motions in liquids.

In fitting a weighted exponential to account for the CI scattering of the CCl_4 data, several values for s, the power for the weighting factor to the exponential, were tried. These values were taken from the models by Levine and Birnbaum[7] for electronic overlap (EO) during binary collisions involving hard spheres on straight line trajectories (s = 1.5), Bucaro and Litovitz[9] for monatomic or isotropic molecular liquids involving deformable shells experiencing EO in binary collisions, (s = 1.571), Bucaro and Litovitz[9] for anisotropic molecular liquids experiencing molecular frame distortion during

binary collisions, (s = 2.714), and for a uniform distribution of critically damped (or Ohmic) oscillators, (s = 1), based on Leggett's work on the dynamics of dissipative systems,[53] which has been used in coherent time domain work.[18,25-30] There was little visible difference between the EO models using a hard sphere and an atomic (isotropic) deformable shell, and therefore results for the hard sphere model (s = 1.5) are not included in Figs. 3.2(a) and (b). Because the overall quality of fit was similar for all three models, Fig. 3.2(a), the collision-induced spectrum alone was fitted by masking out data below 10 cm^{-1}, Fig. 3.2(b). Fitting only the parameter for collision frequency , ω_c, the isotropic model (s = 1.571) provided the best fit visually and in terms of both a linear correlation coefficient (Pearson's r) and minimizing Chi-square. In addition to fitting the CCl_4 spectrum to the models described above, an effort was made to obtain a value for s directly from the observed spectrum by allowing s to vary as an additional parameter. When fitting only the CI spectrum (data points below 10 cm^{-1} masked), s returns a value of 1.53, strongly confirming the choice of an isotropic model and the calculated s = 1.571 value for CI scattering in CCl_4. When the low frequency Lorentzian component is included and the entire experimental spectrum is considered, s returns a value of 1.80 when allowed to vary as a free parameter, again in support of the isotropic model for CCl_4.

Fitting SGS data for CCl_4 with Eqn. [3.5] and s =1.571, values of 2.2 $\pm$ 0.5 cm^{-1} and 17.1 $\pm$ 0.1 cm^{-1} were obtained for Γ and ω_c respectively, Fig. 3.2(c). (It is worth noting that fitting only the CI spectrum with a single component as described above, the value ω_c = 17.0 $\pm$ 0.1 cm^{-1} is obtained. This close agreement in values for ω_c supports the validity of separating the frequency contributions of the diffusive and CI components.) The reported

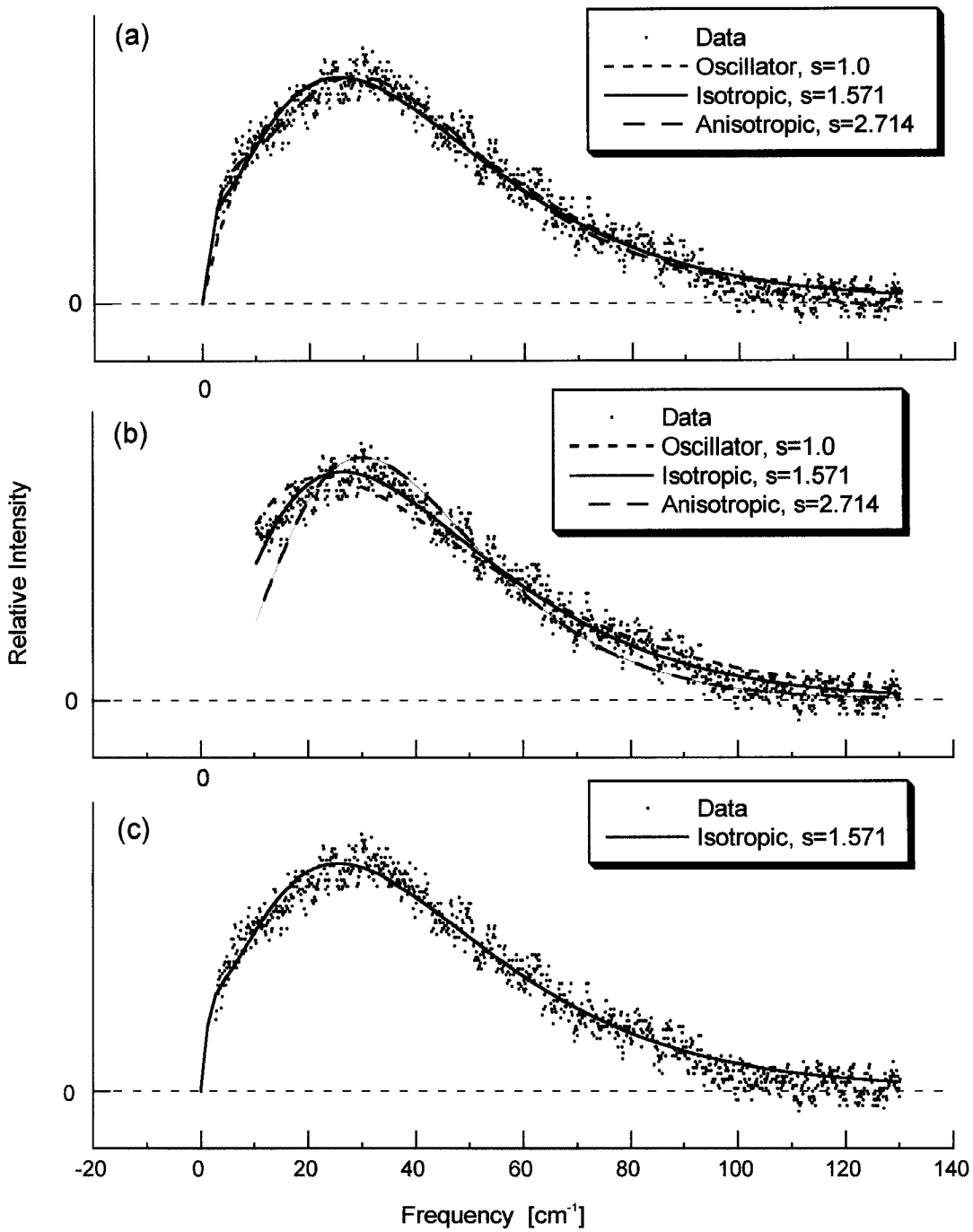

Figure 3.2 The SGS spectrum of CCl_4. (a) Spectrum fitted with dashed line represents the oscillator model, s=1. Quality of fit parameters: χ^2=27,200, r =.983; solid line is the isotropic model, s=1.571 with χ^2=27,000, r =.983; and dotted line is the anisotropic model, s=2.714, with χ^2=26,300, r =.984. (b) Data points below 10 cm^{-1} are removed and the spectrum is fitted with a single CI component. The different fits are as indicated in (a). Quality of fit parameters are now differentiated: oscillator model, χ^2=36,800, r =.977; isotropic model, χ^2=23,094, r =.986; and anisotropic model, χ^2=56,200, r =.964. (c) Best fit to the data employs the isotropic model with s=1.571 and yields values of 2.2$\pm$0.5 cm^{-1} and 17.1$\pm$0.1 cm^{-1} for Γ and ω_c, respectively.

error is the standard error value of the parameters as calculated by the Kaleidagraph® curve fitting program. A comparison of values obtained by different techniques and different fitting models is shown in Table 3-2. Notably the LS spectrum experiments can usually provide either ω_c or Γ reliably, but not both in one experiment due to instrumental limitation. Volterra, et. al.[14] were able to determine both ω_c and Γ, however resulted in an underestimate of ω_c and overestimate of Γ, owing to their choice of s = 2.714. The Stevens[17] value is a measurement of Γ using a high resolution Fabry-Perot interferometer, and is in excellent agreement with the best fitted value to the SGS data. With the exception of Castner et. al.,[19] the time domain experiments did not run a long enough time delay to catch the low frequency Lorentzian component, thus providing no information on Γ. Castner's data has been analyzed in the time domain in terms of two components[54] and recently, further analysis[55] of the same data has shown evidence for an additional intermediate frequency component without resolution of the associated rate. As noted earlier, our efforts to fit CCl_4 with a three-component model indicated that a third term was unnecessary to describe scattering from this symmetric molecule. Since Castner presented his data both as an OKE-RIKES transient signal and in a frequency domain representation, we analyzed his frequency spectrum using s = 1, generally used for time domain work in molecular liquids. This results in the values 2.2 $\pm$ 0.7 and 19.3 $\pm$ 0.3 cm^{-1} for Γ and ω_c, respectively, Table 3-2. Depending on the choice of s value, our results using s = 1.571 (isotropic model) are in general agreement with earlier reported values determined by light scattering and time domain techniques. The ability to simultaneously determine the best

fitted values of ω_c = 17.1 cm^{-1}, Γ = 2.2 cm^{-1}, and s = 1.571 from our SGS data provide added credibility for this result.

Table 3-2. Comparison of dynamical parameters in CCl_4 (in cm^{-1}).

Reference	ω_c	s	Γ
Gabelnick & Strauss (LS)[10]	19.6	1	
Gornall, et. al. (LS)[11]	17.4	1.5	
Volterra, Bucaro & Litovitz (LS)[12,7]	11.9	2.714	4.4
Howard-Lock & Taylor (LS)[13]	14.9	1.571	
Stuckart, Montrose & Litovitz (LS)[14]	20	1	
Stevens, Patterson, Carroll & Alms (LS)[15]			2.2
This work (SGS)	22.4±0.2[a]	1	
	17.7±0.1	1.5	1.8±0.6
	17.1±0.1	1.571	2.2±0.5
	11.7±0.1	2.714	5.4±0.3
Castner, et. al. (OHD-RIKES)[17]	19.3±0.3[b]	1	2.2±0.7[b]
Deuel, Cong, & Simon (OHD-OKE)[16]	16.8	1	
Vohringer & Scherer (OHD-OKE)[18]	17.7[c]		

[a] Since data starts at 2.8 cm^{-1}, it is difficult to accurately get a two-component fit for s=1. Therefore only the value for ω_c is shown for comparison purposes.

[b] See text.

[c] Value for characteristic relaxation time, τ_i = 0.30 ps, converted to cm^{-1}.

3.4 Collision-induced scattering in molecular liquids

Comparison of SGS results in CCl_4 to results for the same model applied to the SGS spectra of other simple liquids can provide additional insight into collision-induced scattering, into CCl_4 specifically, as well as into the quality of the model itself. Previous work in our lab[3,31,44] focused on determining the effects of molecular geometry on the depolarized spectra of simple liquids with the hope of providing new information on the dynamics involved in liquids. The measurement of a spectrum for carbon tetrachloride, a relatively weak scatterer, was attempted earlier without success, and its addition now to the existing SGS body of data has the value of being a more spherical molecule than the other chlorinated methanes previously examined. For comparison purposes, both the simple two-component model of Eqn. [3.5] and an expanded, three-component, model to account for rotational collisions and oscillations in somewhat less isotropic molecules will be applied to the SGS data for chloroform, methylene chloride, and carbon disulfide obtained earlier in our lab,[44] and to the spectrum for benzene measured for this work.

In liquids comprised of asymmetric molecules librational motions contribute additional intensity to the high frequency end of the Rayleigh-wing spectrum. An inhomogeneously broadened Gaussian lineshape is generally used[3,4,29,44-46] to fit the higher frequency contributions, providing a better fit than Lorentzian lineshapes for librational liquid dynamics. That the intermolecular spectrum is inhomogeneously broadened is consistent with scattering that arises from a constantly changing distribution of molecular environments present in a disordered liquid.[56] An antisymmetrized Gaussian

lineshape is used to ensure that the lineshape goes to zero at zero frequency and is given by

$$I_G(\omega) \sim \exp\left[-(\omega-\omega_o)^2/2\alpha^2\right] - \exp\left[-(\omega+\omega_o)^2/2\alpha^2\right] \qquad [3.6]$$

where ω_o is the band center frequency and α is the bandwidth. Combining Eqns. [3.5] and [3.6] results in a three-component model found to fit all the liquids studied well, with the exception of CCl_4 which lacks a librational component. While an association with purely translational CI dynamics is definitely appropriate for ω_c in CCl_4, this designation needs to be expanded for most other molecules in order to encompass the entangled translational/rotational interactions that exist for the less isotropic molecular liquids. To make this difference clear, the parameter ω_c is changed here to $1/\tau$ for the three component fits. As was done for CCl_4 in Chapter 3, fits were made using values of the power parameter, s, corresponding to each of the models for CI scattering (s = 1.00, 1.571, or 2.714) . Also for each liquid a fit was made while allowing s to vary as an additional free parameter. Interestingly, when s is a variable parameter in the three-component fits the value 1.00 is returned for each of the molecules fitted. This result was confirmed by comparing fits using the model-fixed values of s and noting that the fit for s = 1 proved to be the best for each liquid. This is in contrast to values of 1.3 to 1.5 for s when it is treated as a free parameter in the two component fits. As can be seen in Fig. 3.2(b), a smaller weighting factor, s, on the collisional component is associated with a broader linewidth and lower center frequency than for higher s values, suggesting that somewhat longer range mechanisms are responsible for scattering in these liquids than the

purely collisional EO indicated for CCl_4. In a two-component fit, values for s a little lower than 1.571 (purely EO scattering) occur because the less symmetric molecules see a less isotropic environment in which the lower order DID effects are not as completely canceled, thus adding intensity to the lower frequency portions of the spectrum. However, the addition of a third component to model the broad CI scattering has the effect of resolving a higher frequency librational term and shifting an intermediate term toward a lower frequency region of the spectrum so that the power parameter can no longer be directly associated with the models described earlier. The values obtained with the three-component fit (with s = 1), are reported in Table 3-3 and are in good agreement with those published earlier[31,44] which used a model comprised of two Lorentzian components and a Gaussian to fit the same spectra.

The two-component fit of Eqn. [3.5] essentially combines all interaction-induced effects into the one parameter, ω_c without differentiating translational and rotational collisions and higher frequency librational motions. While resolution of various components is less with fewer fit parameters, combining the interaction dynamics into a simple two-component model does offer some additional insight. Specifically here, comparison of the quality of fit for two- vs. three-component models can tell us something about how much of the nondiffusive scattering is due to simple translational collisions as well as indicate those liquids for which multiple scattering mechanisms demand at least one additional term to describe the scattered intensity.

Table 3-3. Fit parameters for the SGS spectra of the liquids studied (in cm^{-1}).

	2 Component Fit	2Component Fit w/ Fixed Value Γ	3 Component Fit
Liquid	**Γ / ω_c**	**Γ / ω_c**	**Γ / (1/τ) /ω_0/α**
CCl_4	2.2±0.5 / 17.1±0.1[a]		
$CHCl_3$	3.10±0.04 / 17.1±0.1[a]	2.69±0.07 / 16.7±0.1[a]	2.69±0.07 / 18±3[c] / 37±5 / 25±4
CH_2Cl_2	3.14±0.04 / 18.0±0.2[a]	2.81±0.09 / 17.3±0.2[a]	2.81±0.09 / 19±5[c] / 44±4/ 20±4
C_6H_6	3.93±0.04 / 29.1±0.1[a]	2.58±0.03 / 27.8±0.1[a]	2.58±0.03/11.1±0.1[c]/59.3±0.8/ 45.5±0.4
	5.09±0.05 / 20.0±0.1[b]	2.58±0.03 / 18.7±0.1[b]	2.58±0.03/11.1±0.1[c]/59.3±0.8/ 45.5±0.4
	3.18±0.05 / 38.0±0.2[c]	2.58±0.03 / 37.0±0.2[c]	2.58±0.03/11.1±0.1[c]/59.3±0.8/ 45.5±0.4
CS_2	3.75±0.06 / 19.5±0.1[a]	3.45±0.04 / 18.9±0.1[a]	3.45±0.04 / 22±2[c] / 48±2 / 21±2

[a] isotropic model fit, s = 1.571 [b] anisotropic model fit, s = 2.714 [c] ohmic model fit, s = 1.0

Again, as was done for CCl_4, the two component fits were made using values of s corresponding to each of the models for CI scattering. The results for the best fits are included with those of the three-component fits in Table 3-3. With the exception of benzene (and CCl_4 which was not fit with three components), values for ω_c in the two-component fits were generally close, 5-7% lower, to those found for $1/\tau$ in the three component fits, while values for Γ were about 9-15% higher. This discrepancy is due, in part, to the weighting factor of s = 1 used in the three-component fits. When the same weighting factor is used for both the two- and three-component fits, ω_c is broader in the two-component fit to incorporate the librational effects, and Γ

is very close in value for both fits as would be expected. Since the three-component fit provides better resolution of individual components, these values for Γ are likely to be more accurate. This led to fitting the spectra with the two-component model while holding Γ fixed at the values determined by the three-component fit. It can be seen, Table 3-3, that the results for ω_c, though depending on s value, are not strongly dependent on the value of Γ used, suggesting that the collision frequency so determined is robust.

Reasonable fits were obtained with the two-component model for all but benzene, most likely due to the much greater difference between the intermediate and high frequency components than for other liquids investigated. As noted in Table 3-3, the isotropic, deformable shell model provided the best two-component fit for the chlorinated methanes, and surprisingly also for CS_2. Further support for the choice of the isotropic model is obtained when s is a free parameter for the two-component fits. As expected, chloroform, with s = 1.48, is very close to the EO model, while methylene chloride, with s = 1.27, seems to experience somewhat longer range effects (less cancellation). Surprisingly, CS_2 at s = 1.35, also fits the EO model well. For reasons not yet clear to us, the CS_2 molecule appears in some way spherical to the probe light and two components provide nearly as good a fit as do three-components, Fig. 3.3. This implies that depolarized scattering in CS_2 is dominated by translational collisions, a conclusion which is also suggested by MD simulation results.[57] For the chlorinated methanes also, EO collisions contribute significantly to the spectrum and the fits compare fairly well with those of the three-component model, Figs. 3.4 and 3.5, especially for frequencies above 20 cm^{-1}. By contrast, the

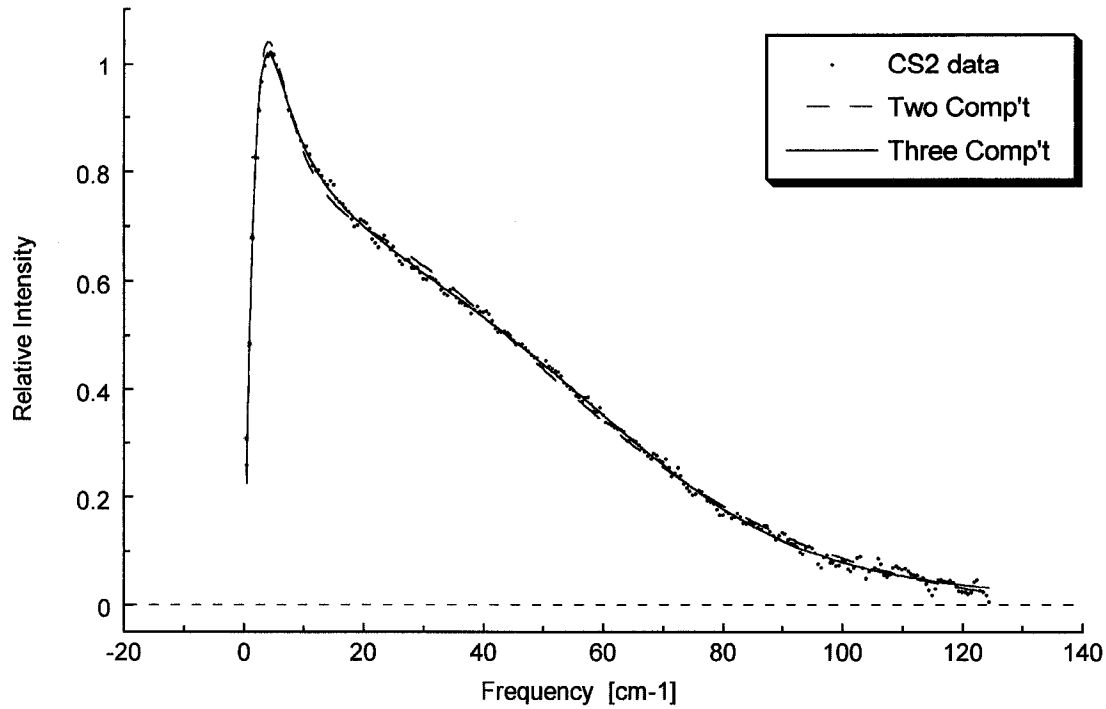

Figure 3.3 The SGS spectrum of CS_2. The two-component isotropic model (dashed line) provides almost as good a fit as the three component model (solid line).

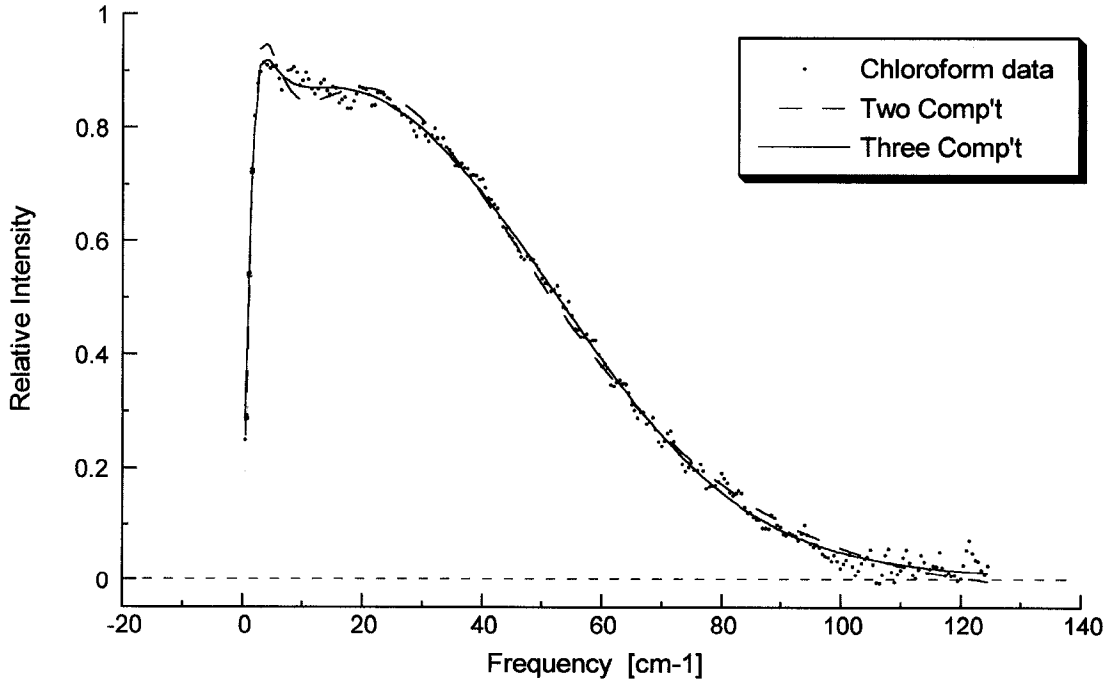

Figure 3.4 The SGS spectrum of $CHCl_3$. Dashed line: The two component isotropic model is fit to the spectrum; Solid line: The three component model is fit.

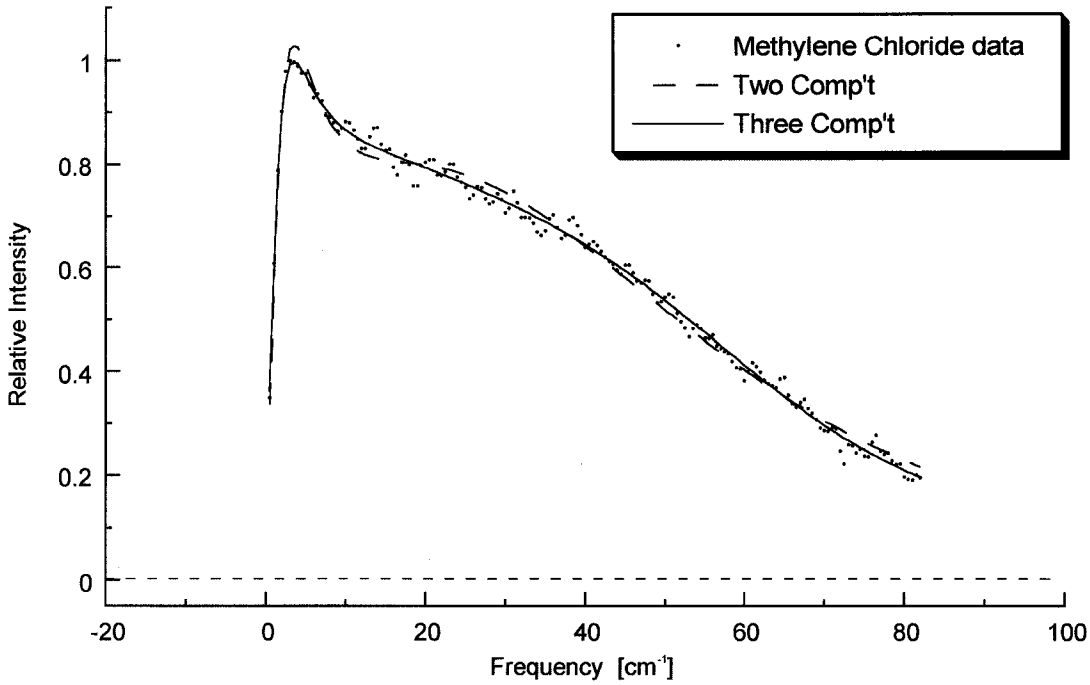

Figure 3.5 The SGS spectrum of CH_2Cl_2. Dashed line: The two component isotropic model is fit to the spectrum; Solid line: The three component model is fit.

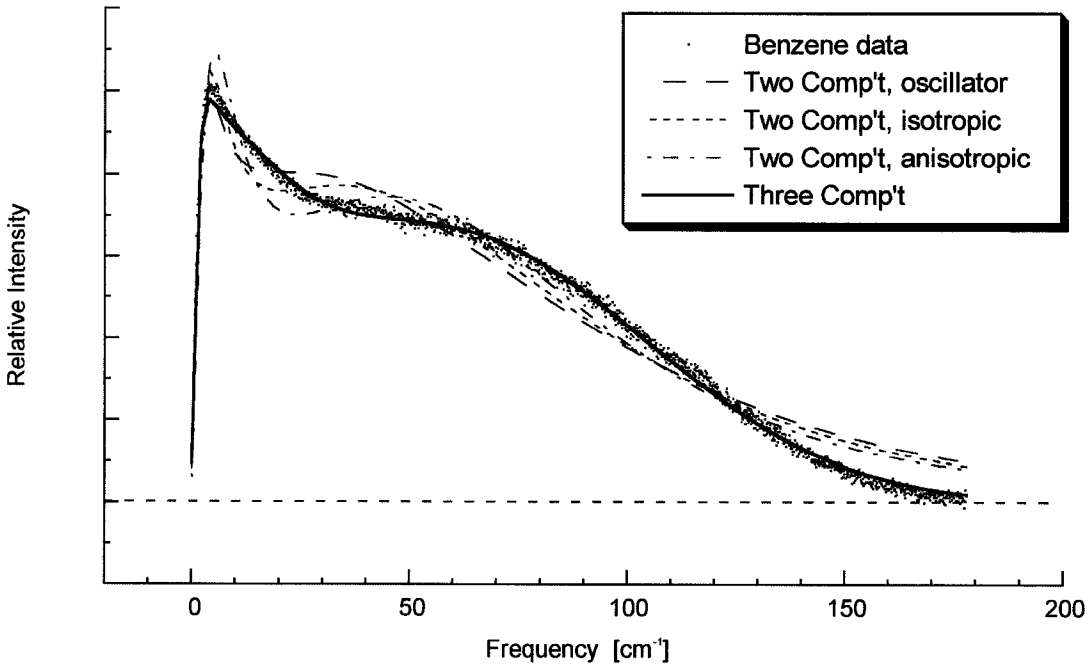

Figure 3.6 The SGS spectrum of C_6H_6. Spectrum is not adequately fit by any two component model: long dash represents the oscillator model, with s=1; short dash the isotropic model, with s=1.571; dot-dash line the anisotropic model, with s=2.714. Solid line: The three component fit, with s=1.0, is fit to the spectrum.

two-component fit for benzene is problematic, Fig. 3.6. In liquid benzene, librational dynamics dominate the depolarized spectrum[54,58] and occur at a higher center frequency, ω_o, than observed in the other liquids. Its collisional component, $1/\tau$, is weaker and relatively narrow. Clearly, combining both of these frequency components into ω_c will cause more problems for the fit to benzene than for the others. The benzene spectrum is shown fitted to all of the two-component models. While the anisotropic (s = 2.714) model provides a marginally better fit to the spectrum, none of the two-component models result in a quality fit to the spectrum, and none can fully account for the spectrum at intermediate frequencies.

3.5 Discussion: Effects of collision and reorientational dynamics on liquid spectra

Microscopic molecular structure and macroscopic (collective) liquid properties both affect the intermolecular interactions that produce depolarized light scattering. Liquid spectra detected with SGS have sufficient resolution to correlate spectral lineshapes to some of these underlying properties. Among the physical properties found to affect diffusive reorientation, intermolecular collisions and librational oscillation are the moment of inertia, mass, and shape anisotropy of the molecule, as well as the density and shear viscosity of the liquid.[44] Table 3-4 lists these parameters for the liquids studied. Values for shape anisotropy are determined by first calculating thelengths of a molecule in the direction of each principle axis, l_x, l_y, and l_z, with the z axis having highest symmetry. The ratio of l_z, and the larger of l_x,

Table 3-4. Physical parameters for the liquids studied, at room temperature and atmospheric pressure)

Parameter	CCl_4	$CHCl_3$	CH_2Cl_2	C_6H_6	CS_2
Shear viscosity, η [cp]	0.969	0.58	0.43	0.652	0.363
Density, ρ [g /cm^3]	1.59	1.48	1.33	0.879	1.26
I_x [10^{-45}kg-m^2]	4.93	2.62	2.74	1.48	2.58
I_y [10^{-45}kg-m^2]	4.93	2.62	0.28	1.48	2.58
I_z [10^{-45}kg-m^2]	4.93	4.97	2.51	2.96	0
I [10^{-45}kg-m^2]	4.93	3.58	2.15	2.10	2.11
Mass [amu]	153.8	119.4	84.9	78.1	76.1
Shape anisotropy, Σ	1.0	1.45	1.45	2.05	1.86
α_1 [Å^3]	10.5	6.68	5.02	12.31	15.14
α_2 [Å^3]	10.5	9.01	8.47	6.35	5.54
α_3 [Å^3]	10.5	9.01	5.96	12.31	5.54

or l_y taken to give a value equal or greater than unity is defined as the shape anisotropy of the molecule, Σ.

Diffusive reorientation reflects collective motion of molecules in a liquid, so is not surprising that diffusion rates are affected by macroscopic liquid properties, such as shear viscosity. Lower diffusion rates, Γ, result with increasing density and viscosity, both of which inhibit the relaxation of density fluctuations in the local structure. Of these, viscosity exerts a stronger influence on diffusion and reorientation rates in molecular liquids, while the effects of density are more clearly seen in molecules with the same general molecular shape, i.e., linear, planar, or quasi-spherical.[44] Within the group of chlorinated methanes, the higher density and viscosity and the

smaller diffusion rate of CCl_4 are as would be expected. Comparing the different values for Γ obtained with the three-component fit shows that an inverse relationship between the shear viscosity of a liquid and its diffusive reorientation rate holds well for each of the liquids examined. The Γ values determined with the two-component fits also are inversely proportional to the viscosity, with the exception of benzene, further emphasizing the need for a three-component model to fit its spectrum adequately.

In confirmation of our earlier results,[44] it was found that higher frequency librational dynamics are dependent on molecular shape anisotropy and moment of inertia. In Table 3-4, the moments of inertia were calculated from bond lengths[59] and Van der Waals radii for the constituent atoms of the molecules.[59] These calculation were made with respect to the x-axis as the most Raman active, so that I_x is the dominant moment of inertia most responsible for determining librational frequency. Comparison of values for ω_o were found to be roughly proportional to I_x^{-1}, seen most noticeably in the much lower value of I_x for benzene and its significantly higher libration frequency.

The intermediate frequency regime, if in fact it is associated predominantly with translational CI dynamics, should be inversely related to molecular mass. In a binary collision, the relationship between ω_c and molecular mass is such that $1/\omega_c = \gamma^{-1}(\mu / k_B T)^{1/2}$, where μ is the reduced mass of a colliding pair of molecules, k_B is the Boltzmann constant and T is the absolute temperature.[13,15] The constant of proportionality, γ^{-1}, is a measure of the separation between two colliding molecules at the point of maximum induced anisotropy.[13] Howard-Lock and Taylor[15] used this relationship as an

additional check on their determination of weighting factors in the models for isotropic/anisotropic liquids. When they plotted values for $1/\omega_c$ corresponding to s = 1.571 for isotropic and s = 2.714 for anisotropic liquids against $(\mu /T)^{1/2}$, a straight line with zero intercept resulted from a least squares fit, reproduced in Figure 3.7(a). When these values for s were reversed, the points fell considerably off the line. This single linear plot both supports the choice of weighting factor for isotropic/anisotropic liquids and may also imply a single distance for maximum induced anisotropy for most liquids. A value of 0.6Å for γ^{-1} was determined independently by both Howard-Lock et.al.[15] and Gornall et. al.[13]

The quality of the fit using the two-component model for a given liquid will depend strongly on the extent to which translational collisions are responsible for the depolarized spectrum. Our results with fits to both the isotropic and anisotropic two-component models are shown in Fig. 3.7(b) on the straight line determined by Howard-Lock and Taylor. Values for CS_2 and the chlorinated methanes fitted to the isotropic model are all within about two wave numbers of the straight line fit, while they fall further from the indicated line if the anisotropic model is used. It is interesting that this plot strongly supports an isotropic model fit for CS_2 just as our fitting results did. The values for benzene support the anisotropic model for this planar molecule, with the anisotropic fit yielding a value for ω_c which is 1.1 cm^{-1} above the straight line fit while the isotropic fit is 8.0 cm^{-1} below. The small deviation of the liquids in Fig. 3.7(b), and in Ref. 13, from a simple straight line fit indicates that mass is an important (though not the only) factor contributing to the complicated dynamics which produce collision-induced spectra. Shape

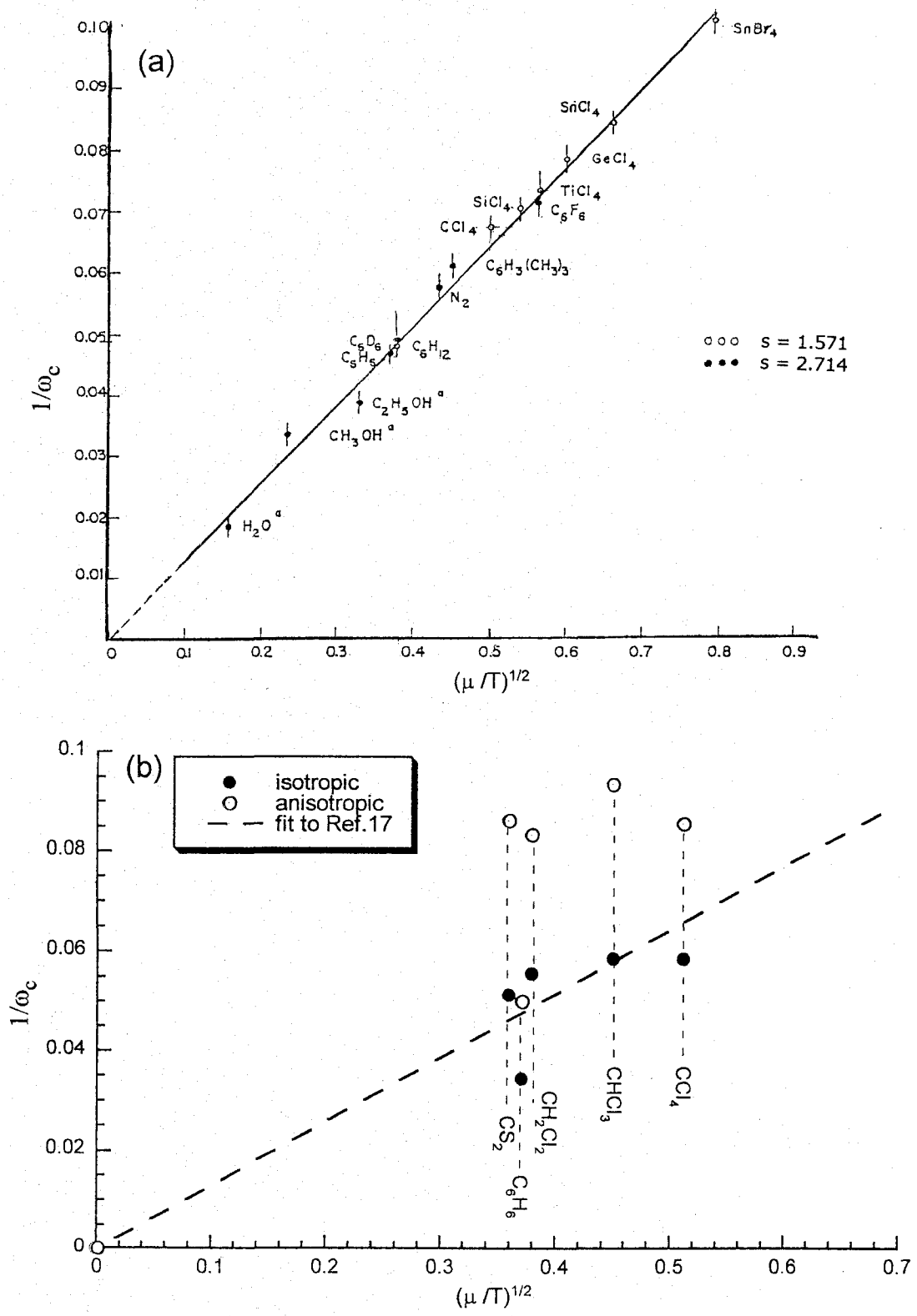

Figure 3.7 (a) Graph of experimental values of $1/\omega_c$ vs. $(\mu/T)^{1/2}$ reproduced from Ref. [15]. (b) Same graph using SGS values and plotted with the least squares fit for the molecular liquids of Ref. [15].

anisotropy, by determining how far a molecule can tip before colliding with a neighbor, also impacts collisional responses.[44] However, the shape anisotropy of liquid molecules plays a lesser role in selecting between models for best fit (or determining s values) than originally expected.

3.6 Conclusions

To summarize, a SGS spectrum for liquid CCl_4 has been fit with a two-component model consisting of a Lorentzian lineshape function with a damping rate, Γ, to represent diffusive relaxation and a weighted exponential function of the form $\omega^s \exp(-\omega/\omega_c)$ with a characteristic frequency, ω_c, corresponding to collision-induced scattering. In the case of CCl_4, a model based on binary interactions resulting in a collision-induced electronic repulsive force with a r^{-9} dependence (s = 1.571) provided the best fit to the liquid spectrum. The fitted values were $\Gamma = 2.2 \pm 0.5$ cm^{-1} and $\omega_c = 17.1 \pm 0.1$ cm^{-1}, in general agreement with earlier measurements from light scattering and coherent time-domain techniques.[1-10]

These results for CCl_4 enable comparison with several other, less symmetric, liquids. While a three-component model which decomposes the CI component into an intermediate frequency term and a librational term is generally best for less isotropic molecules, we found that the two-component model for diffusive reorientation and CI scattering due to translational EO effects was able to account for scattering from the less symmetric $CHCl_3$, CH_2Cl_2 and CS_2 molecules surprisingly well. Thus, even at liquid densities, we find that short-range binary collisions play a primary role in depolarized

scattering. The limited range of values of ω_c (roughly 17 to 20 cm^{-1} with the two-component fits) for these liquids suggests that, in terms of collision-induced effects, these liquids behave similarly with a maximum induced anisotropy occurring at nearly the same interaction distances. The inadequacy of a two-component model for liquid benzene can be attributed to the dominance of fast librational motions requiring a third component to account for the scattered spectrum.

3.7 Recent studies of intermolecular interactions in molecular liquids

Since the completion in 1996 of the SGS experiment reported on here, there have been a few new investigations of intermolecular interactions in liquids, although none of these, to our knowledge has been specific to CCl_4. This section will briefly highlight some of these experiments, as well as new techniques being developed to probe aspects of liquid dynamics different than those observed with SGS.

Recent work (1999-2001) using OHD-OKE spectroscopy has focused on the identification of a new component in the picosecond relaxation dynamics (usually associated with orientational diffusion) of several symmetric top molecular liquids,[6,60] and monosubstituted benzene liquids.[61] Describing the picosecond response as two exponentially decaying functions in time-domain, the faster of these has a relaxation time that is shorter than that for collective reorientational diffusion but longer than the mean collision time in the liquid. The temperature dependence of this relaxation indicates it is related to hydrodynamic effects and strongly correlated with the collective

orientational correlation time.[60] This suggests to us the possibility of a second relaxation mechanism for diffusive reorientation, much as was observed in the SGS spectrum for iodobenzene.[44] The new component in the time-domain data has been analyzed with the application of Kubo theory to OKE spectroscopy[6,60,62] with the suggestion that the exponential relaxation may arise from motional narrowing in the liquid. The time constant derived from Kubo parameters for this exponential component, however, exhibits a temperature dependence opposite to that observed for it in the experimental data.[60,63]

Another possibility is that this faster exponential decay arises from structural relaxation occurring on a picosecond time scale.[61] A theoretical calculation (2002) for the temperature evolution of the OKE spectrum of liquid benzene[63] supports this view, proposing that the instantaneous local order seen in a liquid by a picosecond or femtosecond pulse maintains a quasicrystalline structure. It is these local clusters (comprised of a molecule and its nearest neighbors) that undergo the collective translational and rotational normal mode motions which are responsible for the interaction-induced spectrum.[63] The faster ps relaxation discussed above would be associated with collective translational modes. In this model, the temperature behavior accurately reflects experimental results.

Our analysis of CCl_4, showed no indication of an additional low frequency feature in CCl_4 comparable to that seen in the symmetric top molecular liquids of the time-domain studies. Various three component fits were made to the spectrum, including one comprised of the CI component and two Lorentzians which would correspond to the two exponentially decaying responses seen in the time-domain data. Regardless of the

functional form, in every case the fitted values for one of the three components used were identical, within limits of error, to the values of one of the other two components. Our results thus indicate that a third component is unnecessary for a full description of the CCl_4 spectrum. The absence of a low-frequency shoulder corresponding to the component in the time-domain experiments is somewhat surprising if its origin is indeed in collective translational modes. However, the fact that the picosecond component was evidently augmented at low temperatures may help to explain its absence in the room temperature CCl_4 spectrum.

The last few years have also seen the development of several new experimental techniques for the study of intermolecular interactions in liquids. Among these are techniques utilizing polarization selectivity to access components of the susceptibility tensor different than those probed by SGS or OHD-OKE. In the case of isotropic molecular liquids, symmetry considerations limit this tensor quantity to four nonvanishing elements which obey the relationship

$$\chi^{(3)}_{zzzz} = \chi^{(3)}_{zzyy} + \chi^{(3)}_{zyzy} + \chi^{(3)}_{zyyz}. \qquad [3.7]$$

Furthermore, since the optical frequencies for experiments relevant to intermolecular dynamics are much less than the frequencies of electronic transitions, Kleinman symmetry[64] implies

$$\chi^{(3)}_{zzyy} = \chi^{(3)}_{zyzy} = \chi^{(3)}_{zyyz} = \frac{1}{3}\chi^{(3)}_{zzzz}, \qquad [3.8]$$

leaving just one nonzero independent element. Most third-order experiments measure either the polarized or depolarized component, $\chi^{(3)}_{zzzz}$ or $\chi^{(3)}_{zzyy}$,

respectively. New investigations [38,65,66] are choosing to access what have been termed isotropic and anisotropic components, $\chi^{(3)}_{zzmm}$ and $\chi^{(3)}_{zzyy}$, respectively, where m denotes an axis forming an angle of 54.74° with the z-axis. The anisotropic component is identical to the depolarized component accessed by SGS, but the isotropic component is related to the polarized and depolarized components through[38,65]

$$\chi^{(3)}_{zzmm} = \chi^{(3)}_{zzzz} + 2\chi^{(3)}_{zzyy}. \qquad [3.9]$$

Probing the isotropic and anisotropic components distinguishes between contributions to the molecular dynamics based on symmetry properties. In a molecular liquid, the isotropic response reflects translational density fluctuations, motions that are symmetric in the ensemble average, while the anisotropic response is due to collective reorientational motions (diffusion) and molecular reorientations (libration).[66]

Polarization-selective measurements have been made using diffractive optics and phase-sensitive detection of a transient grating experiment[65] (2000) as well as by using a spatially masked optical Kerr effect (SM-OKE) spectroscopy[66] (2002) in conjunction with conventional OHD-OKE to measure both the isotropic and anisotropic portions of the response function. Both of these experiments offer an advantage for clearly separating the translational collision dynamics from the orientational (diffusion and libration) dynamics in liquids of nonspherical molecules. This advantage would be much less, however, in CCl_4 where the symmetry of the molecule precludes librational dynamics and the small amplitude diffusive component is separable in frequency from the CI component.

Two-dimensional lineshapes derived from multiple types of coherent third-order nonlinear spectroscopies[67] and heterodyne-detection of the fifth-order Raman response[68-70] are other tools being developed for use in conjunction with OHD-OKE measurements as a possible probes of both the structure and the microscopic dynamics of condensed phases.

3.8 References

1. D. McMorrow, W. Lotshaw, and G. Kenney-Wallace, "Femtosecond optical Kerr studies on the origin of the nonlinear responses in simple liquids," IEEE J. Quantum Electron. **24**, 443 (1988).

2. C. E. Barker, R. Trebino, A. G. Kostenbauder and A. E. Siegman, "Frequency-domain observation of the ultrafast inertial response of the optical Kerr effect in CS_2," J. Chem. Phys. **92**, 4740 (1990).

3. J. S. Friedman, M. C. Lee and C. Y. She, "Depolarized stimulated gain spectra of liquid CS_2 and benzene at room temperature," Chem. Phys. Lett. **186**, 161 (1991).

4. Y. J Chang and E. W. Castner, Jr., "Intermolecular dynamics of substituted benzene and cyclohexane liquids, studied by femtosecond nonlinear-optical polarization spectroscopy," J. Phys. Chem., **100**, 3330 (1996).

5. B.-R. Hyun, S. V. Dzyuba, R. A Bartsch, and E.L. Quitevis, "Intermolecular dynamics of room-temperature ionic liquids: Femtosecond optical Kerr effect measurements on 1-akyl-3-methylimidazolium bis(trifluoromethyl)sulfonyl," J. Phys. Chem., **106**, 7579 (2002).

6. M. Ricci, P. Bartolini, R. Chelli, G. Cardini, S. Califano and R. Righini, "The fast dynamics of benzene in the liquid phase. Pt.I. Optical Kerr effect experimental investigation" Phys. Chem. Chem. Phys., **3**, 2795 (2001).

7. H. B. Levine and G. Birnbaum, "Collision-induced light scattering," Phys. Rev. Lett. **20**, 439 (1968).

8. J. P. McTague, P. A. Fluery and D. B. DuPre, "Intermolecular light scattering in liquids," Phys. Rev. **188**, 303 (1969).

9. J. A. Bucaro and T. A. Litovitz, "Rayleigh scattering: Collisional motions in liquids," J. Chem. Phys. **54**, 3846 (1971).

10. W. M. Gelbart, "Review of calculations and analyses of available measurements on depolarized scattering of light by simple fluids," Adv. Chem. Phys. **26**, 1 (1974).

11. G. Birnbaum, ed., *Phenomena Induced by Intermolecular Interactions*, NATO ASI Series B 127 (Plenum, New York, 1985).

12. H. L. Gabelnick and H. L. Strauss, "Low-frequency motions in liquid carbon tetrachloride. II. The Raman spectrum," J. Chem. Phys. **49**, 2334 (1968).

13. W.S. Gornall, H.E. Howard-Lock, and B.P. Stoicheff, "Induced anisotropy and light scattering in liquids," Phys. Rev. A, **1**, 1288 (1970).

14. V.Volterra, J.A. Bucaro and T.A. Litovitz, "Molecular motion and light scattering in liquids," Ber. Bunsenges. Phys. Chem. **75**, 309 (1971).

15. H.E. Howard-Lock and R.S. Taylor, "Induced anisotropy and light scattering in liquids. II," Can. J. Phys. **52**, 2436 (1974).

16. R.A. Stuckart, C.J. Montrose and T.A. Litovitz, "Comparison of interaction induced light scattering and infrared absorption in liquids," Faraday Symp. Chem. Soc. **11**, 94 (1977).

17. J.R. Stevens, G.D. Patterson, P. J. Carroll and G. R. Alms, "The central Lorentzian in the depolarized Rayleigh spectra of liquid CCl_4 and $GeCl_4$," J. Chem. Phys. **76**, 5203 (1982).

18. H. Deuel, P. Cong, and J. Simon, "Probing intermolecular dynamics in liquids by femtosecond optical Kerr effect spectroscopy : Effects of molecular symmetry," J. Phys. Chem. **98**, 12600 (1994).

19. E. W. Castner, Jr., Y. Chang, J. Melinger, and D. McMorrow, "Femtosecond Fourier-transform spectroscopy of low-frequency intermolecular motions in weakly interacting liquids," J. Lumin. **60 & 61**, 723 (1994).

20. P. Vöhringer and N. Scherer, "Transient grating optical heterodyne detected impulsive stimulated Raman scattering in simple liquids," J. Phys. Chem. **99**, 2684 (1995).

21. J. P. McTague and G. Birnbaum, "Collision-induced light scattering in gaseous Ar and Kr," Phys. Rev. Lett. **21**, 661 (1968).

22. V. Volterra, J.A. Bucaro and T. A. Litovitz, "Two mechanisms for depolarized light scattering from gaseous argon," Phys. Rev. Lett., **26**, 55, (1971).

23. A. D. Buckingham and M. J. Stephen, "A theory of the depolarization of light scattered by a dense medium," Trans. Faraday Soc. **53**, 884, (1957).

24. M. Thibeau and B. Oksengorn, "Theoretical study of spectral width of depolarized part of Rayleigh light scattered by a compressed rare gas," Mol. Phys. **15**, 579 (1968).

25. M. Cho, S.J. Rosenthal, N.F. Scherer, L.D. Ziegler, G.R. Fleming, "Ultrafast solvent dynamics: connection between time resolved fluorescence and optical Kerr measurements," J. Chem. Phys. **96**, 5033, (1992).

26. M. Cho, M. Du, N.F. Scherer, G.R. Fleming, and S. Mukamel, "Off-resonant transient birefringence in liquids," J. Chem. Phys. **99**, 2410 (1993).

27. P. Vöhringer, C. C. Arnett, R. A. Westervelt, M. J. Feldstein, and N. F. Scherer, "Optical dephasing on femtosecond time scales: Direct measurement and calculation from solvent spectral densities," J. Chem. Phys. **102**, 4027 (1995).

28. S. Kinoshita, Y. Kai, and Y. Watanabe, "Origin of initial rise process of ultrafast exponential response in liquids," Chem. Phys. Lett. **301**, 183 (1999).

29. N. A. Smith and S. R. Meech, "Ultrafast dynamics of polar monosubstituted benzene liquids studied by the femtosecond optical Kerr effect," J. Phys. Chem. A, **104**, 4223 (2000).

30. M. Neelakandan, D. Pant, E. L. Quitevis, "Structure and intermolecular dynamics of liquids: Femtosecond optical Kerr effect measurements in nonpolar fluorinated benzenes," J. Phys. Chem. A, **101**, 2936 (1997).

31. J. S. Friedman, "Stimulated Rayleigh-Brillouin spectroscopy for studying low frequency dynamics in simple liquids," Ph.D. dissertation, Colorado State University, (1992).

32. A. D. Buckingham and G. C. Tabisz, "Collision-induced rotational Raman scattering by tetrahedral and octahedral molecules," Mol. Phys. **36**, 583 (1978).

33. A. D. Buckingham and G. C. Tabisz, "Collision-induced rotational Raman- scattering by tetrahedral and octahedral molecules," Opt. Lett. **1**, 220 (1977).

34. H. A. Posch, "Collision-induced light scattering from fluids composed of tetrahedral molecules. I," Mol. Phys. **37**, 1059 (1979).

35. G. C. Tabisz, N. Meinander and A. R. Penner, "Interaction induced rotational light scattering in molecular gases," in *Phenomena Induced by Intermolecular Interactions*, edited by G. Birnbaum, NATO ASI Series B 127 (Plenum, New York, 1985).

36. P. M. Madden, "Theory and experimental aspects of collision induced processes," in *Spectroscopy and Relaxation of Molecular Liquids*, edited by D. Steele and J. Yarwood, Studies in Physical and Theoretical Chemistry, Vol. 74 (Elsevier Science Publishers, Amsterdam, 1991).

37. M. Neumann and H. A. Posch, "Interaction induced light scattering from tetrahedral molecules," in *Phenomena Induced by Intermolecular Interactions*, edited by G. Birnbaum, NATO ASI Series B 127 (Plenum, New York, 1985).

38. T. I. C. Jansen, M. Swart, L. Jensen, P. T. van Duijnen and J. G. Snijders, "Collision effects in the nonlinear Raman response of liquid carbon disulfide," J. Chem. Phys. **116**, 3277 (2002).

39. D. Frenkel and J. P. McTague, "Molecular dynamics studies of orientational and collision-induced light scattering in molecular fluids," J. Chem. Phys. **72**, 2801 (1980).

40. B. M. Ladanyi, "Molecular dynamics study of Rayleigh light scattering from molecular fluids," J. Chem. Phys. **78**, 2189 (1983).

41. P. A. Madden and D. J. Tildesley, "Interaction-induced contributions to Rayleigh and allowed Raman bands--A simulation study of CS_2," Mol. Phys. **55**, 969 (1985).

42. L. C. Geiger and B. M. Ladanyi, "Higher order interaction-induced effects on Rayleigh light scattering by molecular liquids," J. Chem. Phys. **87**, 191, (1987).

43. M. Paolantoni and B. M. Ladanyi, "Polarizability anisotropy relaxation in liquid ethanol: a molecular dynamics study," J. Chem. Phys. **117**, 3856, (2002).

44. J. S. Friedman and C. Y. She, "The effects of molecular geometry on the depolarized stimulated gain spectra of simple liquids," J. Chem. Phys. **99**, 4960 (1993).

45. C. Kalpouzos, D. McMorrow, W. Lotshaw, and G. Kenney-Wallace, "Femtosecond laser-induced optical Kerr dynamics in CS_2/alkane binary solutions," Chem. Phys. Lett. **150**, 138 (1988); Chem. Phys. Lett. **155**, 240 (1989).

46. S. Ruhman, B. Kohler, A. G. Joly, and K. A. Nelson, "Intermolecular vibrational motion in CS_2 liquid at $165 \leq T \leq 300$ K," Chem. Phys. Letters **141**, 16 (1987).

47. J. A. Bucaro and T. A. Litovitz, "Molecular motions in CCl_4: Light scattering and infrared absorption," J. Chem. Phys. **55**, 3585 (1971).

48. P.A. Madden, "Depolarized Rayleigh scattering from fluids of spherical molecules," Mol. Phys. **36**, 365 (1978).

49. A. J. C. Ladd, T. A. Litovitz, and C. J. Montrose, "Molecular dynamics studies of depolarized light scattering from argon at various fluid densities," J. Chem. Phys. **71**, 4242 (1979).

50. S-C. An, Montrose, and Litovitz, "Low frequency structure in the depolarized spectrum of argon," J. Chem. Phys. **64**, 3717 (1976).

51. S-C. An, L. Fishman, T. A. Litovitz, C.J. Montrose, "Depolarized light scattering from dense noble gases," J. Chem. Phys.**70**, 4626 (1979).

52. A.H. Narten, "Liquid carbon tetrachloride: Atom pair correlation functions from neutron and x-ray diffraction," J. Chem. Phys. **65**, 573 (1976).

53. A. J. Leggett, S. Chakravarty, A.T.Dorsey, M. Fisher, A. Garg and W. Zwerger, "Dynamics of the dissipative two-state system," Rev. Mod. Phys. **59**, 1 (1987).

54. W. T. Lotshaw, D. McMorrow, N. Thantu, J. S. Melinger, and R. Kitchenham, "Intermolecular vibrational coherence in molecular liquids," J. Ram. Spect. **26**, 571 (1995).

55. D. McMorrow, N. Thantu and J. S. Melinger, "Symmetry breaking in condensed phases: the interaction-induced optical Kerr response of liquid CCl_4," in *Nonlinear Optics '98. Materials, Fundamentals and Applications Topical Meeting*, (IEEE, New York, 1998).

56. D. McMorrow, N. Thantu, V. Kleinman J. S. Melinger, and W. T. Lotshaw, "Analysis of intermolecular coordinate contributions to third-order ultrafast spectroscopy of liquids in the harmonic oscillator limit," J. Phys. Chem. A, **105**, 7960 (2001).

57. L. C. Geiger and B. M. Ladanyi, "Molecular dynamics simulation study of nonlinear optical response of fluids," Chem. Phys. Lett., **159**, 413, (1989).

58. P. Cong, H. P. Deuel and J. D. Simon, "Structure and dynamics of molecular liquids investigated by optical-heterodyne detected Raman-induced Kerr effect spectroscopy," Chem. Phys. Lett., **240**, 72, (1995).

59. R. C. Weast, ed., *CRC Handbook of Chemistry and Physics*, CRC Press (Cleveland, Ohio 1976).

60. B. J. Loughnane, A. Scodinu, R. A. Farrer, J. T. Fourkas, "Exponential intermolecular dynamics in optical Kerr effect spectroscopy of small-molecule liquids," J. Chem. Phys. **111**, 2686 (1999).

61. N. A. Smith and S. R. Meech, "Ultrafast dynamics of polar monosubstituted benzene liquids studied by the femtosecond optical Kerr effect," J. Phys. Chem. A, **104**, 4223 (2000).

62. R. Kubo, "Stochastic Liouville equations," J. Math. Phys. **4**, 174 (1963).

63. B. Ratajska-Gadomska, "Temperature evolution of the low-frequency optical Kerr effect spectra of liquid benzene in quasicrystalline approach," J. Chem. Phys.,**116**, 4563 (2002).

64. P. N. Butcher and D. Cotter, Cambridge Studies in Modern Optics, Vol. 9, *The Elements of Nonlinear Optics*, Cambridge University Press, (1990).

65. M. Khalil, N. Demirdoven, O. Golonzka, C. J. Fecko, and A. Tokmakoff, "A phase-sensitive detection method using diffractive optics for polarization-selective femtosecond Raman spectroscopy," J.Phys. Chem. A, **104**, 5711 (2000).

66. C. J. Fecko, J. D. Eaves, and A. Tokmakoff, "Isotropic and anisotropic Raman scattering from molecular liquids measured by spatially masked optical Kerr effect spectroscopy," J.Chem. Phys., **117**, 1139, (2002).

67. A. Tokmakoff, "Two-dimensional line shapes derived from coherent third-order nonlinear spectroscopy," J. Phys. Chem. A, **104**, 4247 (2000).
68. A. Tokmakoff and G. R. Fleming, "Two-dimensional Raman spectroscopy of the intermolecular modes of liquid CS_2," J. Chem. Phys. **106**, 2569 (1997).

69. A. Tokmakoff, M. J. Lang, D. S. Larsen and G. R. Fleming, "Intrinsic optical heterodyne detection of a two-dimensional fifth-order Raman response," Chem. Phys. Lett. **272**, 48 (1997).

70. K. Okumura, A. Tokmakoff and Y. Tanimura, "Structural information from two-dimensional fifth-order Raman spectroscopy," J. Chem. Phys. **111**, 492 (1999).

4 SGS with High Pressure: Benzene

4.1 Introduction

As noted in the previous chapter, collision induced (CI) scattering presents a difficult theoretical problem because the scattered intensity depends on the polarizability change within a group of interacting molecules, and the time dependence of this change is a function of the intermolecular potential.[1] To date, the spectra which arise from these complex intermolecular dynamics remain difficult to interpret unambiguously. It seems reasonable to expect changes in these interactions when density is increased (collisions should increase in number and duration, reorientations may be more likely to oscillate rather than diffuse) and that these changes will be apparent in the scattered light. Although density effects have been studied by varying temperatures at atmospheric pressure,[2-8] these studies reflect both the change in kinetic energy of the molecules as well as the change in the average volume available for the motion of the molecule. Experiments at high pressures can differentiate the effects of temperature and density on the molecular motions and interactions in a liquid[1,9] and therefore may provide additional insights into the nature of CI scattering.

While there have been relatively few Rayleigh-wing scattering experiments done at high pressure,[1,10-16] those results have been encouraging in terms of noticeable effects of pressure in the 1 - 100 cm^{-1} spectral region. For example, LS experiments under pressure and over a wide range of temperatures carried out by Jonas and coworkers for liquids of spherical[1] and linear[1,13-15] molecules have generally found the characteristic frequencies of these spectra to exhibit a density dependence that is very different than the temperature dependence. Furthermore, the various frequency regions in a given liquid differ in how they respond to further increases in density. In coherent time-domain work, femtosecond ISS[17-18] experiments have also been run as a function of pressure in the study of CS_2. As pressure was increased a weak oscillation, not present at atmospheric pressure, appeared around 650 fs. Low frequency Raman spectra of molecular liquids are also shown to shift with the application of high pressure.[19,20] Together these findings provide additional incentive to incorporate high pressure into our SGS investigation of liquid dynamics.

The particular experimental set-up used here provides flexibility for obtaining either a Rayleigh wing spectrum by tuning the pulsed dye laser (PDL) used for the pump over 300 cm^{-1}, or a 30 GHz Brillouin scan by tuning the continuous-wave dye laser (CWDL) used for the probe beam with only minimal adjustments in the optical components. Thus, even though our primary interest has been in intermolecular interactions, both of these experiments were performed under high pressure conditions for the different kinds of information each had to offer. Section 4.2 will highlight the changes incorporated into the basic SGS experimental set-up of Chapter 2 in order to apply high pressure to the experiment.

Several different simple molecular liquids were considered as our sample liquid, including both carbon disulfide (CS_2) and ethanol (CH_3CH_2OH), each offering its own particular advantages and problems, as will be detailed in Section 4.3. Ultimately benzene was selected as a fairly strong scatterer which was also non-reactive with stainless steel, thereby eliminating the need for an additional internal cell. Incorporating high pressure into the SGS experiment was technically quite challenging, also to be discussed in Section 4.3. Two of the most problematic aspects of working with high pressure deal with scattered pump light and with polarization that is both rotated and scrambled by the sapphire windows used. The spatial separation of the high pressure cell windows limit off-axis travel through the sample and make it very difficult to avoid scattered pump light traveling along the probe beam. Especially when a second interior cell is necessary (as with reactive CS_2), the multiple surfaces and media, and an even narrower unobstructed path through the cell provide a major complication. Difficulties in maintaining a particular polarization are the result of stress applied to the sapphire windows, both when assembling the high pressure cell and when pressure is increased for the experiment. This produces strain-induced anisotropies in the windows resulting in a pressure-dependent scrambling of the polarization which is very difficult to quantify. How these technical challenges were overcome in order to accomplish a depolarized spectrum at 350 bar and Brillouin spectra at 540 and 880 bar in liquid benzene will be reviewed. Encounters with contamination problems and observation of phase transitions will also be discussed.

Section 4.4 deals with applying the model developed in Chapter 3 to curve fit the depolarized benzene spectra. Though only limited pressure was

applied to the sample, the various components did indeed experience that pressure differently, with the low frequency diffusional reorientation rate decreasing with increasing pressure, while collision-induced frequency, ω_c, markedly increases with increased pressure. The librational center frequency, ω_o, and extent of inhomogeneity, α, also change with this pressure increase. Similarly, the Brillouin data was examined for changes with pressure, Section 4.5, and the sound velocity was found to exhibit a shift of 1.92 GHz/kbar.

In all, it was determined that the application of high pressure to the stimulated gain technique is possible and that the technical difficulties with scattering and polarization can be overcome to acquire a signal with as good signal-to-noise as found in a single quartz cell. While only limited data was obtained in the proof of concept experiment, careful analysis has confirmed that the use of high pressure in combination with the SGS technique can provide additional insights into the nature of intermolecular interactions in simple liquids.

4.2 Experimental Procedure

In order to apply high pressure to stimulated gain experiments only a few changes were necessary to the basic experimental set-up described in Section 2.3 other than the substitution of a high pressure cell for the quartz cell used at ambient pressure and a pressure generation system, shown schematically in Fig. 4.1. Pressure generation is accomplished in two steps. The first part utilizes a fluid pump to deliver the pressure generating fluid into the cell. In cases where the sample liquid is reactive with stainless steel, such

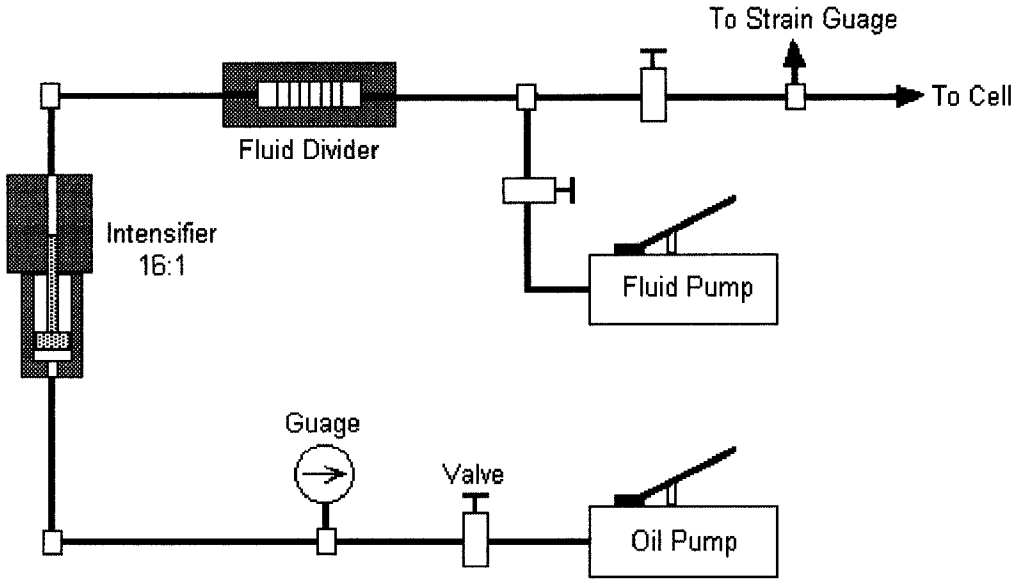

Fig. 4.1 the high pressure generating system.

as CS_2, a pressure generating fluid such as ethanol must be used and the sample is contained within a secondary cell inside the high pressure cell. For non-reactive samples, such as ethanol or benzene, the sample liquid itself fills both the fluid pump and the high pressure cell. The fluid pump can be used to apply pressure up to 1500 bar, or can be isolated from the system and an oil pump amplified by a 16:1 intensifier can be employed to produce up to 7 kbar pressure. Between the oil pump and the high pressure cell is a fluid divider, essentially a 1:1 intensifier, which transfers the pressure from the oil to the sample liquid or pressure medium without allowing them to mix.

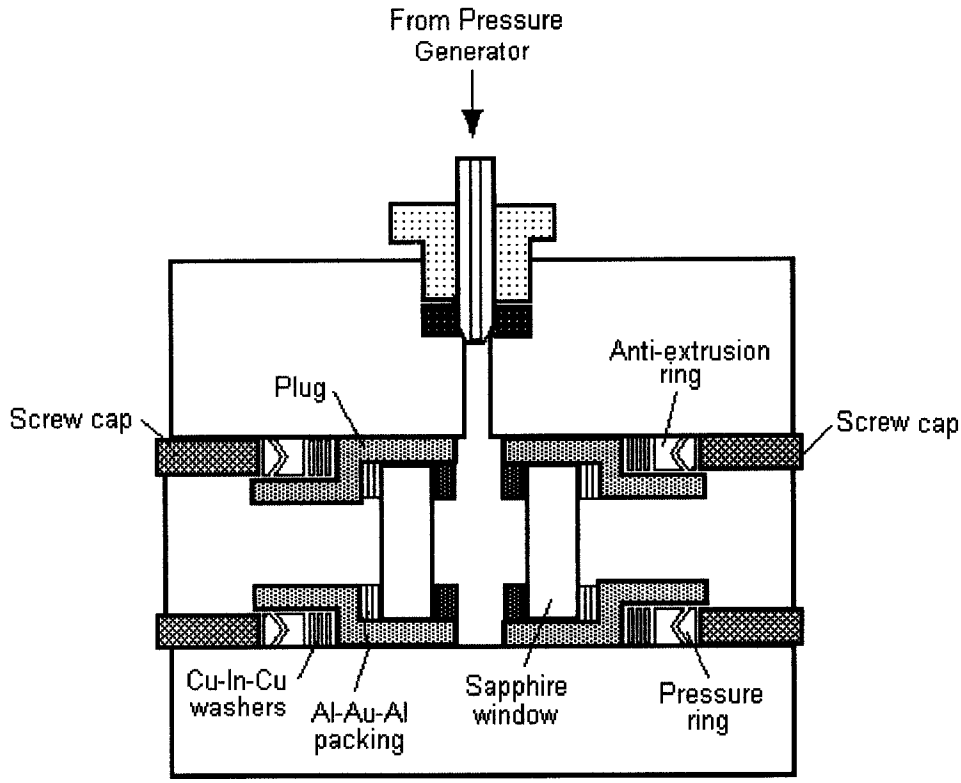

Fig. 4.2 The high pressure cell.

The high pressure cell is depicted in Fig. 4.2. It is a four port design made from stainless steel. For the SGS experiment, two opposing ports are fitted with sapphire windows as entrance and exit ports, and the others are plugged. These windows have a clear aperture of 10 mm and are sealed against high pressure plugs as described by Hochheimer, et. al.[21] It is filled through an additional port on top. The pressurizing fluid is pumped from the fluid pump through the capillary lines and into the top port. While loosely connected, the fluid is pumped into the cell until it overflows. The connection is then tightened to prevent any further passage of fluid or air. For reasons which will be discussed below, benzene was selected as the sample molecular

liquid for these high pressure experiments. Given the volatile and toxic nature of liquid benzene, several precautions were taken to prevent exposure to vapors during the filling and emptying of the cell and pressure lines. Whenever possible, work was carried out under a fume hood. In the laboratory, to vent vapors to the outside, a simple housing was built and a fan rated at 250 cfm was installed into a window. A length of standard dryer flex hose was attached and then was positioned as needed directly over any location where benzene was temporarily exposed to the room. Organic vapor filter masks (3M™ 7000 Series Dual Cartridge Half-Faceplate Respirator) were also worn. The room was evacuated after filling the cell until any remaining vapors were dissipated, also providing time for any bubbles or turbulence in the sample to settle. There was a noticeable reduction in stray scattered pump light when the cell was allowed to stand overnight before data were taken. Beam focus and precise overlap of pump and probe beams are critical to the successful location of the SGS signal. Since the high pressure cell does not allow a visual check of the beams from the side or top as with the simple quartz cells, a great deal of care had to be taken to eliminate as much trial-and-error in alignment as possible. In order to accomplish this, a stage was built for the high pressure cell with independent micrometers for x- and y-translation as well as for rotation about its center in order to turn the cell windows off-axis to the beam path to help minimize stray scattered pump light. The experiment is set up first without the sample in place, aligning both the pump and probe beams to travel parallel to the tabletop at the correct height for the high pressure cell, with both focusing as nearly as possible at the same location in air. This approximate focal point is marked, both on the tabletop and by suspending a small plumb bob overhead. The high pressure

cell is then put into place at the focal point. Care is taken to align one translation micrometer with the beam path and the cell is rotated so that the windows are approximately 5° off perpendicular to the beam path. The new focal point for the probe beam is calculated based on travel through the sapphire window and liquid under investigation. The cell is then translated to the calculated probe focus and the pump lens is also translated to once again align the two foci. The probe beam is then sent through and balanced with the reference beam at the diodes.

To further facilitate locating the SGS signal in the high pressure cell, an alternate path through a quartz cell of the sample liquid was added to provide a simple means of precisely setting the laser frequency difference. By propagating the beams through a clear unobstructed quartz cell, the focus and overlap can easily be checked visually and then, while monitoring the signal at the oscilloscope, the laser frequency difference can be set precisely for Brillouin signal. This eliminates frequency as a variable in the search for a signal in the high pressure cell. Switching between these two paths was accomplished by inserting four additional mirrors, M1-M4, while keeping the probe path length equal to that of the reference beam, and required no adjustments to the optics aligned for the high pressure experiment. A schematic view of the high pressure SGS experiment is shown in Fig. 4.3.

Additional half-wave plates and polarizers, P1 and P2, as shown, were also added to mitigate polarization problems introduced by the sapphire windows and stress-induced birefringence which will be discussed in the next section. This particular placement for the polarizers also ensured a simple means of switching between a polarized and a depolarized experiment without the need for realigning optics.

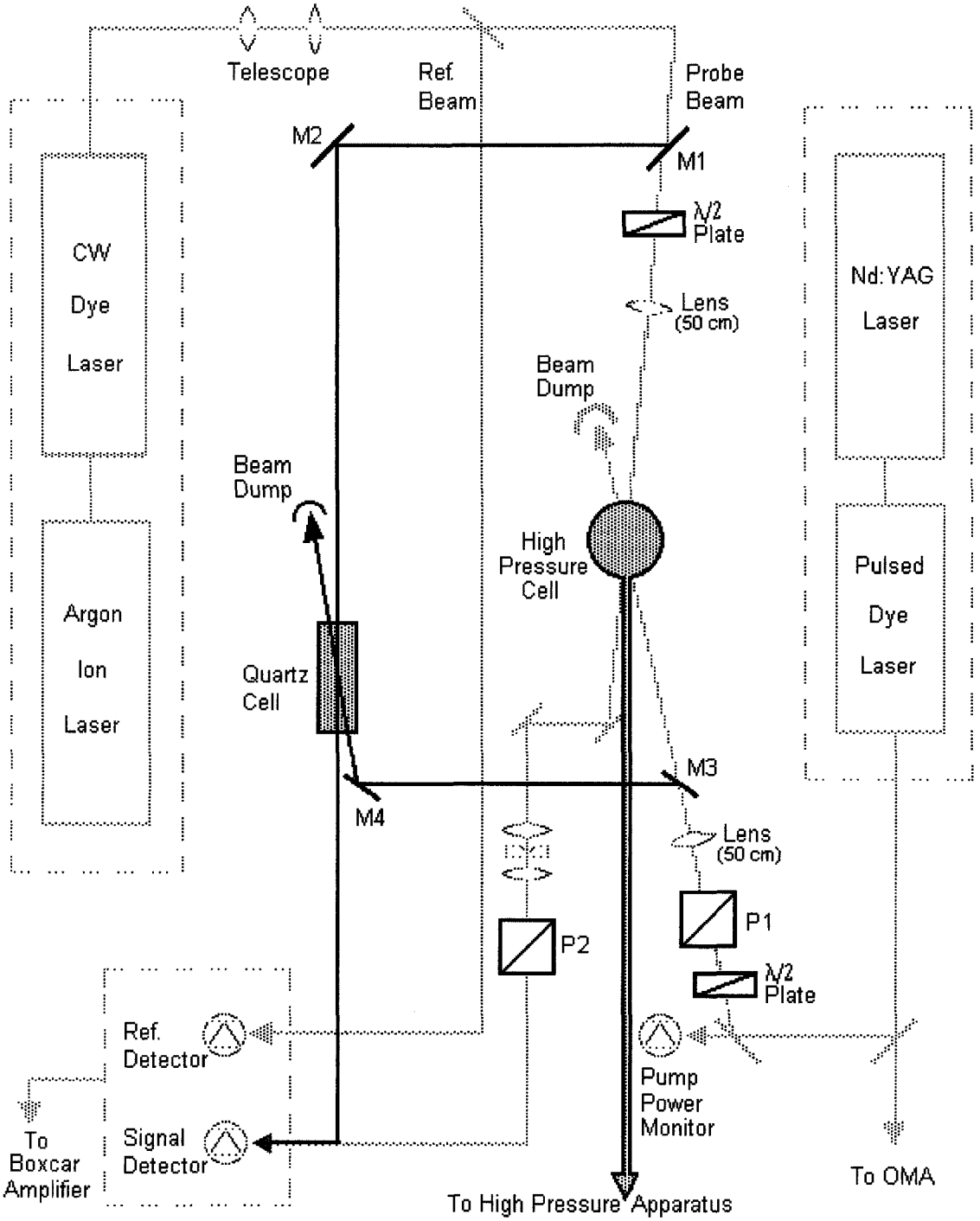

Fig. 4.3 Schematic of the SGS experiment as modified for application of high pressure. The dotted lines represent apparatus used in the basic SGS experiment and solid lines show changes made for the high pressure experiment. Mirrors M1 and M3 direct the probe and pump beams along an alternate path used to precisely set the frequency difference between the lasers and then are removed during the high pressure experiment. See text.

4.3 Technical Challenges

Despite reliably finding and maintaining small signals using SGS at ambient pressures, application of high pressure introduces several new challenges to be overcome. As noted in the previous section, in order to locate the SGS signal in the high pressure cell, measures needed to be taken to compensate for reduced visibility. The high pressure cell also introduces new difficulties associated with scattered pump light and with randomization of laser polarization. A few surprises were also encountered, in the form of unexpected complications from contamination problems and unrecognized phase changes.

Scattered pump light

Carbon disulfide (CS_2) was first selected for the high pressure study in order to ensure a strong signal and because of prior personal experience with this liquid using SGS techniques at ambient pressures. CS_2, however, is very reactive with stainless steel and would pose significant problems with etching both the cell and capillary lines, if placed in direct contact. A small Teflon cell was therefore used to contain the sample and ethanol was used as the pressure generating fluid. The internal cell consisted of snap fit sapphire windows, over each of which a Teflon washer was placed and a metal end cap was tightened. In order to avoid additional scattering at the new surface-fluid interfaces, the sides of the window in contact with ethanol were anti-reflection coated (indices of reflection: $n_{sapphire}$=1.765, $n_{ethanol}$=1.360). It was unnecessary to coat the interior surfaces, since CS_2 has an index of n_{CS2}=1.63, resulting in a reflectance of only about 0.16% at the uncoated

CS_2/sapphire interface compared to 1.7% at the uncoated ethanol/sapphire interface.

The inner cell was loaded under a fume hood while submerged in a beaker of filtered CS_2 in order to eliminate large air bubbles when snap fitting the windows. The filled cell is then put into place in the ethanol-filled high pressure cell and left overnight to allow turbulence and the minute bubbles from filtering the liquid to settle out. Despite the anti-reflection coatings, the fact that the interior cell further restricted the clear path through the cell and required working nearly perpendicular to the several interfaces resulted in pump light being scattered back along probe beam. The strongest scattered peak seen on the oscilloscope was at least the same order of magnitude as the signal, and often five times greater. Interestingly, it was noted that this scattered peak was delayed by up to 5 ns, indicating a travel distance of about 150 cm further than the probe beam signal, most likely due to multiple reflections within the high pressure cell.

In an effort to eliminate much of the scattered light problem and simplify the initial experiment, the internal Teflon cell was removed and the experiment was attempted with ethanol as both the sample and the pressure generating medium. This greatly reduced the amount of stray scattered light, eliminating multiple scattered peaks from the signal field on the oscilloscope, including the strong 5 ns delayed pump light. However, ethanol is a very weak scatterer and coupled at that point in time with very low power output from the argon laser, the depolarized signal was very difficult to reliably locate. It should also be noted that this was attempted before many of the improvements to the basic SGS technique were put in place. Particularly, if the polarizers (P1 and P2, Fig. 4.3) used to correct rotation of the beam

polarization had been in place, locating this signal would have been much more likely. It should be noted that the depolarized signal was easily picked up on the alternate optical path through the quartz cell at ambient pressure where there are no polarization problems. Also, the Brillouin signal, at about ten times the intensity of the depolarized signal, was fairly easy to locate in the high pressure cell despite the scrambled laser polarization. It was Brillouin signal in ethanol that was used in an earlier proof-of-concept experiment combining SGS techniques with high pressure.[22]

At this point in time, a different sample liquid was sought and benzene was selected on the basis of being both non-reactive with stainless steel and having a reasonably strong scattering cross-section. While still requiring the cautions necessary for working with a toxic and volatile substance, it did offer distinct advantages over the previous liquids and greatly simplified the high pressure experiment.

Polarization

The windows used in the high pressure cell are of sapphire, a material of superior strength and hardness and possessing a high transmittance over a wide range of wavelengths. The birefringence of sapphire, $(n_o - n_e)$ is reported to be only 0.008,[23] which for incidence at small angles off-axis should have little effect. These windows, however, do exhibit pressure-dependent scrambling of polarization, apparently due to strain-induced anisotropies in the material. As pressure is applied, strain produces a deformation of the atomic network such that the average distance between nearest neighbors differs in the direction parallel and perpendicular to the strain.[24-25] One feature of our high pressure cell is that it allows the sapphires to be stressed

at the time of cell assembly. While this prestressing improves the safety of the experiment[21] and provides a seal at very low pressures, it is sufficient to produce a significant amount of rotation and randomization of the polarization even before the sample liquid is pressurized. Efforts have been made to quantify pressure-induced polarization scrambling by optical windows of quartz and of float glass.[24] As was also found in our experiment using sapphire, there was considerable variation from window to window in these materials. Additionally, these studies noted that the amount of polarization scrambling observed changed with the duration of pressurization for both the quartz and float glass windows. This may be understood in terms of a viscoelastic material which, given time will first experience shear relaxation to a virtually unstressed birefringence coefficient, and then, as the application of stress continues, the glassy material will begin to flow.[24]

The fact that polarization rotation and randomization are different with each individual window and that they vary differently depending on the angle of incidence, the spatial location of incidence on a given window face, the duration of pressurization, as well as the input polarization, all make efforts to fully quantify polarization changes too complex to be practical during an experiment. A more useful approach is to incorporate additional half-wave plates and polarizers into the SGS experimental set-up as seen in Fig. 4.3. One half-wave plate is set in the probe beam before the sample and polarizer P_1 is initially used as an analyzer after the sample. By changing the direction of the linear input polarization before the sample, a beam polarization can be selected which results in somewhat less randomization, as determined by a maximum amount of light transmitted at some rotated angle at analyzer P_1. For depolarized experiments P_1 is then set to the minimum for the transmitted

probe beam and then placed in the pump beam before the sample, as shown in Fig. 4.3. A second half-wave plate is then used to rotate the pump beam to match the polarization of P_1. A second polarizer, P_2, is set to match the maximum of the transmitted probe beam and placed before the signal diode to help eliminate stray pump light. This arrangement thus provides a means for optimizing the polarization of the pump and probe beams with respect to one another, and for easy compensation of any further polarization changes due to small movements of the high pressure cell and/or probe beam made while adjusting focus or overlap. As a further aid in locating the SGS signal, the polarization of the pump beam can now easily be adjusted while viewing the oscilloscope monitor in order to intentionally leak a small amount of polarized light and provide strong Brillouin scattering. After the signal is located, adjustments at P_1 are again made to clean up the depolarized signal by eliminating the Brillouin scattering signal. Additionally, the change from a depolarized to a polarized experiment can now be quickly made with minimal change to the optics involved.

Contamination Problems

With success in overcoming scattering and polarization problems, SGS signal could be reliably located and maintained through the high pressure cell at ambient pressures, and we anticipated interesting results with an increase in the sample pressure. As is often the case with experimental science, we met with unexpected problems.

After capillary lines were filled and loosely connected to the cell, benzene was pumped in until there was a small overflow at the port connection and the port was then sealed. When the pump and probe laser

beams were directed through the high pressure cell, they surprisingly emerged at 2 mm and 2.5 mm, respectively, below the entry level for the beams and traveled at a downward angle much as if reflected from a curved internal interface. The possibility was considered that turbulence could be causing the problem, and the cell was allowed to "rest" overnight. Though the problem remained after about seven hours, by the next day the beams were again traveling through the cell without deflection. However, it became difficult to balance the dc power levels on the probe and reference beams. A chopper located after the CWDL provides a 7 ms wide square pulse on the probe and reference beams and it was noted that about 24% of the probe intensity was being absorbed after 5ms. This indicated a contamination problem which was confirmed after the cell was opened. Benzene in the capillary lines had changed to a golden color and had evidently also contaminated the liquid in the high pressure cell despite its remaining nearly clear in appearance. Some of the liquid from the cell was kept and analyzed using an Elmer-Perkins spectrophotometer. As seen in Fig. 4.4, a reduced transmittance in the recovered sample compared to pure benzene verified the presence of a contaminant. The high pressure cell was then thoroughly cleaned and repolished, the fluid divider was disassembled, cleaned and new parts tooled to prevent any possible leakage of oil into the system. The capillary lines were repeatedly flushed until liquid benzene came through clear and then were flushed twice more with benzene from a new bottle. This eliminated the contamination and absorption of the probe beam through the high pressure cell.

Continuing laser problems prevented another attempt to locate the depolarized SGS signal within the time that the high pressure equipment was

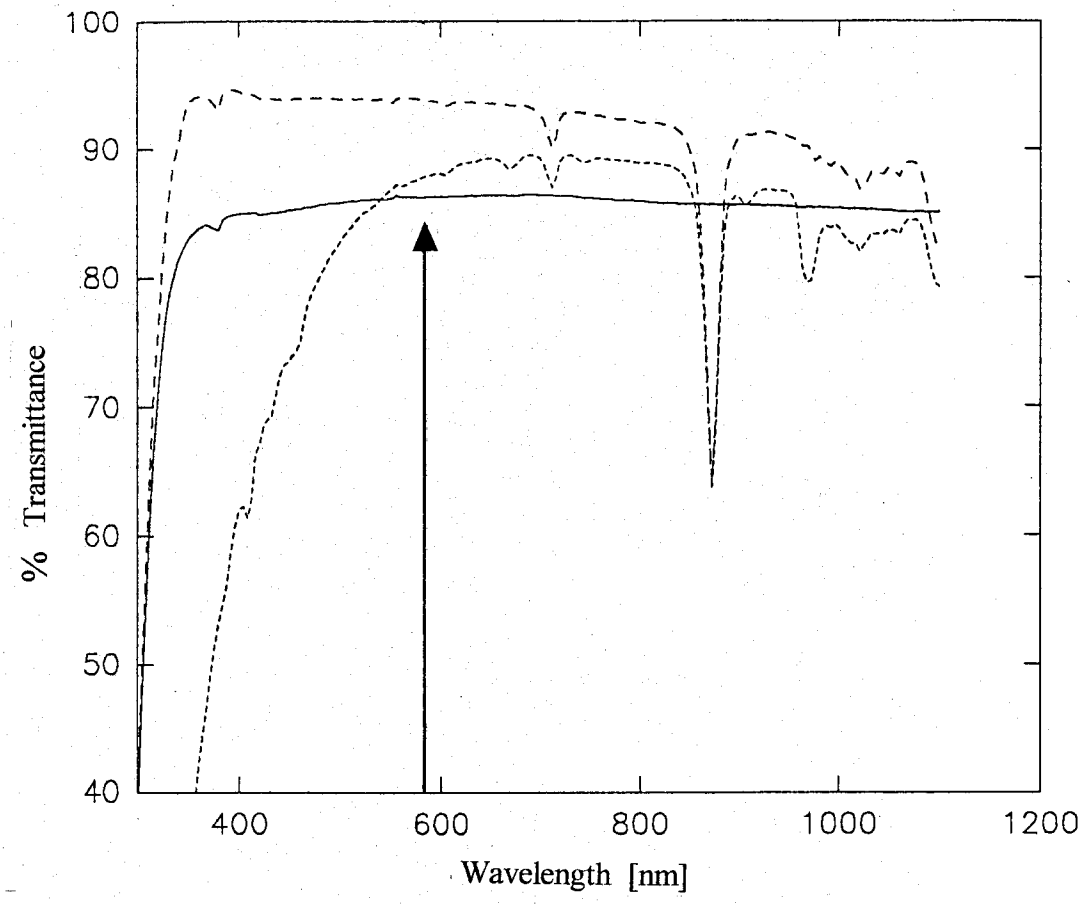

Fig 4.4 Spectrophotometric analysis of contaminated benzene. —— Solid line: Transmittance of clean glass (offset by 10% to avoid overlapping curves); – – – – Long dash: Clean, filtered benzene in glass; ------ Short dash: Benzene sample from the high pressure cell in glass. Laser wavelength (corresponding to zero on frequency scale for measured spectra) is shown at 585 nm.

Continuing laser problems prevented another attempt to locate the depolarized SGS signal within the time that the high pressure equipment was available to us. By the time the apparatus was again available, extremely low argon laser power led to the decision to try to obtain the higher intensity Brillouin signal in benzene at high pressures, which will be discussed in section 4.5.

attempt again showed signs of contamination which was traced to oil leakage at a new pressure gauge. With this new contamination problem located and resolved and the cell recleaned and polished, depolarized data was finally obtained at 350 bar. Pressure was then increased to 1 kbar and the sample checked. The benzene appeared clear and transmission was good and the sample was allowed to rest. Several hours later, a probe beam sent through the cell had about 50% of its power absorbed, and the benzene appeared murky. However, it was noted that this change was reversible and when pressure was lowered the beam no longer experienced absorption and the liquid visibly cleared with the exception of several small spots of residue that had been deposited on the inside of the windows. Unfortunately, due to all the previous contamination problems we did not immediately associate this behavior with a gradual phase change in benzene.

In order to better understand what was occurring, the probe beam alone was sent through the sample in the high pressure cell and the transmitted power was measured using a FND-100 photodiode. A white screen which could easily be moved into the exiting beam was also used to make a visual check for absorption or diffuse scattering in the liquid. The pressure was then raised in approximately 100 bar increments while transmitted power and beam quality were monitored. Quite a "light show" ensued, and although unfortunately no camera was in place, sketches were made and included with the tabulated results in Table 4-1. The sketches of the beam's appearance are as viewed in darkened room, so that white within the circles represents the laser light. Initially, the sample was kept at each pressure change forapproximately seven to ten minutes. As pressure was increased above 900 bar, the beam quality as viewed on the screen suddenly deteriorated. Much

Table 4-1. Transmitted power and appearance of liquid benzene under high pressure.

Pressure [bars]	Transmitted Power [mV]	Appearance on screen
200	120	Clean beam spot, A
500, 600, 700, 800, 900	120	Unchanged
930	10	Beam is scattered, diffuse glow, B
800	95	Beam spot is more visible, some diffuse glow
575	120	Clean beam spot, A
800	100	Clean beam spot, A
925	70 5, after 10 sec <1, after 25 sec	Diffuse, B Beam is unevenly scattered, blotchy appearance, C Homogeneous, very low intensity glow
1000	undetected	Dark
900, 825, 770	<1	Homogeneous, very low intensity glow
625	90	Diffuse, though brighter. Changing during next 3 min: Large, bright scatter spot moves across screen and back, D Several bright flashes and streaks, in motion, E Finally, a fairly clean beam spot, though spatially shifted
525	90	Unchanged
625	95	Brighter, cleaner beam, even as pressure is increased
700	100 120, after 5 min	Unchanged
810	120	Unchanged
880	120 <20, after 3 min <10, after 5 min	A changing interference pattern, F Final appearance, G. Remained stable for over 30 min

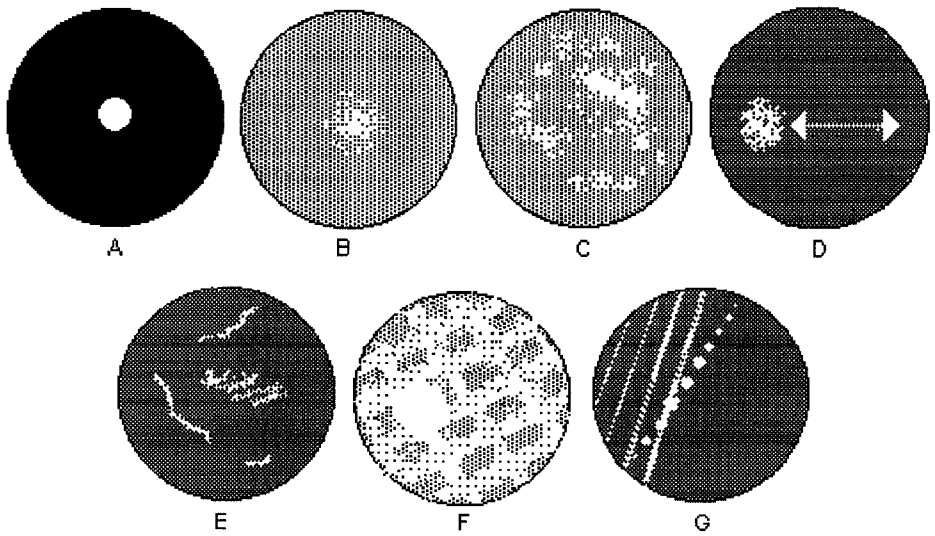

of the beam was scattered throughout the liquid resulting in a diffuse glow from the port with a brighter center spot (Circle B, Table 4-1). As indicated in the Table 4-1, the pressure was then reduced and the changes visible at 930 bars of pressure were reversed. When the pressure was increased a second time, the beam was again diffusely scattered at 925 bars pressure. However, the appearance of the transmission quickly altered to an unevenly scattered, blotchy appearance (Circle C) and a half minute later transmitted light was reduced to less than 1 mV on the diode detector. The application of 1 kbar pressure eliminated essentially all of the transmitted light. The sample behaved differently when the pressure was reduced the second time, with the transmitted light indicating movement of scatterers in the sample. First, the beam was deflected from one side of the screen to the other, then several bright flashes and moving streaks were seen until after about three minutes a fairly clean beam spot again emerged, although spatially shifted. The changes induced at high pressures were no longer immediately reversible. Interestingly, as pressure was once again increased gradually from 525 to 810 bars, the transmitted beam showed a slight improvement in both power and appearance. At 880 bars, the power dropped after three minutes and a changing interference pattern (Circle F) was seen. A few minutes later, a final very interesting pattern (Circle G) was obtained and remained stable for at least a half an hour. Later reference to a pressure-temperature diagram[26] confirmed suspicions of solid matter in the sample, likely due to a partial phase change in the pressurized liquid. Without the earlier contamination problems, perhaps this phase change would have been more readily recognized. Pressure versus temperature data for benzene is shown in Figure 4.5. Room temperatures in the lab tend to be fairly warm, often ranging from

25 - 28 °C, temperatures for which benzene would begin to solidify around 725 to 850 bars pressure. No effort was made to control the sample temperatures, which may have been somewhat warmer than the surrounding room temperature due to heat added by the laser beams, thus enabling us to reach somewhat higher pressures before noting pressure freezing effects. This portion of the experiment did produce data at both ambient conditions and at 350 bar which have been carefully analyzed and will be discussed in the next section.

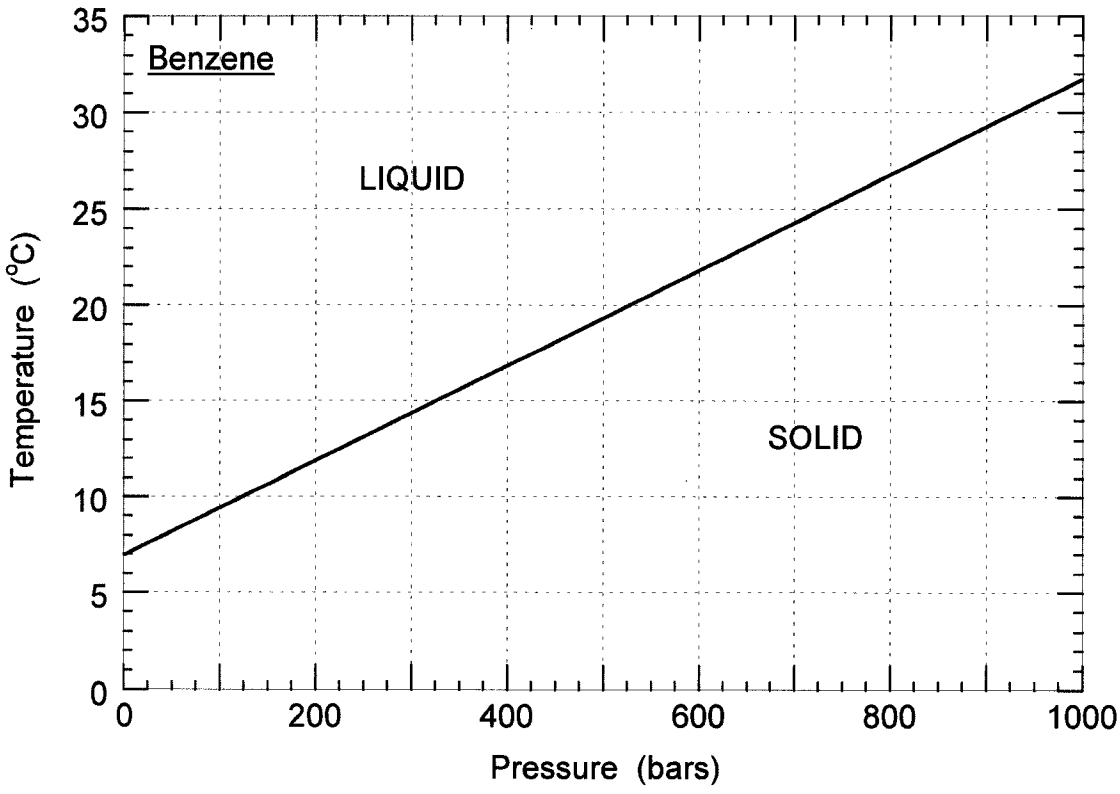

Fig. 4.5 Pressure versus temperature diagram for benzene from Ref. 26.

4.4 Depolarized SGS at High Pressures

Following the methodology discussed in section 4.2 with special attention paid to beam focus, the ambient pressure SGS signal from liquid benzene was readily located in the high pressure cell. Data was taken on two different days, providing a total of fourteen individual spectra which were added together for the spectrum of Fig. 4.6a. The signal-to-noise for an individual spectrum obtained through the high pressure cell was generally about 9:1, as good as noted for the 10 cm quartz cell. The three component fit of Chapter 3,

$$g(\omega) = \mathrm{Im}[G(\omega)] = A\omega[1/(\omega^2+\Gamma^2)] + B\omega^s\exp(-\omega/\omega_c)+ \{\exp[-(\omega-\omega_o)^2/2\alpha^2]-\exp[-(\omega+\omega_o)^2/2\alpha^2]\} \qquad [4.1]$$

with s=1.0, was applied to the spectrum and the results shown in Table 4-2. These values compare well those reported in the literature,[7,8,27-31] including SGS results obtained in this lab several years ago[27,28] which were fitted to a model consisting of two Lorentzian terms and an inhomogeneously broadened Gaussian. One notable difference in the SGS fits seems to be the value for the rate of diffusive reorientation, for which this work reports a higher value. In order to eliminate model-dependent differences, the current data is also fitted to the earlier model[27,28] and a value of 2.09 cm^{-1} is obtained for Γ as compared to the 1.94 cm^{-1} reported earlier. Diffusive reorientation rates are somewhat temperature dependent, as has been shown by OKE data for benzene at various temperatures.[7] When converted to wavenumbers, those collective reorientational times indicate that near room temperature, a change of just 6 °C (11 °F) would be sufficient to account for the 0.15 cm^{-1} difference

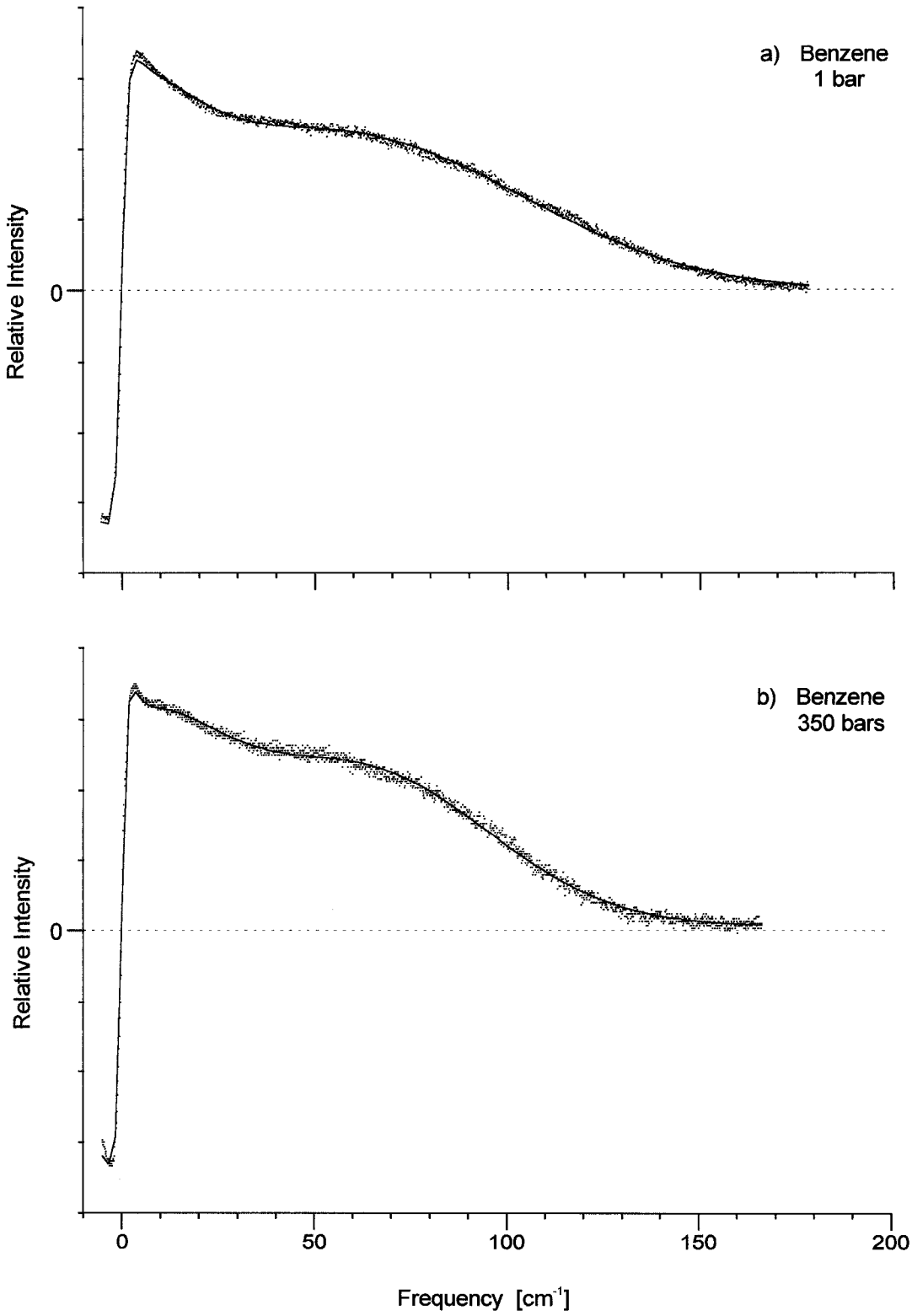

Figure 4.6 SGS spectra of liquid benzene at a) ambient pressure and at b) 350 bars.

in the two sets of SGS data applied to the same Friedman model. As seen in Table 4-2, the values reported for Γ using other techniques would support either of the values.

Due to the problems enumerated in Section 4.3 a pressurized spectrum was not obtained immediately and thus potentially introduces more variation in the experimental conditions than is optimum. Furthermore, data at only one increased pressure (350 bar) was obtained, Figure 4.6b. Even these limited results show a shift with respect to atmospheric pressure measurements, which is tabulated in Table 4-3, along with Δ, the percentage change in going from ambient conditions to 350 bar.

Table 4-2. Comparison of dynamical parameters in benzene (cm^{-1}) at 1 bar pressure.

Reference	Γ	ω_c	ω_o	α
This work (SGS)	2.58±.03	11.1±0.1	59.3±0.8	45.6±0.5
Friedman[28] (SGS)	1.94	11.9	58.2	38.1
McMorrow[29] (OHD-OKE)	2.59	13.8	48.2	68.8
Vohringer[30] (OHD-OKE)	2.1	9.5	41	
Loughnane[7] (OHD-OKE)	1.87	5.58		
Ricci[8] (OHD-OKE)	1.7	12	43	
Dill[31] (LS)	2.27			

Increasing liquid density inhibits the relaxation of density fluctuations in the local structure and results in lower diffusive reorientation rates, Γ. This is evident both when the reorientation rates of several liquids with different densities are compared (Section 3.3) as well as when the density of a single liquid is increased. Using experimental values given by Fujita[32] for the density of benzene under pressure indicated that the density is increased by 3% in applying 350 bar pressure. This density change corresponds to a 17% decrease in the SGS values for reorientation rates Γ. Dill[31] and coworkers found a similar pressure dependence in their depolarized light scattering study of reorientation in benzene, with a reported 16% decrease in Γ at 250 bar and, by a linear extrapolation of their values, a 23% decrease at 350 bar.

Table 4-3. Fit parameters for the SGS spectra of liquid benzene (in cm^{-1}).

Pressure (bar)	**Density** ($g\ cm^{-1}$)	Γ (cm^{-1})	ω_c (cm^{-1})	ω_0 (cm^{-1})	α (cm^{-1})
1 bar	0.874	2.58±0.03	11.1±0.2	59.3±0.8	45.5±0.5
350 bar	0.901	2.13±0.02	14.7±0.3	66.3±0.5	31.4±0.3
Δ	+3%	-17%	+32%	+12%	-31%

As noted in Chapter 3, the characteristic frequency for collision-induced dynamics, ω_c, describes the line shape arising from purely translational collisions in CCl_4. For more anisotropic molecular liquids however, molecular reorientations result in contributions from the time

dependent permanent anisotropy of the molecule, as well as from induced anisotropy due to both translational and rotational multi-body interactions. An increase in density results in more frequent collisions which means a shorter duration for a given interaction before the next collision occurs and any correlation or 'memory' of the previous influence is lost. These shorter times produce a broader line shape with contributions to the spectral density at higher frequencies and thus increase the characteristic frequency, ω_c. Tighter molecular packing at higher densities also produces a cancellation effect in scattering from DID interactions giving quadrupole-dipole and higher order interactions a relatively more significant impact on the scattered intensity, thus again contributing to a higher characteristic frequency for the interaction-induced scattering. Comparison of the spectra in Fig. 4.6 reveals relatively more intensity near 15 cm^{-1} in the 350 bar spectrum. This is indicative of a broadening of this collision induced component, as well as an increase in its contribution to the spectral intensity due to the more frequent collisions. Of the three characteristic frequencies comprising this model, it is the one for collision-induced dynamics, ω_c, that has the strongest pressure dependency with a 32% increase over the 1 bar value at 350 bar.

As might be expected, strong pressure sensitivity has been observed for this region of the spectrum by other researchers in several other molecular liquids. For the spherical molecular liquids CH_4[1,11] and SF_6[1] at ambient pressure, the spectra can be characterized by three regions, each fitted by an exponential function of the form A $\exp(-\omega/\Delta)$. As pressure is applied, the angular frequency Δ_{int} corresponding to the intermediate frequency region between 25-85 cm^{-1} shows a strong increase with density in both liquids. Similarly for the triatomics, CO_2[1,13] and CS_2,[1,15] each displays three distinct

frequency regions at ambient conditions and each experiences a dramatic increase in its Δ_{int} with increasing pressure, with no similar increase in Δ representing the low or high frequency regions. In contrast to this pressure dependence, data taken at constant pressure indicated an insensitivity to temperature in the intermediate frequency region for either the quasi-spherical or more linear molecular liquids. These experimental results imply that for this component of the spectrum, volume changes are much more important for determining molecular dynamic behavior than are changes in the kinetic energy of the molecules, consistent with a collision-induced model. In the case of CS_2, when pressure is increased to 3.5 kbars, a fourth distinct spectral region at 155-215 cm^{-1} is noted[1,15] and is most likely associated with a CIRRS mechanism.[15]

That librational motions are also affected by high pressures may be understood in terms of "caging" effects by near neighbors around any given molecule.[33] As density is increased, local ordering in the liquid should also increase leading to stronger "caging" effects. These effects will be apparent in both stronger intermolecular forces leading to a higher librational frequency, ω_o, and a reduced inhomogeneity in those forces, α. Close examination of the 1 bar and 350 bar spectra in Fig. 4.6 does reflect a shift of ω_o to a somewhat higher frequency with pressure, along with a narrowing of this component, as indicated by the values of ω_o and α in Table 4-3.

Carbon disulfide is one of the most popular and extensively studied substances using high pressure, and while structurally quite different may provide an informative contrast and comparison to results in benzene. Kohler and Nelson have investigated CS_2, using a femtosecond time-resolved impulsive stimulated light scattering (ISS) technique and separately varying

pressure (using a diamond anvil cell) and temperature.[17] Results were fitted to a model representing a diffusional component and librational oscillations,

$$G(t) = A\exp(-\Gamma t) + B\exp(-\alpha^2 t^2/2)\sin(\omega_A t) \qquad [4.2]$$

where G(t) is the impulse response function, Γ is the rate of reorientational diffusion, and ω_A and α describe the average and width of the distribution of librational frequencies. In order to compare to the benzene values determined here, the Kohler and Nelson results were prorated for a similar 3% density increase (500 bars in CS_2). Table 4-4 lists their 1 bar values and the calculated 500 bars values along with both the percentage change in these values, Δ_{CS2}, and the change in benzene parameters, Δ_{C6H6}, repeated from Table 4-3.

Table 4-4. Changes in the fit parameters due to a 3% density change compared for the molecular liquids, CS_2 (from Ref. 17) and C_6H_6 (this work).

Pressure/	Γ	ω_A		α
Percentage change	(cm^{-1})	(cm^{-1})		(cm^{-1})
1 bar	6.4	22.8		26.0
500 bars	5.4	31.8		22.5
Δ_{CS2}	-16%	+39%		-13%
		ω_c	ω_o	
Δ_{C6H6}	-17%	+32%	+12%	-31%

As mentioned above, carbon disulfide and benzene liquids are structurally very different. In CS_2, scattering by translational motions is responsible for a significant portion of the intensity, as suggested by our two component fit of Chapter 3, as well as by molecular dynamics simulations.[6,34] The molecules tend to be aligned parallel with one another yet the orientational correlation in the liquid phase is small.[35,36] By contrast, the scattering in benzene is dominated by a broad distribution of librational motions[6] with a relatively high average frequency. In its liquid state, the molecules tend to be perpendicular to the nearest neighbors in a configuration similar to that of crystalline benzene.[37,38] In using ω_A and β to represent librational motions in CS_2 in a two component fit, as Kohler and Nelson have done, ω_A will of necessity incorporate scattering from translational collisions as well. The ambient value for ω_A (22.8 cm^{-1}) is very close to our SGS value for ω_c (21 cm^{-1}) in CS_2, Table 3-2. Kohler and Nelson interpreted their findings in terms of molecular orientational motion which becomes oscillatory at increased densities. In benzene, the dominance of oscillatory motions in the ambient liquid may make the increase in librational frequency, ω_o, less dramatic than is the case for CS_2. Instead, the larger effect of increased density on librational motion in benzene seems to be to strongly narrow the distribution of frequencies while at the same time moderately increasing the center frequency. It is interesting to note that the center frequency moves toward one of the crystalline libron modes (which have appreciable Raman intensities at 53 and 73 cm^{-1})[35] as pressure is increased. This may help to explain why liquid benzene shifts to a solid at a relatively low pressure.

4.5 Stimulated Brillouin Gain Spectra of Benzene at High Pressure

As noted in Chapter 2, Brillouin scattering in liquids can reveal information about the collective dynamics of the molecules, particularly thermally excited acoustic waves.[39,40] Accessing this information has been accomplished using spontaneous Brillouin scattering with a Fabry-Perot interferometer[39,41,42] and more recently with coherent techniques in both frequency-[43-45] and time-domain.[46-48] Recent experiments by MacPhail and coworkers[49-51] have clearly demonstrated the excellent resolution possible with cw stimulated Brillouin gain spectroscopy (SBG) revealing various underlying relaxation processes. To date however, relatively few studies have combined these techniques with the application of high pressures to molecular liquids[22,52-56] due to the technical difficulties involved in introducing high pressure to the scattering experiment. It is precisely this lack of data that makes the opportunity to obtain Brillouin spectra at various pressures attractive. When the argon laser used to pump the CW dye laser was no longer able to supply sufficient power for the depolarized experiment, the SGS experimental set up could be changed in a matter of minutes to take high resolution Brillouin data. The Brillouin signal is an order of magnitude larger than the depolarized signal, making it easy to locate and maintain despite the seriously compromised laser stability and power. The argon laser problems did make it impossible to maintain a good modelock over a full 30 GHz scan as was usual for the Coherent 599-21 (CWDL), so that only 25 GHz scans were run for both the 540 and 880 bar scans.

Fig.4.7(a) shows Brillouin spectra obtained at ambient conditions indicating a Brillouin shift of 7.28 GHz. A comparison with literature values

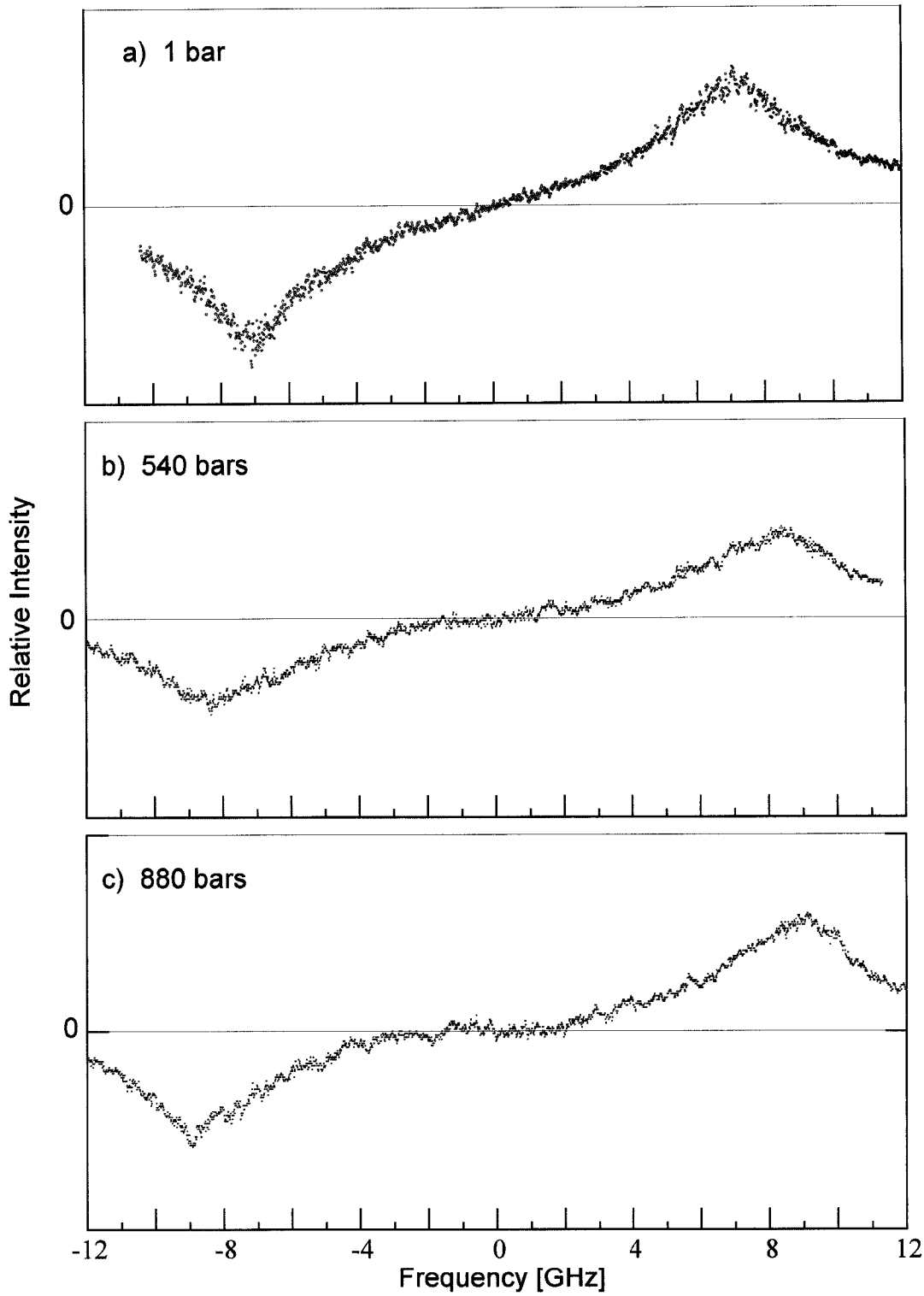

Figure 4.7 Stimulated Brillouin gain spectra of liquid benzene at a) 1 bar, exhibiting a frequency shift of 7.28 GHz, b) 540 bars, with a Brillouin frequency shift of 8.34 GHz, and c) 880 bars, with a shift of 8.97 GHz

is shown in Table 4-5 where the reported Brillouin shifts have been corrected to the scattering wavevector used in the measurement (178^{o} scattering angle and a laser wavelength of 600 nm) according to the equation for Brillouin shift, Eqn. 2.3. The MacPhail and Eastman values were measured at $22^{o}C$, and the remainder at $25^{o}C$.

Fig 4.7 also shows (b) data at 540 bar, with a Brillouin shift = 8.34 GHz and (c) data taken at a pressure reading of 880 bar, with a Brillouin shift = 8.97 GHz. In Fig. 4.8, the Brillouin frequency versus pressure is plotted. The resulting pressure shift is 1.92 GHz/kbar, a value which confirms the spontaneous Brillouin results of Asenbaum and Hochheimer[55] (1.94 GHz/kbar) and Medina and O'Shea[53] (1.96 GHz/kbar).

Table 4-5 Brillouin shifts for liquid benzene at 1 atmosphere.

This work	Stimulated Brillouin Gain	7.28 GHz
MacPhail, et. al.[49]	Stimulated Brillouin Gain	7.42 GHz
Asenbaum & Hochheimer[55]	Spontaneous Brillouin	7.27 GHz
Medina & O'Shea[53]	Spontaneous Brillouin	7.31 GHz
Eastman, et. al.[57]	Spontaneous Brillouin	7.32 GHz

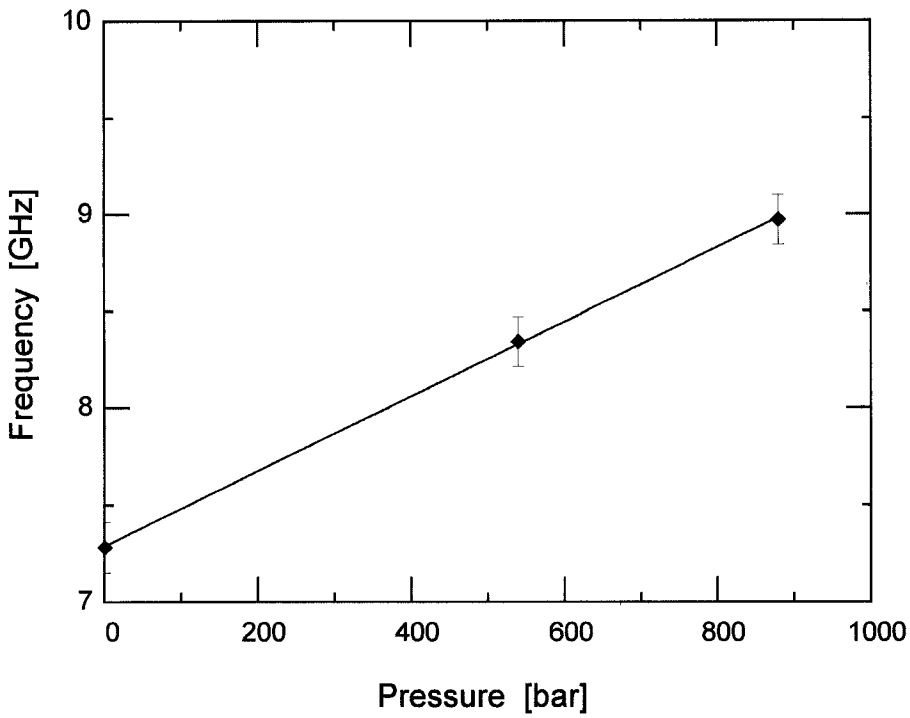

Figure 4.8 Graph of Brillouin frequency shift vs. pressure in liquid benzene.

4.6 References

1. J. Jonas, "Pressure--An essential experimental variable in spectroscopic studies of liquids," in *Phenomena Induced by Intermolecular Interactions*, NATO ASI Series B 127(Plenum, New York), 525 (1985).

2. S-C. An, C. J. Montrose, and T. A. Litovitz, "Low frequency structure in the depolarized spectrum of argon," J. Chem. Phys. **64**, 3717 (1976).

3. S-C. An, L. Fishman, T. A. Litovitz, C. J. Montrose, "Depolarized light scattering from dense noble gases," J. Chem. Phys. **70**, 4626 (1979).

4. A. Waldman, U. Banin, E. Rabani, and S. Ruhman, "Temperature dependence of light scattering from neat benzene with femtosecond pulses: Are we seeing molecules librate?" J. Phys. Chem. **96**, 10842 (1992).

5. E. W. Castner, Jr., Y. Chang, J. Melinger, and D. McMorrow, "Femtosecond Fourier-transform spectroscopy of low-frequency intermolecular motions in weakly interacting liquids," J. Lumin. **60 & 61**, 723 (1994).

6. W. T. Lotshaw, D. McMorrow, N. Thantu, J. S. Melinger, and R. Kitchenham, "Intermolecular vibrational coherence in molecular liquids," J. Ram. Spect. **26**, 571 (1995).

7. B. J. Loughnane, A. Scodinu, R. A. Farrer, J. T. Fourkas, "Exponential intermolecular dynamics in optical Kerr effect spectroscopy of small-molecule liquids," J. Chem. Phys. **111**, 2686 (1999).

8. M. Ricci, P. Bartolini, R. Chelli, G. Cardini, S. Califano and R. Righini, "The fast dynamics of benzene in the liquid phase. Pt.I. Optical Kerr effect experimental investigation," Phys. Chem. Chem. Phys., **3**, 2795 (2001).

9. H. D. Dardy, V. Volterra, and T. A. Litovitz, "Rayleigh scattering: Orientational motion in highly anisotropic liquids," J. Chem. Phys. **59**, 4491 (1973).

10. P. A. Fleury, W. B. Daniels, and J. M. Worlock, "Density and temperature dependence of intermolecular light scattering in simple fluids," Phys. Rev Lett. **27**, 1493 (1971).

11. F. Medina, W. Daniels, "Collision-induced light scattering from fluid methane at high densities," Phys. Rev. **A17**, 1474, (1973).

12. F. D. Medina and J. M. Dugas, "Density dependence of the light scattering spectrum of fluid nitrogen," J. Chem. Phys. **75**, 3252 (1981).

13. X. Song, J. Jonas, and T. W. Zerda, "Total intensity measurements of depolarized Rayleigh scattering from linear molecules," J. Phys. Chem. **93**, 6887 (1989).

14. Hegemann and J. Jonas, "Temperature study of Rayleigh and Raman line-shapes in liquid carbonyl sulfide," J. Phys. Chem. **88**, 5851 (1984).

15. B. Hegemann, K. H. Baker, and J. Jonas, "Temperature and pressure effects on the collision-induced depolarized Rayleigh line-shapes of liquid carbon disulfide," J. Chem. Phys. **80**, 570 (1984); B. Hegemann and J. Jonas, "Separation of temperature and density effects on collision-induced Rayleigh and Raman line shapes of liquid carbon disulfide," J. Chem. Phys. **82**, 2845 (1985).

16. V. Friedrich, G. Tarjus, and D. Kivelson, "Study of the integrated intensity of depolarized light scattering spectra of tetrahedral molecules," J. Chem. Phys. **93**, 2246 (1990).

17. B. Kohler and K. A. Nelson, "Femtosecond molecular dynamics of liquid carbon disulphide at high pressure," J. Phys: Condens. Matter **2**, SA109 (1990).

18. B. Kohler and K. A. Nelson, "Femtosecond impulsive stimulated light scattering from liquid carbon disulfide at high pressure: Experiment and computer simulation," J. Phys. Chem. **96**, 6532 (1992).

19. K. Goosens, L. Smeller, and K. Heremans, "Pressure tuning spectroscopy of the low-frequency Raman spectrum of liquid amides," J. Chem. Phys. **99**, 5736 (1993).

20. J. Jonas and Y. T. Lee, "NMR and laser Raman scattering studies of fluids at high pressure," J. Phys: Condens. Matter **3**, 305 (1991).

21. H. D. Hochheimer, M. L. Shand, J. E. Potts, R. C. Hanson, and C. T. Walker, "Pressure dependence of the Raman scattering by copper halides," Phys. Rev. **B14**, 4630. (1976).

22. J. S. Friedman, B. L. Bracewell, H. D. Hochheimer, and C. Y. She, "Stimulated Brillouin gain spectroscopy at high pressures," in *Proceedings of NATO Advanced Research Workshop,* Frontiers of High Pressure Research, Ed. by H. D. Hochheimer and R. D. Etters, Series B:Physics **Vol. 286**, 209 (Plenum 1991).

23. Melles Griot, *Optics Guide 5*, 13-2 (1990).

24. D. M. Cantor, J. Schroeder, and J. Jonas, "Polarization scrambling by optical windows used for light scattering experiments at high pressures," Appl. Spect. **29**, 393 (1975).

25. S. Perry, P. T. Sharko, and J. Jonas, "Technique for measuring the amount of pressure-induced polarization scrambling by optical windows in high pressure light scattering cells," Appl. Spect. **37**, 340 (1983).

26. *International Critical Tables*, Vol.III, National Research Council of the USA (McGraw-Hill, New York), 41, (1928).

27. J. S. Friedman, "Stimulated Rayleigh-Brillouin spectroscopy for studying low frequency dynamics in simple liquids," Ph.D. dissertation, Colorado State University, (1992).

28. J. S. Friedman and C. Y. She, "The effects of molecular geometry on the depolarized stimulated gain spectra of simple liquids," J. Chem. Phys. **99**, 4960 (1993).

29. D. McMorrow, W. T. Lotshaw, and G. A. Kenney-Wallace, "The structure and dynamics of molecular liquids probed with femtosecond optical Kerr effect spectroscopy," in *Advances in Laser Science III*, Optical Science and Engineering Series 9, (American Institute of Physics, New York), 674 (1987).

30. P. Vöhringer and N. F. Scherer, "Transient grating optical heterodyne detected impulsive stimulated Raman scattering in liquids," J. Phys. Chem **99**, 2684 (1995).

31. J. F. Dill, T. A. Litovitz and J. A. Bucaro, "Molecular reorientation in liquids by Rayleigh scattering: Pressure dependence of rotational correlation functions," J. Chem. Phys. **62**, 3839 (1975).

32. Y. Fujita and S. Ikawa, "High-pressure study of the far-infrared collision-induced absorption of nondipolar liquids," J. Chem. Phys. **103**, 3907 (1995).

33. R. M. Lynden-Bell and W. A. Steele, "A model for strongly hindered molecular reorientation in liquids," J. Chem. Phys. **88**, 6514 (1984).

34. C. Geiger and B. M. Ladanyi, "Molecular dynamics simulation study of nonlinear optical response of fluids," Chem. Phys. Lett. **159**, 413 (1989).

35. T. Hattori, A. Terasaki, T. Kobayashi, T. Wada, A. Yamada, H. Sasabe, "Optical-heterodyne-detected induced phase modulation for the study of femtosecond molecular dynamics," J. Chem. Phys. **95**, 937 (1991).

36. L. J. Lowden and D. Chandler, "Theory of intermolecular pair correlations for molecular liquids--Applications to liquid carbon tetrachloride, carbon disulfide, carbon diselenide and benzene," J. Chem. Phys. **61**, 5228 (1974).

37. E.G. Cox, D.W.F. Cruickshank, and J.A.S. Smith, "The crystal structure of benzene at -3 degrees C," Proc. Soc. London, Ser. **A247**, 1 (1958).

38. T. Hattori and T. Kobayashi, "Ultrafast optical Kerr dynamics studied with incoherent light," J. Chem. Phys. **94**, 3332 (1991).

39. B. J. Berne and R. Pecora, *Dynamic Light Scattering* (Wiley, New York, 1976).

40. G. D. Patterson and P. J. Carroll, "Light scattering spectroscopy of pure fluids," J. Phys. Chem. **89**, 1344 (1985).

41. R. Y. Chiao and B. P. Stoicheff, "Brillouin scattering in liquids excited by the He-Ne Maser," J. Opt. Soc. Am. **54**, 1286 (1964).

42. W. S. Gornall, G. I. A. Stegeman, B. P. Stoicheff, R. H. Stolen, and V. Volterra, "Identification of a new spectral component in Brillouin scattering of liquids," Phys. Rev. Lett. **17**, 297, (1966).

43. A. G. Jacobson and Y. R. Shen, "Coherent Brillouin spectroscopy," Appl. Phys. Lett. **34**, 464 (1979).

44. C. Y. She, G. C. Herring, H. Moosmuller, and S. A. Lee, "Stimulated Rayleigh-Brillouin gain spectroscopy in pure gases," Phys. Rev. Lett. **51**, 1648 (1983); C. Y. She, G. C. Herring, H. Moosmuller, and S. A. Lee, "Stimulated Rayleigh-Brillouin gain spectroscopy," Phys. Rev. A **31**, 3733, (1985).

45. S. Y. Tang, C. Y. She, S. A. Lee, "Continuous-wave Rayleigh-Brillouin-gain spectroscopy in SF_6," Opt. Lett. **12**, 870 (1987).

46. Y. X. Yan and K. A. Nelson, "Impulsive stimulated light scattering. I. General theory," J. Chem Phys. **87**, 6240 (1987).

47. Y. X. Yan, L. T. Cheng, K. A. Nelson, "The temperature-dependent distribution of relaxation times in glycerol. Time-domain light scattering study of acoustic and Mountain-mode behavior in the 20 MHz -3 GHz frequency-range," J. Chem Phys. **88**, 6477 (1988).

48. S. M. Silence, A. R. Duggal, L. Dhar, and K. A. Nelson, "Structural and orientational relaxation in the supercooled liquid triphenylphosphite," J. Chem Phys. **96**, 5448 (1992).

49. K. Ratanaphruks, W. T. Grubbs, R. A. MacPhail, "Cw stimulated Brillouin gain spectroscopy of liquids," Chem.Phys.Lett.**182**, 371(1991).

50. W. T. Grubbs and R. A. MacPhail, "High resolution stimulated Brillouin gain spectroscopy of liquid carbon disulfide: Dependence of the linewidths and peak gain on scattering angle," J. Chem. Phys. **97**, 19 (1992); W. T. Grubbs and R. A. MacPhail, "Rotational-translational coupling and asymmetric lineshapes in the high resolution stimulated Brillouin gain spectra of liquid carbon disulfide," J. Chem. Phys. **97**, 8906 (1992).

51. W. T. Grubbs, and R. A. MacPhail, "High resolution stimulated Brillouin gain spectrometer," Rev. Sci. Instrum. **65**, 34 (1994).

52. J. H Stith, L. M. Peterson, D. H. Rank, and T. A. Wiggins, "Hypersound speeds in carbon disulfide, acetone, and benzene at high pressure," J. Acoust. Soc. Am., **55**, 785 (1974).

53. F. D. Medina and D. C. O'Shea, "Brillouin scattering from liquid benzene at high pressures," J. Chem. Phys. **66**, 1940 (1977).

54. A. Asenbaum and H. D. Hochheimer, "Brillouin scattering from liquid CCl_4 at high pressures," J. Chem. Phys. **74**, 1 (1981).

55. A. Asenbaum and H. D. Hochheimer, "Brillouin scattering in liquid benzene under high pressure," Z. Naturforsch. **38a**, 980, (1983).

56. H. B. Bohidar, "Brillouin scattering study of equation of state of single component liquids," J. Appl. Phys. **64**, 1810 (1988).

57. D. P. Eastman, A. Hollinger, J. Kenemuth and D. H. Rank, "Temperature coefficient of hypersonic sound and relaxation parameters for some liquids," J. Chem. Phys. **50**, 1567 (1969).

5 Summary and Conclusions

5.1 Summary and Conclusions

Stimulated gain spectroscopy has been shown to be an excellent tool for the investigation of the low frequency dynamics of molecular liquids, providing sufficient resolution and signal-to-noise ratio to reflect intermolecular interactions. Liquid CCl_4 was selected for investigation because its isotropic polarizability ensures that depolarized scattering arises only from intermolecular interactions (predominantly translational collisions). This makes CCl_4 a good test for various models for collision-induced anisotropy based on different power dependences of the interaction distance, r, while the resolution of the SGS technique enables a careful curve fitting analysis to distinguish between these distinct models. The data was fit with a two component model comprised of a Lorentzian lineshape function with a damping rate, Γ, to represent diffusive relaxation and a weighted exponential function of the form $\omega^s \exp(-\omega/\omega_c)$ with a characteristic frequency, ω_c, corresponding to collision-induced scattering. Values for the power parameter s derive from interaction distances corresponding to different sources for the induced anisotropy and provide distinct models for fitting to the experimental data. A model in which the weighted exponential

corresponds to a collision-induced electronic repulsive force with a r^{-9} dependence (s =1.571) provided the best fit to the CCl_4 liquid spectrum. The best fitted values are $\Gamma = 2.2 \pm 0.5$ cm^{-1} and $\omega_c = 17.1 \pm 0.1$ cm^{-1}, in general agreement with earlier results from light scattering and coherent time-domain techniques, which were usually unable to determine all three parameters from a single measured spectrum.[1-10]

The successful SGS measurement of s, Γ and ω_c for CCl_4 permits a systematic comparison with other liquids comprised of quasi-spherical molecules ($CHCl_3$ and CH_2Cl_2), a linear molecule (CS_2), and a planar molecule (C_6H_6). While a three-component model which decomposes the CI component into an intermediate frequency term and a librational term is generally best for less isotropic molecules, the application of the two component model for diffusive reorientation and CI scattering fit many molecules surprisingly well. Especially in the case of CS_2, the two-component fit is nearly comparable to the three-component fit, an indication that, for many molecular liquids, binary collisions dominate depolarized scattering even at liquid densities.

Similarities found for all the liquids investigated include diffusion rates which are ordered inversely to their density and shear viscosity, as expected,[11] and comparable collision frequencies, ω_c, with values ranging from 17.1 to 20.0 cm^{-1}. The isotropic, electronic overlap model (s = 1.571) provided the better fit to the data for the quasi-spherical molecules as well as, surprisingly, CS_2, while benzene, as had been expected, was better fit by an anisotropic model (s = 2.714). Although the CI component for $CHCl_3$, CH_2Cl_2, and CS_2 may be further decomposed into an intermediate frequency term and a librational term, such decomposition may not be necessary since a

single mechanism for induced anisotropy dominates the collisional effects for these molecules. For a planar, disk-like molecular liquid such as benzene, collision-induced effects are more complex, involving multiple mechanisms to produce two well separated depolarized scattering components. Along with the reorientational term, the SGS spectra for these molecular liquids require two additional terms for the decomposition of collision-induced effects as done previously.

At the time that the depolarized spectra for CCl_4 was measured, CI scattering was the only objective and a small amount of polarized light was allowed to pass through to provide some Brillouin signal for alignment purposes. The Brillouin signal affects only the data below 2.8 cm^{-1}, which was assumed to be insignificant to the CI scattering picture. Later curve fitting analysis revealed the presence of an additional narrow Lorentzian component at very low frequencies. Data smoothly ranging from negative to positive frequency differences, including a zero frequency measurement, would have improved resolution of this component. A purely depolarized spectrum for CCl_4 can be acquired by using the first vibrational Raman line as an alternate means of alignment, thus fully resolving the very low frequency scattering component due to diffusive relaxation.

To obtain more information about intermolecular interactions than can be extracted from a third order nonlinear process alone, an additional variable in the form of high pressure was introduced into the SGS experiment. As discussed in Chapter 4, new problems with alignment, stray scattered light and scrambled polarization were encountered when high pressure was added to the experiment. Rather than using the weakly scattering CCl_4, liquid benzene was selected as a strong scatterer whose signal would be easier to

locate and maintain while the technical difficulties of incorporating a high pressure capability into the SGS experiment were minimized. With careful methodolgy and several improvements to the initial experimental set-up these difficulties were overcome and a depolarized stimulated gain signal was obtained with a signal-to-noise ratio comparable to the experiment at ambient pressure. Benzene spectra at atmospheric pressure and at 350 bars were analyzed using a curve-fitting model comprised of a low frequency diffusive reorientational term, a high frequency librational term, and an intermediate frequency term.

A comparison of fitted values reveals frequency shifts in these spectral components when high pressure is applied. Diffusive reorientation rates, Γ, decrease with the application of pressure, as increasing the liquid density inhibits the relaxation of density fluctuations in the local structure. In benzene, this was seen as a 17% decrease in Γ at 350 bars pressure. This inverse relationship is also evident when comparing the reorientation rates of several liquids with different densities in Section 3.5. The higher frequency librational motions are also affected by high pressures as increasing density increases the local ordering in the liquid leading to stronger caging effects. As a result, stronger intermolecular forces produce a 12% higher librational frequency, ω_0, in benzene at 350 bars with a 31% reduction in the inhomogeneity in those forces, α, leading to a narrowing of the librational component. The strongest pressure sensitivity was observed for the intermediate frequency component, which for benzene is the result of contributions from both translational and rotational multi-body interactions. Increasing density results in more frequent collisions with shorter durations. This effect is observed in the 350 bar spectrum as a 32% higher characteristic

frequency, ω_c, for the interaction-induced scattering. When compared to the 1 bar spectrum, this component is broadened with the application of pressure and shows a significant increase in its contribution to the spectral intensity. Although high pressure studies of the Rayleigh wing of molecular liquids are few, comparisons were made to results of previous studies.[12-17] Particularly, an analysis applying a curve-fitting model consisting of components for reorientational and librational motions in CS_2 at various pressures[16] was compared and contrasted with our results in benzene.

Finally, Chapter 4 demonstrated stimulated Brillouin gain spectroscopy with the Brillouin spectra of liquid benzene at 1, 540 and 880 bar. Results indicating a shift with pressure of 1.92 GHz/kbar are in excellent agreement with results published earlier.[18,19] A vast improvement in the resolution of the Brillouin gain experiment can be obtained with the use of 2 cw lasers.[20-23] A fully cw set-up allows a laser linewidth limit of 1 MHz as opposed to the 500 MHz imposed by the pulsed dye laser and would provide sufficient resolution for analysis of the Brillouin lineshape. The primary focus of this research, however, was the intermolecular interactions contained in the broad Rayleigh wing and the pulsed dye laser provided the necessary tunability for spectra of 250 cm^{-1}.

In summary, SGS studies in liquids at higher pressures can help to delineate the behavior of different low-frequency components resulting from intermolecular interactions with enough accuracy to challenge existing theoretical models dealing with molecular dynamics of simple liquids.

5.2 References

1. H. L. Gabelnick and H. L. Strauss, "Low-frequency motions in liquid carbon tetrachloride. II. The Raman spectrum," J. Chem. Phys. **49**, 2334 (1968).

2. W.S. Gornall, H.E. Howard-Lock, and B. P. Stoicheff, "Induced anisotropy and light scattering in liquids," Phys. Rev. A, **1**, 1288 (1970).

3. J. A. Bucaro and T. A. Litovitz, "Rayleigh scattering: Collisional motions in liquids," J. Chem. Phys. **54**, 3846 (1971).

4. V. Volterra, J.A. Bucaro and T. A. Litovitz, "Molecular motion and light scattering in liquids," Ber. Bunsenges. Phys. Chem. **75**, 309 (1971).

5. H.E. Howard-Lock and R.S. Taylor, "Induced anisotropy and light scattering in liquids. II," Can. J. Phys. **52**, 2436 (1974).

6. R.A. Stuckart, C.J. Montrose and T.A. Litovitz, "Comparison of interaction induced light scattering and infrared absorption in liquids," Faraday Symp. Chem. Soc. **11**, 94 (1977).

7. J.R. Stevens, G.D. Patterson, P. J. Carroll and G. R. Alms, "The central Lorentzian in the depolarized Rayleigh spectra of liquid CCl_4 and $GeCl_4$," J. Chem. Phys. **76**, 5203 (1982).

8. H. Deuel, P. Cong, and J. Simon, "Probing intermolecular dynamics in liquids by femtosecond optical Kerr effect spectroscopy : Effects of molecular symmetry," J. Phys. Chem. **98**, 12600 (1994).

9. E. W. Castner, Jr., Y. Chang, J. Melinger, D.McMorrow, "Femtosecond Fourier-transform spectroscopy of low-frequency intermolecular motions in weakly interacting liquids," J. Lumin. **60 & 61**, 723 (1994).

10. P. Vöhringer and N. Scherer, "Transient grating optical heterodyne detected impulsive stimulated Raman scattering in simple liquids," J. Phys. Chem. **99**, 2684 (1995).

11. J. S. Friedman, M. C. Lee and C. Y. She, "Depolarized stimulated gain spectra of liquid CS_2 and benzene at room temperature," Chem. Phys. Lett. **186**, 161 (1991).

12. J. Jonas, "Pressure--An essential experimental variable in spectroscopic studies of liquids," in *Phenomena Induced by Intermolecular Interactions*, NATO ASI Series B 127 (Plenum, New York), 525 (1985).

13. F. Medina, W. Daniels, "Collision-induced light scattering from fluid methane at high densities," Phys. Rev. **A17**, 1474, (1973).

14. X. Song, J. Jonas, and T. W. Zerda, "Total intensity measurements of depolarized Rayleigh scattering from linear molecules," J. Phys. Chem. **93**, 6887 (1989).

15. B. Hegemann, K. H. Baker, and J. Jonas, "Temperature and pressure effects on the collision-induced depolarized Rayleigh line-shapes of liquid carbon disulfide," J. Chem. Phys. **80**, 570 (1984); B. Hegemann and J. Jonas, "Separation of temperature and density effects on collision-induced Rayleigh and Raman line shapes of liquid carbon disulfide," J. Chem. Phys. **82**, 2845 (1985).

16. B. Kohler and K. A. Nelson, "Femtosecond molecular dynamics of liquid carbon disulphide at high pressure," J. Phys: Condens. Matter **2**, SA109 (1990).

17. J. F. Dill, T. A. Litovitz and J. A. Bucaro, "Molecular reorientation in liquids by Rayleigh scattering: Pressure dependence of rotational correlation functions," J. Chem. Phys. **62**, 3839 (1975).

18. F. D. Medina and D. C. O'Shea, "Brillouin scattering from liquid benzene at high pressures," J. Chem. Phys. **66**, 1940 (1977).

19. A. Asenbaum and H. D. Hochheimer, "Brillouin scattering in liquid benzene under high pressure," Z. Naturforsch. **38a**, 980, (1983).

20. S. Y. Tang, C. Y. She, and S. A. Lee, "Continuous-wave Rayleigh-Brillouin-gain spectroscopy in SF_6," Opt. Lett. **12**, 870 (1987).

21. S. Y. Tang, "Light scattering in fluids," Ph.D. dissertation, Colorado State University, (1992).

22. K. Ratanaphruks, W. T. Grubbs, and R. A. MacPhail, "Cw stimulated Brillouin gain spectroscopy of liquids," Chem. Phys. Lett. **182**, 371 (1991).

23. W. T. Grubbs, and R. A. MacPhail, "High resolution stimulated Brillouin gain spectrometer," Rev. Sci. Instrum. **65**, 34 (1994).